PRECIPITATION, RECRYSTALLIZATION AND SOLUTE STRENGTHENING IN MICROALLOYED STEELS

by

© Melek G. Akben

A Thesis Submitted to the
Faculty of Graduate Studies and Research
in Partial Fulfilment of the Requirements for the
Degree of Doctor of Philosophy

Department of Mining and Metallurgical Engineering
McGill University
Montreal, Canada

December 1980

ABSTRACT

Constant strain rate compression and torsion tests were carried out isothermally at temperatures of 875 to 1075°C on a series of six steels. The base steel had a composition of 0.06% C and 1.43% Mn and the others contained one of the following sets of additions: (i) 0.035% Nb; (ii) 0.035% Nb + 0.115% V; (iii) 0.035% Nb + 0.30% Mo; (iv) 0.035% Nb + 1.90% Mn; (v) 0.115% V. The tests were conducted to determine the effects of Mn, Mo, Nb and V, singly and in combination, on the high temperature flow and recrystallization behavior of the materials. The dynamic precipitation kinetics for Nb(CN) and VN were determined by the Weiss method. The two PTT curves were similar, with the nose of the VN curve being situated at a slightly lower temperature (885 vs. 900°C) and at a somewhat longer time (26 vs. 16 s), in agreement with the lower equilibrium solution temperature of VN. The dynamic precipitation kinetics of Nb(CN) were retarded by the addition of Mn, V or Mo. This retardation is attributed to the increased carbonitride solubility that follows the addition of these elements because of the way in which they decrease the C and N activity coefficients.

RTT curves were constructed for dynamic recrystallization in the six steels investigated. These were derived from the peak strains of the compression flow curves, as determined at a strain rate of $3.7 \times 10^{-2} s^{-1}$. Recrystallization occurred earliest in the plain C steel followed fairly quickly

by the 0.115% V steel. All of the Nb bearing steels recrystallized considerably later, with the greatest retardation being noted in the 0.3% Mo steel, where it was nearly twice that due to Nb addition alone. This very large effect, and the retardation due to each of the transition elements, is explained in terms of the electronic differences between iron and the particular element. The effect of the atomic size differences with respect to iron is also considered.

The strengthening due to the presence of Mn, Mo, Nb and V in solution was determined from the yield strengths of these steels. The increment in yield strength over that of the plain C steel was determined as 70% and 7% per 0.1 at.% of Nb and V when each is added singly. The strengthening increased to 80% and 8% respectively for these elements when present jointly in austenite. The strength increments were 9% for Mo and 1.3% for Mn per 0.1 at.% when added to a 0.035% Nb steel. The rank order of these effects is also explained in terms of the electronic and atomic size differences, and a possible reason for the synergistic effect (e.g. in the case of Nb and V in a Nb-V steel) is proposed.

RESUME

Des essais de compression et de torsion, isothermes à des températures de 875 à 1075°C, ont été effectués sur une série de six aciers. L'acier de base avait une composition de 0.06% C et 1.43% Mn et les autres contenaient respectivement les éléments d'addition: (i) 0.035% Nb, (ii) 0.035% Nb + 0.115% V, (iii) 0.035% Nb + 0.30% Mo, (iv) 0.035% Nb + 1.90% Mn, (v) 0.115% V. Les essais ont été faits de manière à déterminer les effets de Mn, Mo, Nb et V, pris séparément ou ensemble, sur l'écoulement à haute température et la récristallisation des matériaux. La cinétique de précipitation dynamique pour le Nb(CN) et VN a été déterminée par la méthode de Weiss. Les deux courbes PTT étaient semblables, avec le nez de la courbe étant situé à une température légèrement inférieure (885 vs. 900°C) et à un temps un peu plus long (26 vs. 16 s), en accord avec une température de la solution en équilibre, inférieure, du VN. La cinétique de précipitation dynamique du Nb(CN) a été retardée par l'addition de Mn, V ou Mo. Ce retard est attribué à la solubilité accrue du carbonitride qui suit l'addition de ces éléments à cause de la façon dont laquelle ils décroissent les coefficients d'activité du C et N.

Les courbes RTT ont été faites pour la recristallisation dynamique dans les six aciers etudiés. Elles ont été déduites des définitions au pic de contrainte des courbes de compression. À une vitesse de $3.7 \times 10^{-2} s^{-1}$, la recristallisation est apparue plus tôt dans l'acier au C, suivie de

près par l'acier 0.115% V. Tous les aciers contenant Nb ont recrystallisé beaucoup plus tard. Le plus retardé étant l'acier 0.3% Mo, où l'effet était environ deux fois plus marqué que celui dû à l'addition de Nb seul. Cet effet très important, et le retard dû à chaque élément de transition, est expliqué en termes de différences électroniques entre le fer et l'élément particulier. L'effet de la différence de taille des atomes par rapport au fer est aussi considéré.

Le renforcement dû à la présence de Mn, Mo, Nb et V en solution a été déterminé à partir de la limite elastique de ces aciers. L'incrément de la limite élastique divisé par celui de l'acier au C a été trouvé 70% et 7% par 0.1 at.% de Nb et V quand chacun est ajouté séparément. Cette mesure augmente à 80% et 8% respectivement pour ces éléments lorsqu'ils sont tous deux présents dans l'austénite. Les incréments pour le Mo, et le Mn ajouté à l'acier 0.035% Nb, ont été de 9% et 1.3% par 0.1 at.% respectivement. L'importance relative de ces effets est aussi expliqué en termes de différences électroniques, et de différences de taille atomiques, et une raison possible de l'effet conjoint (ex. dans le cas du Nb et V dans l'acier Nb-V) est proposée.

ÖZET

Manganez, molibden, niyobyum ve vanadyumun % 0,05 karbon, % 1,25 manganezli çelikelrin yüksek sıcaklıktaki akımı üzerine tek başına veya birlikte etkisini araştırmak için iki mekanik deney türü kullanılmıştır. 875 ila 1075 ^{o}C sıcaklıkları arasında, sabit sıcaklık ve sabit doğru gerilim hızıyla kompresyon deneyleri yapılmıştır. Bu tür deneyde erişilen en yüksek hız saniyede 0,74, ve en yüksek doğru gerilim 0,80 idi. Daha yüksek hızlara (saniyede 3 azami doğru gerilim hızı) ve gerilimlere torsiyon deneyleriyle erişilmiştir. Bu deneyler 875 ve 925 ^{o}C sicakliklarinda yapilmistir.

Bu elemanların (Mn, Mo, Nb ve V) solüsyonda veya çökerti yapıcı olarak etkilerini ayırt edebilmek için, I. Weiss'in geliştirdiği yöntemle, mikroalaşım karbonitrürlerinin çökerme hızları ölçülmüştür. Bu yontemin temeli, en yüksek basınctaki doğru gerilimin (E_p) çökerme hızına olan hassasiyetidir. Çökerme olmayan çeliklerde E_p, doğru gerilim hızının logaritmasiyla doğrusal olarak artar. Çökerme başlayan hızda, olağanın üstünde bir artış görülür. Bu yolla Nb(CN) ve VN'nin dinamik (yani akım sırasındaki) çökerme hızları ölçülmüştür. Bu iki sistemin çökerme eğrilerinin yakın zamanlerda olduğu görülmüştür. VN eğrisinin burnunun biraz daha düşük sıcaklıklarda oluşu ve biraz daha geç başlamasının nedeni, VN'nın östenitteki solüsyon sıcaklığının daha düşük oluşudur. Nb(CN)'nin çökermesi yüksek Mn katkısıyla, veya 0,115 V(yüzde olarak), veya 0,30 Mn ilavesiyle geciktirilmektedir. Bu gecikmelerin nedeninin bu ilavelerin Nb- karbonitrürlerin östenitteki erirgenliği üzerine olan

etkisinden olduğu önerilmistir. (Bu elemanlar erirgenliği arttırmaktadir.) Erirgenliğin artısı, bu elemanların C ve N aktivasyon katsayılarını azaltmasından ileri gelmektedir.

İncelenen altı çeliğin rekristallizasyon- zaman- sıcaklık (RTT) ĕgrileri, saniyede $3,7 \times 10^{-2}$ gerilim hızında, 875 ila $1075^{o}C$ sıcaklıkları arasında belirlenmistir. Bu veriler, azami gerilimin (E_p) doğru gerilim hızına oranlanmasıyla elde edilmistir. Rekristallizasyon en erken sade karbon çeliğinde baslamaktadır. Sabit bir zaman farkıyla (logaritmik eksende) bunu V çeliği takip etmektedir. Bütün niyobyumlu çeliklerde rekristallizasyonda aşırı bir gecikme görülmüstür; karbon çeliğine oranla V un iki katı kadar. $925^{o}C$'dan daha aşağıdakı sicakliklarda, RTT eğrilerinde bir kamburlaşma görülmektedir. Bu kamburlasmanin nedeni, Nb(CN) nin çökermesinin rekristallizasyondan önce baslamasindandir. Nb'lu çelikler arasinda, en fazla gecikme, 0,30 Mo li çelikte görülmüstür. Bu gecikme, sadece Nb'un etkisinin iki misli kadardir. Bu aşiri etki, ve her elemanin etkisinin derecesi de) , elemanin elektronik yapisinin demirinkinden farki, ve atom çap farklari açisindan incelenip açiklanmistir.

Nb ve V'un çeliğin yüksek sicakliktaki direncine tek olarak katkisi, benzer temel alaşimdaki karbon çeliğinin direnciyle alaşimli çeliklerin dirençlerinin oranlanmasiyla elde edilmistir. Atomik orande % 0,1 Nb ilavesi direnci % 70 oraninda arttirmistir. Ayni miktarda V direnci % 7 kadar arttirmaktadir. Bu iki elemanin beraberkenki etkileri, Nb için % 80 ve V için % 8'e artmaktadir. Yüzde 0,035 Nb'lu çeliğe % 0,1 (atomik) Mo veya Mn ilavesi direnci,sirasiyla % 1,3 ve % 9 kadar attirmaktadir. Dirence her elemanin katkisi elektronik yapi ve atomik çaplar

farkiyla, ve bir öneri olarak, birlikte iki elemanin etkisinin teker olarak katkisinin daha yüksek olusu, elemnlarin birbirinin aktivasyon katsayilarini arttirmasina bağlanmistir.

ACKNOWLEDGEMENTS

The author is most thankful to her thesis supervisor, Professor John J. Jonas, for his guidance, many useful comments and encouragement throughout the course of this research as well as for his personal generosity. His genuine enthusiasm to try and gain scientific insight into the practical aspects of making of HSLA steels and the opportunities he has created to interact with other experts in this subject area have added a very interesting dimension to this study.

Much gratitude is due to the author's parents and sister for their great moral support from across the world. Special thanks are extended to her brother, who has always been there when needed and who has given her valuable advice.

Many thanks are also due to Paul Marchand for his unspoken support, encouragement and patience, especially during the writing of this thesis.

The friendly and pleasant work environment created by past and present fellow graduate students along with their suggestions on technical matters has been appreciated, particularly the assistance of Isaac Weiss (now a professor of materials science at Wright State University, Dayton, Ohio) in the earlier stages of this investigation.

The author is indebted to her colleagues at CANMET, particularly to Drs. G.E. Ruddle and J.D. Boyd, as well as to

Drs. J.M. Gray (Microalloying International) and M. Korchynsky (Union Carbide Corp.) for their useful comments and suggestions. She is indebted to PMRL, CANMET, for providing the experimental materials and for the financial support of this investigation, and to Dr. M.J. Stewart (Dominion Engineering Works, Ltd.) who initiated the project while at CANMET.

Last, but not least, she expresses her gratitude to Louis Vroomen, Jr. for the many improvements related to the compression testing computer programs, and to Martin Knoepfel, Bruno Grondin, Oscar Muehling, Ben Stafford and George Dedic for specimen preparation, and for assistance with the repair and construction of the experimental equipment.

TABLE OF CONTENTS

LIST OF FIGURES

LIST OF TABLES

CHAPTER 1

INTRODUCTION

High Strength Low Alloy (HSLA) steels were developed in response to the increasing need for inexpensive, strong, tough and weldable steels. With each passing year, larger tonnages of these materials are being produced. Many of the advances associated with the development of these steels have depended, and still do, on the control of recovery and recrystallization in deformed austenite. In the case of flat HSLA steel products, this is accomplished by controlled rolling, a process in which the temperature and reduction at each stage of hot forming are manipulated according to an overall plan or schedule. The delay or prevention of recrystallization, when required, is achieved by making microalloying additions (i.e. additions in amounts well under 1% by weight). Whether the elements added fulfill their purpose as solutes on the one hand, or as precipitate formers on the other has been subject to great debate . Some of this can be found, for example, in the book entitled "The Hot Deformation of Austenite", edited in 1977 by J.B. Ballance. The controversy is still continuing and has not been resolved, as can be seen from the proceedings of the October 1980 International Conference on Steel Rolling in Japan. The papers presented at this conference include ones claiming either that the microalloying additions produce strong solute retardation effects, or inversely that these additions retard recrystallization principally via the formation of precipitates.

An understanding of the effects of the microalloying additions, singly and in combination, on the softening processes mentioned above is of importance for several reasons. The first of these is that, in order to obtain the desired final properties, it would be useful if the chemistry could be selected on the basis of rational principles. Once the chemistry has been determined, a rolling schedule must also be designed. The latter should enable the steels to be formed without damage to the equipment and also produce the required final mechanical properties. A well developed set of rules regarding the conception and design of such schedules would also be of great utility to steel processors.

The dual aim of (i) rational alloy design, and (ii) rational rolling schedule design requires, however, that the roles of each of the alloying additions be clearly understood. For example, why should certain alloy additions such as Nb be more effective than others, e.g. V? Similar remarks apply to the influence of Mo or Al, as other examples. The present investigation was undertaken, in part, to try to answer these questions. The project involved a series of six steels containing Mn, Mo, Nb and V singly and in combination. The solute and/or precipitate effects of these elements on retarding recrystallization during or after high temperature deformation were investigated. As will be seen below, it was possible to distinguish between these two kinds of effects to a certain extent. In addition, the contribution of each element to the hot strength

of austenite was also studied systematically. Finally, a possible scientific or rational basis was drawn up and is recommended for the explanation of these effects. It is the author's hope that such a rationalization may be of some use with respect to the design of both alloys and rolling schedules.

CHAPTER 2

A REVIEW OF THE LITERATURE ON THE HIGH TEMPERATURE FORMING OF HSLA STEELS

2.1 Development of HSLA Steels

2.1.1 A Brief History

The development of High Strength Low Alloy (HSLA) steels has occurred in response to demands by design engineers for improved tensile and impact properties, as well as to social and economical pressures to achieve higher cost and material efficiencies in production. The most important property to be controlled is the yield strength. It can be increased by grain refinement, by solid solution alloying, by precipitation in austenite and ferrite, and finally by controlling the transformation behavior. In addition, for low temperature applications in plate form, e.g. arctic pipeline grades, the impact transition temperature (ITT) must be sufficiently low. In the case of Canadian applications, this temperature may be required to be as low as - 65°C (1). Good weldability is also a requirement for the heavy plate applications (e.g. bridges, offshore oil and gas rigs, pipelines, etc.), and even for some sheet metal uses in the automotive and other industries. The following is a brief history of the development of HSLA steels.

From the beginning of the century up to the early 1930's, the strength requirements for steels were met through C and Mn additions up to 0.35% and 1.5% respectively (2,3). By 1933, Cor-Ten (2,4), the first commercial low alloy steel

was introduced. This product made use of two or more of the following addition agents: Cr, Cu, Mn, Mo, P and Si. The total alloy concentration was in the range of 2-4%. This product had a combination of high strength, improved impact properties and good corrosion resistance, all of which made it widely useful, and therefore applied. The structural steel plate grades had yield strengths in the range 345-415 MPa (3,4).

By the beginning of the next decade, the strengthening effect of Nb (or Cb) additions of as little as 100-500 ppm was discovered (2). Although this development led to a slight loss in corrosion resistance, it enabled the total alloy additions to be reduced to 1-1½%, including Al, Mn and Si which comprised most of the additions. In the same decade, the similar effects of Ti and V were also recognized (4). V was used successfully in structural, plate and sheet grades. The use of Nb was limited until the 1940's when its availability increased and the cost decreased.

The form of the dependence of the yield stress on the ferritic grain size was demonstrated by Hall (5) and Petch (6) in the early 1950's. This allowed the different strengthening contributions attributable to grain refinement and to solute addition to be distinguished (7). Initially, grain refinement was achieved by the use of Al and N (3,8). Some of the reasons for the limited current use of these elements as grain refiners, particularly for controlled rolling operations, is an important subject area of this thesis, and will be elaborated on in the Discussion. Since then, Mo, Nb, Ta,

Ti and V have also been used as grain refiners. The greater effectiveness of Nb than of the other elements was stressed by Leslie (9), Morrison and Woodhead (10), and Morrison (11) as early as 1963. Morrison was also able to single out the effects of precipitation from those of grain refinement (11).

Prior to the development of practical TMT schedules, HSLA and plain carbon steel products were manufactured in a similar way. The forming operations (e.g. hot rolling) were performed and heat treatments may or may not have followed to produce the required properties. The two main disadvantages of this practice were (i) that the optimum properties of the alloyed grades were not generally reached (2), and (ii) that the costs involved were often higher than necessary (largely because of the inefficient use of the alloy additions). Furthermore, because some of the microalloying additions precipitate below a given temperature, and because this leads to significant increases in rolling load, plain C steel production methods are no longer employed for HSLA steels. As early as 1958, there were reports that deliberate finish-rolling at lower than conventional temperatures led to a refinement of the ferrite grain structure and to a corresponding improvement in the mechanical properties (12). This eliminated the need for further heat treatment. Such low finish rolling is called control rolling, and if carried out in the appropriate manner, produces the optimum properties in the as-rolled product. This type of procedure is now commonly used for HSLA sheet and thin plate production. Hot forming

with subsequent heat treatment is still used, however, for certain plate and heavy sections, for the reasons discussed in the next section.

2.1.2 Controlled Rolling of HSLA Steels

Controlled rolling is a process whereby the properties of a steel can be improved to a level equivalent to those of a more highly alloyed or heat treated steel (12). Its first purpose is to refine the austenite grain size by natural or accelerated cooling during passage of the steel through the mill. This can be achieved by means of controlling the rolling process to a high degree. There are three stages involved in such an operation: soaking, roughing and finishing, after which the material is coiled if it is thin enough. For complete success, the time and temperature at the start and end of each of these stages must be carefully regulated.

The second important aim of the rolling process is to produce a very fine grained ferrite after transformation. Because grain refinement is the principal source of ferrite strengthening, the carbon levels can be reduced to below 0.15%. In this way, the yield strengths of control-rolled steels can be raised considerably from the C-steel level, to the range 350-700 MPa (13,14). The reduction in the C concentration, along with the presence of microalloying agents, results in crackfree weldability and in increased hardness in the heat affected zone of the weld, both of which are particularly important in the pipeline grades (15).

The soaking temperature of the HSLA steels is generally in the range 1200-1300°C. The minimum is set by the solubility temperature of the microalloy carbonitrides. The effective use of the microalloying elements, particularly Nb and V, depends on their being in solution at the start of rolling, and then on their presence in supersaturated form as the temperature decreases during rolling. In this way, they are available for precipitation during the hot forming operation. (Precipitation results in the retardation of recrystallization, as is described in more detail in Section 2.2 below.) The final strength and toughness of the HSLA product is thus strongly influenced by the soaking temperature (16,17), because the latter determines the amount of carbonitride available for precipitation.

High soaking temperatures lead to coarse austenitic grain sizes (250-1000 μm), and are therefore undesirable (16). As a result, lower soaking temperatures (which must still be above the solubility temperature) have three distinct advantages. The first of these is a smaller initial grain size, which is a help in producing fine grained ferrite. The amount of deformation (bite per pass) required for the onset of both static and dynamic recrystallization decreases with decreasing initial grain size. Thus smaller initial grains make further refinement easier, although they have little or no bearing on the final austenite grain size once recrystallization has occurred (17,18). The second of these is related to the hold time, which is the time the steel has to be held between passes

for the temperature to drop to the necessary level. Higher soaking temperatures lead to longer hold times and sometimes to lower mill output. The third of these is related to the energy costs involved in heating to higher temperatures. This saving is, however, somewhat offset by the lower rolling loads required at the higher temperatures.

Roughing is carried out between 1150 and 1050°C. The initial coarse austenite grains are refined to the range 60-250 μm by at least one complete cycle of recrystallization. For this to be effective, it must take place without any substantial grain growth following recrystallization. The number of cycles depends on the temperature, the reduction per pass and the initial grain size (17-19). At these temperatures, recrystallization takes place within seconds, or even fractions of a second, after each pass (this is less than the inter-pass time). In this manner, repeated recrystallization, in the absence of appreciable grain growth, leads to a finer austenite grain size, which in turn results in a finer ferrite grain size (12).

In opposition to the roughing process, during finishing, it is necessary to avoid recrystallization completely. This is possible through the control of temperature and time, and most importantly, by appropriate microalloying. The time to the onset of recrystallization increases somewhat at lower temperatures; it is also reduced as the amount of deformation is increased at a given temperature. However, recrystallization

can be delayed by more than an order of magnitude in time (with respect to the plain C behavior) by the microalloying additions. This retarding effect has often been attributed to the precipitation of the carbonitrides (12,19-23). A more detailed discussion of the interaction between recrystallization and precipitation will be given in the next section, along with a different approach to the effect of the microalloying additions.

According to several authors, the product from the finishing mill should have a uniformly 'pancaked' structure (17,19,24). The greater austenite grain boundary area provides more nucleation sites for the ferrite grains. In addition, the deformed state of the austenite, as well as the presence of deformation bands, increases the nucleus density still further above the level pertaining to equiaxed (undeformed) grains. This results in a fine and uniform ferrite grain structure after transformation. When austenite recrystallization occurs in the finishing stage, despite the precautions described above, the final ferrite grain size is mixed, or in the best possible case, larger than desirable (17,25). This leads to a deterioration in the fracture properties.

Austenite grain growth is avoided once the material leaves the finishing stands by quenching or accelerated cooling (19). In some cases, finishing is even carried out below the Ar_3 temperature, as is done for some dual phase steels. Under these conditions, the presence of the fine precipitates introduced by microalloying can delay or prevent ferrite grain growth (12,17,26). In their absence, grain growth cannot be

prevented, and the refinement of the ferrite grains by rolling is difficult to achieve. When rolling is carried out below the Ar_3, the final structure is generally comprised of elongated ferrite grains containing subgrains. The deformed state of the ferrite can lead to unfavorable texture effects, particularly in pipeline grades.

Controlled rolling is especially effective for the production of thin plates and strip mill products. For heavy gauge plate production, e.g. 40 mm, the lower cooling rates in the centre of the plate are responsible for poor mechanical properties. For these products, normalizing heat treatments are required after rolling to produce uniform properties.

The choice of the rolling schedule depends on characteristics of the product, such as thickness, strength and toughness. These determine the finishing and coiling temperatures, and whether further heat treatment is required. A high finishing temperature in Nb-steels, for example, will produce maximum precipitation strengthening in the ferrite after transformation, but little or no grain refinement. Though the yield strength may be comparable to that produced with the aid of lower finishing temperatures, there is a loss in toughness because of the heavier reliance on precipitation strengthening. When low finishing temperatures are used, on the other hand, there is much less precipitation strengthening. Its place is taken by a substantial component of Hall-Petch strengthening due to the finer grain size, and the toughness is simultaneously improved (3,13,19,25).

Lower finishing temperatures necessitate the use of either a lower soaking temperature or a hold-time before finishing. The former may lead to excessively high rolling loads in the roughing stands, either due to solute effects, or to the retardation of recrystallization by precipitation. The insertion of hold-times is also unpopular, because it can lower mill output. Most mill operators define mill productivity in tons per hour output, rather than in dollar value produced. The delays involved in schedules with hold-times are unwelcome for this reason and not readily accepted for implementation, particularly where tonnage shift bonuses are awarded (12). This penalty can be avoided by scheduling several slabs on a single series of mills. The rolled plates can then be held on run out tables, provided they are long enough, or else removed temporarily from the line.

Each steel company has its own preferred rolling schedule for different grades of products (e.g. see references 12 and 25). As already suggested above, however, most schedules involve soaking at 1200-1300^{o}C, roughing between 1250-1050^{o}C, and finishing at or below 900 or 850^{o}C. After a brief hold of approximately one minute, the material is rapidly cooled to 650^{o}C and coiled. The desired product properties are obtained by controlling the recrystallization of austenite by means of its interaction with the precipitation process. This subject will be considered in the next section.

2.2 Recrystallization in Austenite

2.2.1 Types of Recrystallization

The recrystallization behavior of an alloy depends on three main factors: its chemistry, and the amount and temperature of the deformation it has undergone. In addition, the strain rate of deformation also has a distinct, but smaller effect. For a given temperature and chemistry, the time and rate of recrystallization are primarily determined by the prior or accumulated strain. During hot forming, there are three types of recrystallization: (i) static, or classical recrystallization; (ii) dynamic recrystallization; and (iii) metadynamic recrystallization (24,27). The type that predominates depends on the conditions of deformation. Static recrystallization requires a minimum or critical amount of prior deformation. This is of the order of 8% (27); it is the slowest of the three processes in terms of R_s (recrystallization start time). It generally takes place in between rolling stands and on the runout table. As described in Section 2.1.2, it is desirable for R_s to be short in the roughing temperature range and long in the finishing temperature range. It is also necessary that R_f (recrystallization finish time) not be too long during roughing, so that recrystallization is complete at a given stage. Otherwise the grain size is unlikely to be uniform.

Dynamic recrystallization occurs concurrently with deformation, e.g. while the material is being rolled or forged. The higher the temperature and the lower the forming rate, the smaller the strain required, and the more likely it is to

occur. The onset of dynamic recrystallization is marked by a drop in flow stress (load) while forming. The strain (or deformation) at the maximum stress is referred to as the peak strain (ε_p) and is used as a parameter to follow this type of recrystallization (21,28). Strictly speaking, recrystallization commences before the peak is reached (28), but for most practical purposes, this difference can be neglected.

The peak strain for a given chemistry increases with deformation rate and grain size (18) and decreases with an increase in temperature. The R_s time for this process is very short, and can be less than a second (21,29,30), in contrast to roughly 30 seconds in the static case for a 0.035% Nb steel deformed to 1.33 strain in torsion at 3.6 s^{-1} and 900°C (28).

The third type of recrystallization occurs when the material is under no load but is distinguished from the classical type by the fact that dynamic recrystallization must have been initiated prior to the interruption of straining. That is, it only occurs after the material has been deformed beyond the peak strain. Like classical recrystallization, this type of recrystallization can also take place between rolling stands. At a given temperature and deformation rate, the R_s time decreases with increasing pre-strain. Thus the possible start times are always less than the static case. As pointed out above for dynamic recrystallization, the higher the strain rate, the greater the critical strain (ε_p) for the onset of metadynamic recrystallization.

2.2.2 Effects of Small Alloy Additions on Recrystallization

The effect of alloy chemistry on the three types of recrystallization is similar to that of strain. The retardation of recrystallization by alloy additions can be attributed to their presence as solutes, as precipitates, or to a combination of the two causes. Before examining these effects in more detail, there will be a brief recapitulation of the principal recrystallization mechanisms.

The nucleation of recrystallization can occur by two alternative processes: (i) the bulging of high angle, i.e. grain, boundaries; and (ii) by subgrain coalescence (24). In addition, it is also possible to have recrystallization take place without any nucleation whatsoever, through the process of 'in situ recrystallization' (31). The first of these occurs in materials that have not undergone large strains. The latter requires that the deformation be sufficient for a well developed substructure to have formed. Increased amounts of deformation or of holding time lead to larger misorientations at the sub-boundaries, until coalescence occurs.

Recrystallization is generally preceded by some form of recovery. In materials that recover with ease, i.e. those with high stacking fault energies such as Al and α-Fe, both static and dynamic recrystallization are retarded, or may not even occur. Enhanced recovery prevents the formation of a well-defined substructure with a minimum of misorientation, making the nucleation of recrystallization more difficult.

Both solute atoms and second phase particles (in this case, precipitates) can affect the recrystallization. Stüwe (31) has presented an excellent summary of the contribution of these two factors to the "dragging force" opposing recrystallization. The major difference in their effects is due to the mobility that single atoms have in a lattice at high temperatures. They can move with a dislocation or with a boundary provided that the rate of motion of the latter is not too high. When a dislocation or a boundary moves, the solutes can create a substantial dragging force. Precipitates, on the other hand, are invariably sessile, and thus can only provide static pinning. When they are coarse, they are no longer able to act as barriers (21,29,30) and can sometimes even enhance recrystallization (32). The effects of solutes on recrystallization can be summarized as follows:

- Solutes can lower the stacking fault energy and therefore hinder recovery. Consequently, recrystallization is delayed or prevented completely (33).
- When the presence of solutes obstructs dislocation rearrangement, subcells cannot readily form nuclei and recrystallization is delayed (34).
- Sub-boundary motion can become more sluggish due to solute segregation to dislocations. This often promotes the occurrence of dynamic recrystallization when it might have otherwise been absent (33). (This is also related to lower recovery rates.)

- The presence of solutes on moving grain boundaries can affect the motion in one of three ways: if the grain boundary motion is slow, the solute atoms will move with it; if the motion is very fast, the boundary will break away from the solutes; at intermediate velocities, there will be a solute drag which will impede the boundary motion and, therefore, retard recrystallization (31).

Fine precipitates prevent or restrain sub-boundary migration, i.e. the motion of groups of dislocations rather than single ones (13,24,33-35). They tend to stabilize the substructure, thus retarding recrystallization (24). Fine precipitates on grain boundaries also produce a drag-force (Zener drag), resulting in a delay or elimination of precipitation.

The retardation of recrystallization due to non-precipitating alloy additions is readily accepted when these are present in substantial amounts, e.g. the effect of a 5.2% Mn addition in γ-iron is well known (36). Whether there is a solute-retarding effect of elements such as Nb and Ti (which are present in much smaller amounts) has been the subject of considerable controversy (37). The observed delay in the recrystallization of Nb-micro-alloyed steels has generally been attributed to the effect of fine precipitates, with the exception of a few investigators who could not detect preci-

pitation directly or indirectly (21,28-30,37). In order to shed light on this debate, several researchers have attempted to distinguish between the individual effects of solutes and precipitates in Nb-HSLA steels (21,29,30,34,38). The most recent of these is the work of Weiss and Jonas (21,29,30). With a high temperature, isothermal compression testing technique, they were able to determine precipitation and recrystallization kinetics in undeformed, deforming and deformed steels. They demonstrated that, at high temperatures and high strain rates, where dynamic recrystallization starts prior to the onset of dynamic precipitation, recrystallization (i.e. the peak strain, ε_p) is nevertheless delayed in comparison with a plain carbon steel of similar composition. (This delay occurs in the absence of observable precipitates.) When precipitation starts before recrystallization, the latter is delayed still further by more than an order of magnitude in time. The most pronounced case was observed at 900°C, at which temperature the nose of the PTT curve is located. These results agree in general terms with the previous ones of Le Bon et al. (28), and of Lamberigts and Greday (39), as well as with the more recent data of Hansen et al. (13). The former two reports are based on torsion data and the latter involves a combination of compression testing and microscopy.

The second of these investigations is that of Roberts (34). His study consisted of a series of hot isothermal compression experiments carried out on Nb and V microalloyed

steels. The author reported that he observed an increase in peak stress and that Nb(CN) particles were not present. He did not, however, conclude that the effect was due to solute drag. In an earlier study (40), carried out in 1977, he claimed that solute retarded recrystallization was unlikely in HSLA steels, such delays as were observed being attributable to fine precipitates. His more recent study (1978) led him to conclude that there is definitely a solute-drag component of retardation of dynamic recrystallization in the presence of Nb and V. The results of White and Owen (41) for V, Nb and Nb-V HSLA steels published in 1980 agree with Roberts' work, although the authors did not themselves come to the same conclusions.

Both of the above studies were carried out in steels containing C and N along with Nb and/or V. The third study was performed by Luton, Dorvel and Petkovic (28). They tested three steels: a 0.055% C, 0.41% Mn, 0.005% N plain carbon steel, and two 0.054% Nb steels with 0.92% Mn. The first of these Nb-steels contained 0.05% C and 0.005% N; the second was decarburized and denitrided with wet hydrogen to reduce the interstitial levels to 0.0014% C and 0.001% N. That is, they produced a nearly "interstitial free" steel. They found that an increase of 0.56% in the concentration of the substitutional solute alone led to a 1-1½ order of magnitude delay in recrystallization at 900-1000°C without the formation of precipitates. They also showed that when dynamic and post-dynamic precipitation occurs, it retards static recrystalliza-

tion when the particle size in in the 20 nm range. Furthermore, if the volume fraction of precipitate attains 0.02% or more, static recrystallization can be completely suppressed.

In this author's view, the effect of solutes such as Nb in retarding recrystallization is reasonably well established under the conditions of deformation and temperature described above. However, as it is still a subject of debate in the technical literature, we will return to this question and consider it in greater depth in the Discussion.

2.3 Methods of Following Precipitation in Austenite

The austenite phase in HSLA steels is stable only at high temperatures. Thus, any room temperature method of following precipitation requires the use of indirect measurements, either on martensite or on the transformed α-phase. A direct measurement method at high temperature is also possible, and is based on compression or torsion testing. The room temperature methods are based on one of the following four approaches: (i) physical property measurement; (ii) mechanical property measurement; (iii) quantitative metallography or microscopy; and (iv) quantitative chemical extraction.

2.3.1 Direct Methods (High Temperature Mechanical Testing)

A method was devised by Weiss (21,29,30) to determine the PTT curves of two Nb-HSLA steels for the undeformed (static), pre-deformed, and deforming (dynamic) states of the material. The method involves isothermal, constant strain

rate, uniaxial compression testing. The peak strain (ε_p) determined from the resulting flow curves is the parameter used to establish the precipitation start (P_s) and finish (P_f) times. After a half hour soak at the solution temperature, the material is cooled to the test temperature and then one of three procedures is applied.

(i) It can be held for various times and then tested at a given strain rate. This provides data for the (undeformed) static case.

(ii) The samples may be pre-deformed immediately at a given strain rate to a specific strain, held for various times and the deformation is continued, possibly at another strain rate. This method provides data for the pre-deformed static case.

(iii) Finally, samples can be tested without interruption over a range of strain rates to furnish information for the dynamic case.

The P_s times for the undeformed and pre-deformed static conditions are the holding times corresponding to the first deviation of ε_p from a maximum and constant value. In a similar manner, the P_f times are associated with the holding times where the ε_p reaches a second, and minimum plateau. In the dynamic condition, the P_s and P_f times are calculated from the ε_p vs. log $\dot{\varepsilon}$ (log strain rate) curves. (The details of this method will be described in the Discussion chapter below.)

The PTT curves obtained by these mechanical methods are comparable with the results obtained from the indirect methods which are reported in literature. For example, although the curves and precipitation kinetics reported by Le Bon et al. (28) and Simoneau et al. (42) are somewhat slower than those of Weiss, those obtained by Watanabe et al. (43) are slightly faster. As will be demonstrated later, the differences in the kinetics can to some extent be accounted for by the differences in steel chemistry and in the amount of pre-deformation.

White and Owen (41) have also used isothermal compression tests to follow the precipitation of Nb, V and Nb-V steel, but they employed constant cross head speeds instead of constant true strain rates. The change in flow stress of the pre-strained samples was measured after various holding times. These data were supplemented by electron microscopy but the results were not treated so as to lead to PTT curves. Similar methods, but under constant true strain rate conditions, were used by Roberts (34,40). Once again, these were not employed to deduce PTT curves but, with the aid of accompanying electron microscopy, the results contributed to an understanding of precipitation kinetics and precipitate morphology in Nb, V and Nb-V steels.

2.3.2 Indirect Methods

2.3.2.1 Physical property measurement methods

The electrical resistivity of a material is sensitive to its structure. In order to follow the progress of precipitation, Simoneau et al. (42) measured the resistivity components ρ'_t and ρ_r. Here ρ'_t is the increase in resistivity due to the temperature being higher than $4^{\circ}K$, and ρ_r has three contributing factors:

$$\rho_r = \rho_r(I) + \rho_r(Nb) + \rho_r(D)$$

where $\rho_r(D)$ is the contribution due to the presence of dislocations, the density of which is measured by an x-ray line broadening technique; $\rho_r(Nb)$ is the contribution attributable to the Nb left in solution, and $\rho_r(I)$ is due to the non-precipitating interstitials, whose concentration is assumed to remain constant. In order to eliminate possible differences in resistivity due to variations in the C and N levels, all samples were annealed 16 hours at $300^{\circ}C$. At $900^{\circ}C$ they determined the P_s times for static precipitation of two Nb alloys. They detected the start of precipitation at approximately 1000 and 3500 seconds for a 0.19% C, 0.65% Mn, 0.05% Nb, 0.0072% N, and a 0.07% C, 0.88% Mn, 0.04% Nb, 0.0103% N steel, respectively. For both materials, the onset of precipitation was delayed at higher temperatures. These times are much longer than any others reported in literature (see Ref. #21 for a recent review) and probably reflect the insensitivity of the method for determining precipitation kinetics.

Davenport et al. (44) used an x-ray diffraction technique to determine the volume fraction and size distribution of Nb(CN). These results were verified by means of the dark field examination of thin foils. The observed precipitation-time-temperature behavior followed a C-curve, with the nose at around 1090°C. The effect of pre-strain on the rate of precipitation, and the effects of time and temperature were also obtained.

Mishima et al. (45) followed the progress of precipitation of "VC" in austenite with the aid of two methods. The results obtained agreed with one another, the methods being based on measurement of the thermoelectric potential and of the martensite transformation temperature (M_s). The thermoelectric potential drops when precipitation starts. It is reported to have a "high sensitivity to atomic concentration and relative insensitivity to the presence of defects" (45). Thus it is said to be more precise than the electrical resistivity method described above. The M_s temperature rises after holding the sample at a given "ausaging" temperature. This is because, once precipitation starts, the C concentration in solution drops.

2.3.2.2 Mechanical property measurement methods

Microhardness measurements were utilized by Amin and Pickering (46), LeBon et al. (28), Jizaimaru et al. (47) and Ouchi et al. (48). The precipitation of Nb in the austenitic range reduces the amount available for precipitation

during or after transformation to ferrite. This causes a loss in the secondary hardening potential. Amin and Pickering (46) applied a combination of reheat temperatures and of rolling/holding temperatures and times with reductions of 20% or 50% prior to cooling to room temperature at 400°C/min (6.7°C/sec). The effects of these parameters and of stoichiometry on precipitation strengthening with Nb(CN) was followed in this way.

In the latter three references, a microalloyed steel and a plain carbon steel were tempered at 600°C for an hour to evaluate the progress of isothermal precipitation. Changes in hardness vs. aging time in the austenite range allowed the determination of P_s and P_f, which are times at which the hardness level begins to drop and levels out respectively.

2.3.2.3 Quantitative metallography and microscopy

Although the precipitation kinetics can be determined with the aid of the above methods, they produce little or no information about the size, volume fraction and shape of the individual precipitates. For these purposes, thin foil and extraction replication can be used to better advantage. With the replication method developed by Ashby and Ebeling (49) for precipitates in the Cu-SiO_2 system, accurate size distributions and interparticle spacings can be determined. It leads, however, to inaccuracies in volume fraction which arise from statistical errors. These can be overcome using the Fullman expression (50) for determining the number of particles

per unit volume. The number of Nb(CN) precipitates per unit volume after different rolling schedules has thus been calculated (50). Phillipo and Crane (51) adopted this method to get the P_s times for carbide precipitation after various amounts of reduction followed by aging at 1000°C.

Hansen et al. (13) applied the technique, using carbon replicas, to determine the PTT curve for Nb(CN) formation, as well as the particle size distribution and particle area-density statistics for both the Nb(CN) and AlN systems. White and Owen (41) also followed the static precipitation of Nb(CN) and V(CN). They noted evidence of a V-rich precipitate which they assumed to be VN in 0.1 and 0.2 V steels. They excluded the possibility of quantitative electron microscopy to detect the start of VN precipitation due to the small size of precipitates and to their being widely scattered. In the V and Nb bearing steels, they found no evidence of V in the Nb(CN) precipitates. Chandra et al. (52) studied the dynamic coarsening rate of Nb(CN) as affected by temperature in samples that were compressed at different strain rates. They found that in a 0.05 C, 0.018 Nb, 0.004 N steel, at 925°C, dynamic precipitation produced fine particles (3 to 8 nm). When static precipitation preceded straining, the mean particle size produced dynamically dropped to below the statically precipitated size (at about 15% strain at $1.2 \times 10^{-3} s^{-1}$ strain rate) and then grew. Straining beyond the end of dynamic precipitation led to coarsening. The rate of coarsening was higher at lower temperatures. This was attributed to the higher

dislocation densities present under these conditions.

Particle volume fractions were measured by transmission electron microscopy by many authors. Cahn and Nutting (53), and Hilliard (54) described the corrections required for the effect of overlapping images when the mean particle diameter is small in comparison to the foil thickness. Sellars and Smith (55) developed another method for the same purpose. Additionally, they established a separate correction for the particles intersecting the foil surfaces. In their more recent investigations, Davenport et al. (56) showed how to differentiate the particles which remained undissolved during reheating from those that precipitated during the rolling schedule. Their Nb(CN) precipitation study involved the use of dark field procedures in the TEM.

2.3.2.4 Quantitative chemical methods

The amount of Nb(CN) present at the different stages of aging was followed by Hoogendorn and Spanraft (57) using a chemical extraction method. Aging was carried out in the austenite phase, then the samples were oil or water quenched. The carbide particles were separated by dissolving the ferrite matrix. The volume fraction was estimated from the weight of the residue left after filtration. Watanabe et al. (43) attempted to determine the chemical composition and crystalline structure of Nb(CN) with a similar method. They had the subsidiary aim of checking for the presence of Mo in the carbonitrides in a series of Nb-Mo microalloyed steels. After

thermomechanical treatment, the samples were cut, polished, ultrasonically cleaned, dried and weighed. With the aid of further ultrasonic vibration, electrolytic extraction of Nb(CN) from the matrix was carried out. The washed and dried samples were re-weighed to determine the weight loss. The solution was filtered and the amount of Nb was also determined by spectrophotometric analysis. The loss of Nb in this procedure was reported to be less than 3% of the total amount. The lattice parameter measurements of the precipitates by x-ray diffraction did not reveal the presence of Mo in the Nb(CN) phase.

Each of the indirect methods described above involves some complications. None is carried out at the temperature for which the information is required. Furthermore, the chemical method is not sensitive to the presence of coherent particles. Likewise, the metallographic method is inaccurate due to the denseness of the quenched microstructure. Thus, the sampling errors can be significant. Although the microhardness technique does not suffer from the latter two deficiencies, as the measurements are carried out in a quenched and tempered phase, they can be influenced by other aging and hardening phenomena.

The mechanical testing method has two advantages. One is that testing is carried out on the phase of interest, i.e. the austenite phase, and not on a transformed phase. The second is that bulk, rather than local, properties are measured, so that the sampling errors are reduced. This

technique, followed by electron microscopy to obtain the particle size distribution and volume fraction, can produce the most detailed and reliable information. Even without microscopy, the use of mechanical testing is an efficient and relatively accurate way of determining PTT curves, and it is the method selected for the present study.

CHAPTER 3

EXPERIMENTAL MATERIALS AND PROCEDURE

3.1 Experimental Materials

With the purpose of investigating the effects of Mn, Mo, Nb and V singly and in combination on the dynamic recrystallization and on the high temperature flow behavior of austenite, a series of six steels was prepared in the Physical Metallurgy Research Laboratories of the Department of Energy, Mines and Resources, Ottawa. The series was comprised of a reference plain carbon steel and five HSLA steels, with the chemical compositions shown in Table 3.1.

The steels were prepared as follows: They were melted in 230 kg heats in an induction furnace and Al-killed. Each heat was cast into three 70 kg cylindrical ingots. Both ends were cropped and the ingots were cut into two cylindrical sections weighing roughly 23 kg each. They were soaked in an oil-fired furnace for two hours at 1200°C before being forged down to 67 mm thick slabs. These slabs were soaked for two hours at 1250°C in an electric Globar furnace, then hot rolled down to a final thickness of 13 mm in a reversing mill.

For the reasons described below (in Sections 3.4 and 3.5), two testing methods were adopted: compression and torsion. All the test samples were prepared from the 13 mm thick plates with their longitudinal axes along the rolling direction.

TABLE 3.1

Chemical Composition of the Steels Investigated, wt.%

Steel Type	C	Mn	S	Al	Si	Nb	V	Mo
Plain C	0.06	1.43	0.012	0.025	0.24	-	-	-
V	0.05	1.20	0.012	0.030	0.25	-	0.115	-
Nb	0.05	1.25	0.012	0.030	0.27	0.035	-	-
Mn-Nb	0.06	1.90	0.010	0.030	0.225	0.035	-	-
Mo-Nb	0.06	1.33	0.012	0.025	0.205	0.040	-	0.30
Nb-V	0.05	1.18	0.013	0.020	0.24	0.035	0.115	-

N ≈ 0.006, P ≈ 0.006

3.2 Heat Treatment of the Tested Materials

Two separate heat treatments were carried out on all the samples tested. Preliminary compression tests resulted in elliptical samples due to the rolling texture in the as-received material. To eliminate this effect, all samples were heat treated at 1000°C for two hours under vacuum, and then water quenched. This heat treatment was carried out in batches of 10-20 specimens for the compression samples, and in batches of four for the torsion samples. The samples were enclosed in stainless steel annealing envelopes.

The second heat treatment, the austenitization, was carried out immediately prior to the testing of each specimen. The sample was held at T_{aus} (austenitizing temperature) for half an hour in the test chamber in an argon atmosphere. These temperatures are given in Table 3.2. The choice of T_{aus} for each steel was based on two considerations: (1) To ensure the complete dissolution of the microalloy carbonitrides, and (2) to obtain approximately the same initial austenite grain size for all the six steels. The matter of the austenite grain size will be considered in more detail in the next section.

The equilibrium solubility temperatures of VN and V_4C_3 for 0.05% C, 0.115% V and 0.006% N were calculated from (2):

$$\log (V)(N) = -\frac{7733}{T} + 2.99$$

and,

TABLE 3.2

Heat Treatment* and Austenite Grain Sizes of the Steels Investigated

Steel Type	Austenitizing Temperature (^{o}C)	γ-Grain Size (μm)
Plain C	1030	110
V	1045	100
Nb	1100	130
Mn-Nb	1100	120
Mo-Nb	1100	130
Nb-V	1100	120

*All samples were heat treated at 1000^{o}C for two hours and water quenched prior to austenitization.

$$\log(V)^{4/3}(C) = -\frac{10\,800}{T} + 7.06,$$

where (V), (N) and (C) are the concentrations in weight percent of V, N and C respectively, and T is the absolute temperature.

In this way, the equilibrium solubility temperature of VN was estimated to be 984°C and that of V_4C_3 to be 850°C. For this steel, T_{aus} was selected as 1045°C. This is approximately 60°C above the nitride solubility temperature, and according to Cordea (2), such an annealing temperature should lead to approximately the same austenite grain size as when plain carbon and Nb-steels are heated to 1030 and 1100°C, respectively.

The equilibrium solubility temperature for 0.035% Nb and 0.05% C was calculated as 1041°C from the following equation (2):

$$\log(Nb)(C) = -\frac{7510}{T} + 2.96 ,$$

where (Nb) and (C) are the concentrations of Nb and C in weight percent and T is the absolute temperature. If the carbon equivalent of 0.006% N is taken as 12/14 (N), the calculated solubility temperature becomes 1050°C.

All of the Nb-bearing steels were austenitized at 1100°C, which is 50 to 60°C higher than the calculated equilibrium solubility temperature. The effects of the other alloying and microalloying elements on this temperature are

considered extensively in the Discussion section below (Chapter 5).

Once the half-hour austenitizing treatment was complete, the system was cooled to the test temperature at an approximate rate of 1°C/sec. Each sample was tested as soon as the temperature was stable within 5°C of the required value. This took between 3 to 6 minutes from the start of the cooling operation.

3.3 Metallography

In order to determine the initial austenite grain sizes of the materials tested, a series of samples was heat treated, as described above, and ice-water quenched. The quenched specimens were mounted in resin and hand polished by standard methods down to 5 μm grit diamond polishing compound.

A number of etchants was tried, including nital and a hot (80°C), saturated aqueous picric acid solution containing a wetting agent (Teepol). The most successful one was the modified aqueous picric acid solution developed by the Republic Steel Co.*, which is comprised of the following ingredients:

---

*The author is indebted to E.L. Brown for this information from his thesis.

6 drops hydrogen peroxide

2 grams ammonia persulphate

2 grams wetting agent (Teepol, Calsoft)

per 100 ml saturated aqueous picric acid.

The mounted sample was immersed in this solution and swabbed regularly with cotton wool to remove the dark deposit formed due to the chemical attack.

The grain sizes were determined by the intercept method (ASTM #E112) using a circular 200 mm length grid. The grain sizes determined in this way are shown in Table 3.3.

3.4 Compression Testing

One of the aims of this investigation was to determine the dynamic precipitation kinetics of VN and Nb(CN), along with the effects of Mn, Mo and V on the precipitation kinetics of Nb(CN). In order to do so, a series of isothermal, constant true strain rate tests was carried out. The range of strain rates that could be obtained with the present equipment and specimen sizes was 3.2×10^{-5} to 0.74 s^{-1}. The maximum true strain that could be applied without risk of damaging the experimental apparatus was 0.8. Where higher strains or strain rates were required, torsion testing was carried out (see below).

3.4.1 Specimen Preparation

Compression samples were machined from the as-received plates with the compression axis along the rolling direction (Fig. 3.1). The sample sizes used were based on the load capacity of the Instron machine and load cell, as well as on the strain rate used. The sample height-to-diameter ratio was kept constant at 1.5. The sample heights used were 13.1 mm, 11.4 mm and 8.4 mm.

The end surfaces of the specimens were grooved to retain the glass lubricants used to minimize the friction between the ends of the sample and the test equipment. Thus, after testing, the samples were approximately cylindrical, with no apparent barrelling. The groove geometry was based on the work of Luton (58) and allows for the maximum retention of lubricants. The grooves were flat-bottomed, and wider at the base than are the ridges between them. They were made with a modified 2 teeth/mm thread chaser.

3.4.2 Compression Testing Equipment

High temperature compression tests were carried out on an Instron machine modified for constant true strain rate operation. The details of this apparatus are described in detail elsewhere (21,29,30). The compression tooling, illustrated in Fig. 3.2, was comprised of an upper anvil assembly connected to the moving crosshead, and a stationary lower anvil attached to the load cell. An Inconel muffle surrounded the specimen and tools, which allowed for testing in a vacuum of about 10^{-3} torr, or in an argon atmosphere.

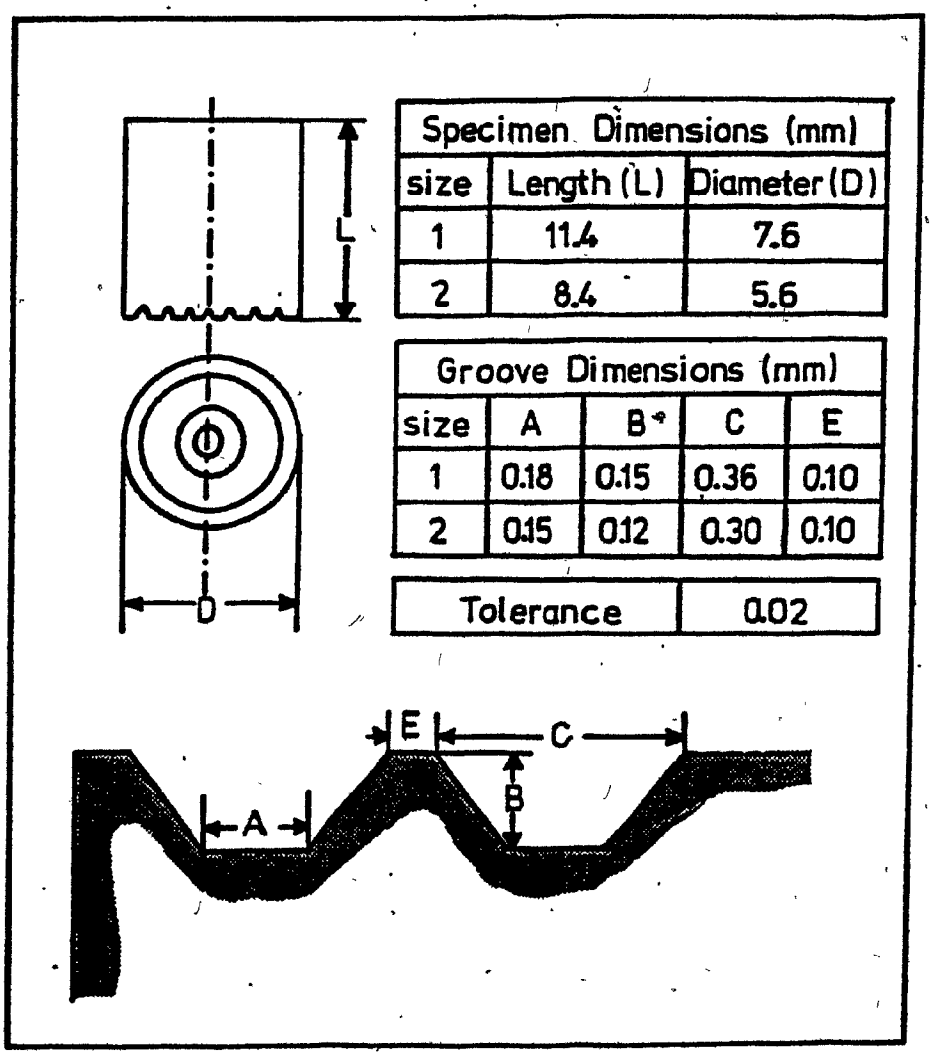

Specimen Dimensions (mm)		
size	Length (L)	Diameter (D)
1	11.4	7.6
2	8.4	5.6

Groove Dimensions (mm)				
size	A	B*	C	E
1	0.18	0.15	0.36	0.10
2	0.15	0.12	0.30	0.10

Tolerance	0.02

Figure 3.1 Compression test sample geometry and groove design.

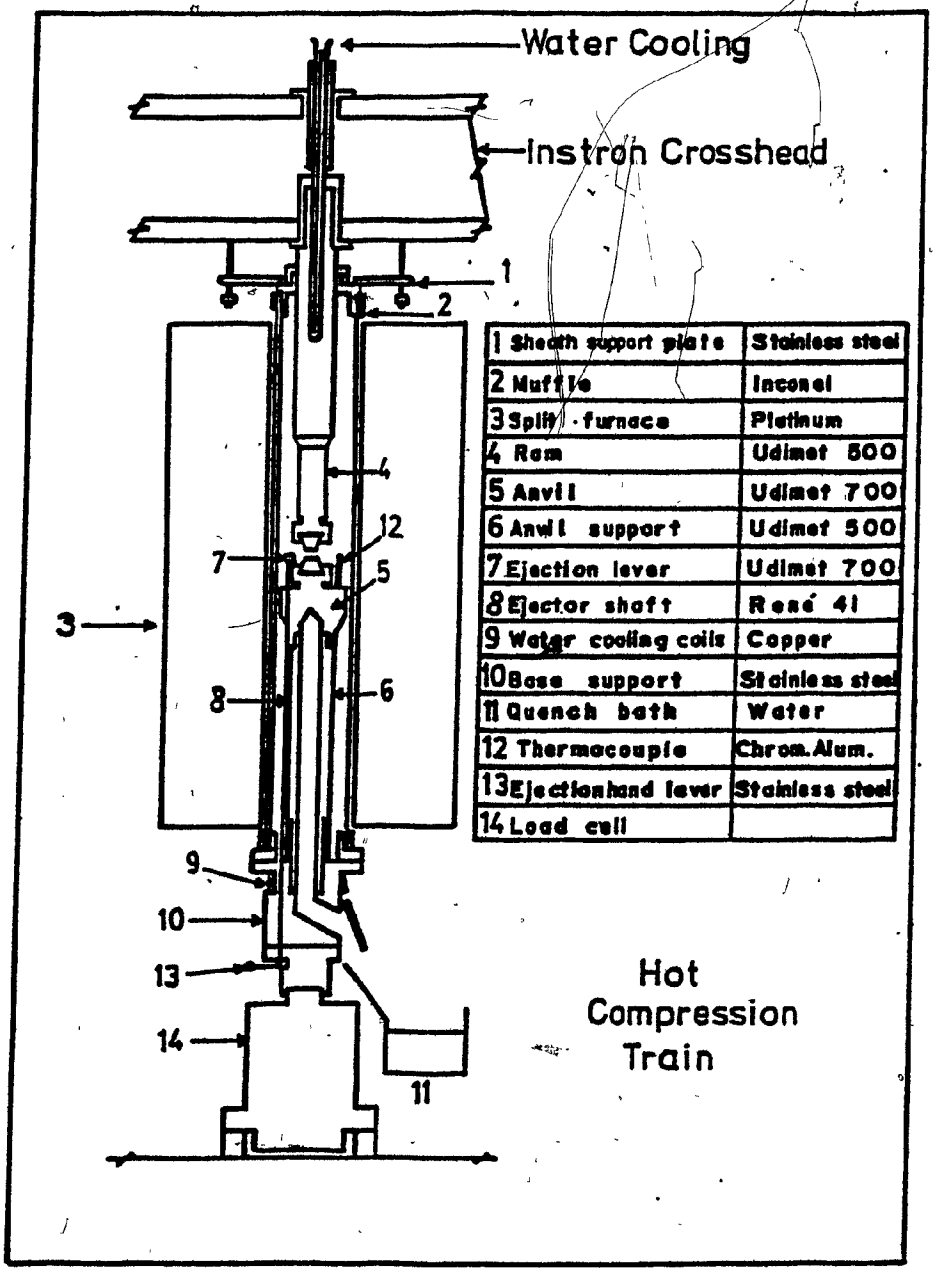

1 Sheath support plate	Stainless steel
2 Muffle	Inconel
3 Split - furnace	Platinum
4 Ram	Udimet 500
5 Anvil	Udimet 700
6 Anvil support	Udimet 500
7 Ejection lever	Udimet 700
8 Ejector shaft	René 41
9 Water cooling coils	Copper
10 Base support	Stainless steel
11 Quench bath	Water
12 Thermocouple	Chrom.Alum.
13 Ejectionhand lever	Stainless steel
14 Load cell	

Figure 3.2 Schematic diagram of hot compression train (after Weiss (78)).

SiN inserts were placed at the ends of the anvils and were held in position by superalloy nuts. The smoothly ground SiN inserts formed a good, minimally deforming compression surface for the samples.

The tests were performed with the aid of a Honeywell 4020 process control computer. The load measurements were taken from the load cell and the displacement measurements from a Linear Variable Displacement Transducer (LVDT). The LVDT rod was attached to the moving crosshead and the coil to the Instron frame. These data were stored by the computer on a scratch file. True stress/true strain plots were obtained immediately after each test, after which the data were transferred on tape for permanent storage, so that they could be recalled at will at a later date.

The high temperatures required for the austenitizing treatment were obtained by means of a Satec split three-zone platinum resistance furnace with a capacity of 14.5 amperes per zone. This furnace was connected to a Leeds & Northrup Electromax-III, series 6435 controller.

3.5 Torsion Testing

The range of strain rates and strains attainable with the compression testing equipment is limited to maxima of 0.74 s^{-1} and 0.8, respectively. Particularly at the lowest temperature (875°C), dynamic recrystallization does not start below a strain of 0.75-0.8 at the higher strain rates. Thus it is impossible to establish the onset of dynamic recrystal-

lization by means of compression testing under these experimental conditions. With the purpose of overcoming these difficulties, some torsion tests were performed. The maximum equivalent strain rate that could be reached was 3 s^{-1}. There was no practical limit (except for fracture) to the strain that could be attained, so that the peak strain could always be determined in this way.

3.5.1 Specimen Preparation

The torsion specimens were machined from the as-received plates with their axes along the rolling direction (Fig. 3.3). The samples were cylindrical, with a gauge length of 25.4 mm and a diameter of 6.35 mm. One end of the sample was threaded for insertion in the grip at the torque cell (fixed) end of the apparatus. The end of the sample inserted in the rotating grip was kept flat to allow for thermal expansion and contraction during austenitization and cooling, as well as for length changes due to anisotropy or elastic interaction effects during testing.

3.5.2 Torsion Testing Equipment

The torsion tests were performed on a closed loop hydraulic torsion machine of the MTS type. The details of the apparatus, shown schematically in Fig. 3.4, have been described elsewhere (59). This machine was interfaced with a PDP 11/04 minicomputer for the purpose of running the test and to enable data acquisition, as described by Canova *et al.* (62). The computer

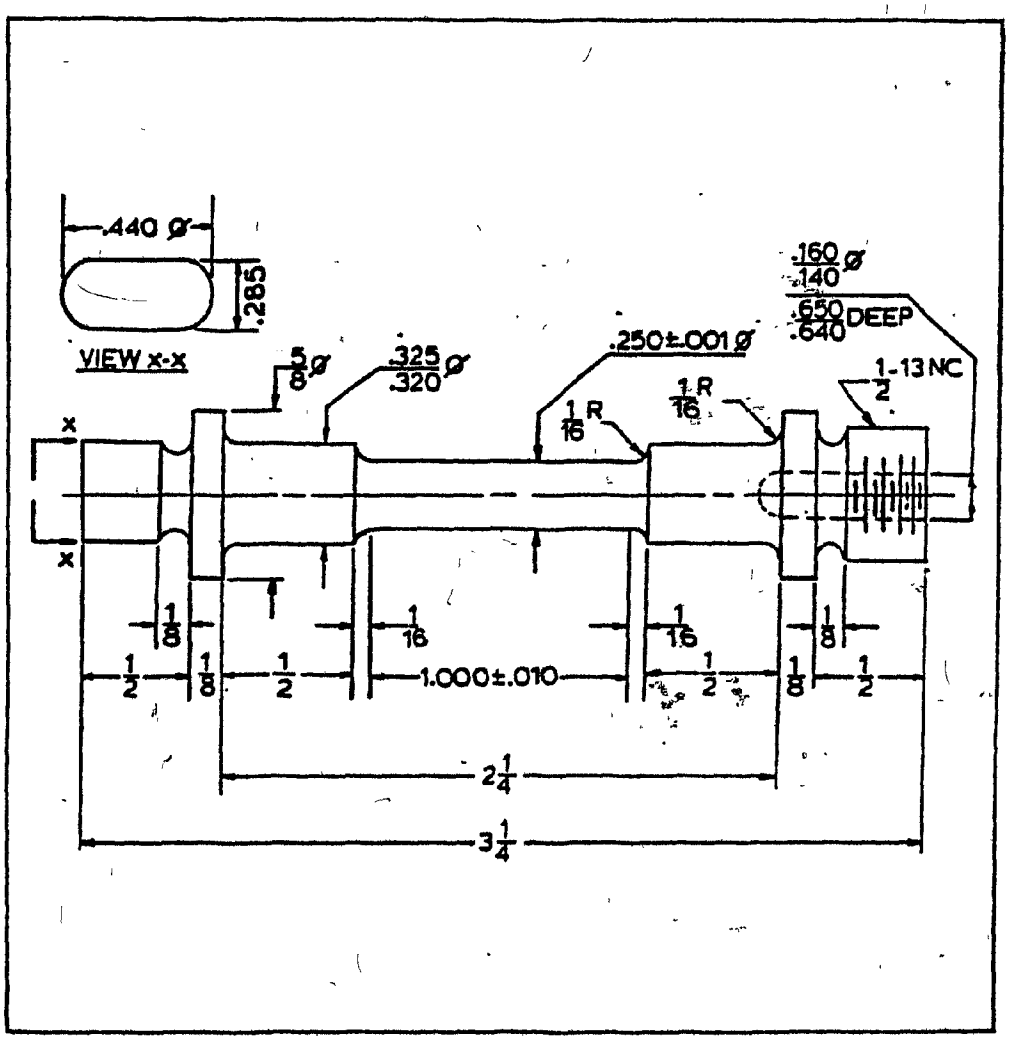

Figure 3.3 Torsion test sample geometry.

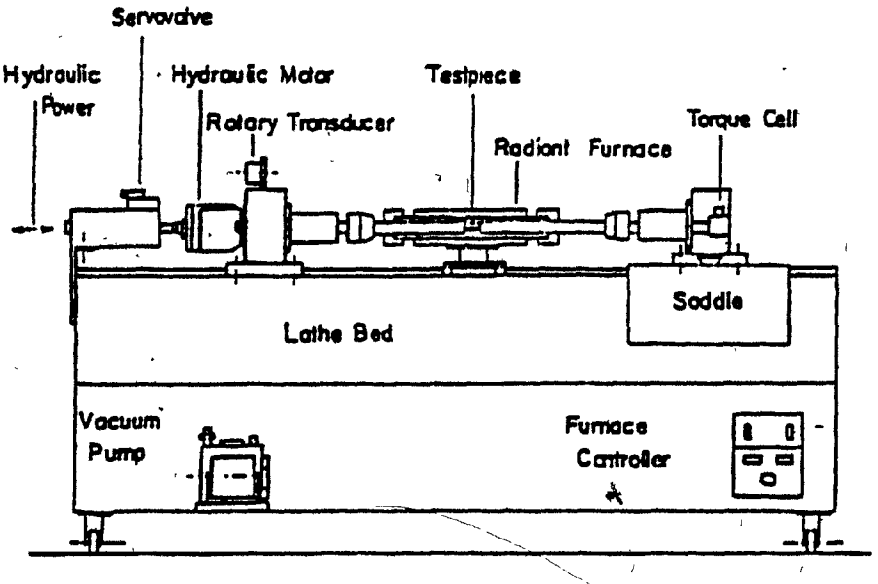

Figure 3.4 Schematic diagram of the hot torsion train (after Fulop et al. (59)).

generated the desired input signal to the servo controller by means of real-time programming (see Appendix A). The digital input signal from the hardware segment generator was converted into analog form before being fed to the two controllers.

The displacement, i.e. the angle of twist of the sample, was measured through a transducer on the rotating grip. These measurements were converted to equivalent strains using the relations given in Section 4.3. The torques were monitored from the torque cell at the end of the fixed grip. The equivalent stress, σ_{eq}, was determined from the torque as described in Section 4.3.

The torque vs. time, torque vs. equivalent strain and log (torque) vs. log (equivalent strain) plots were displayed immediately after each test on a Tektronix 4010-1 video terminal interfaced with the computer. A copy of each plot was obtained from the Tektronix 4631 hard copy unit, also connected to the terminal.

The samples were heated in a Research Inc. dual elliptical radiant heater. The furnace was water cooled. A Thermac 6000 series controller was used to control this furnace. To reduce oxidation, a positive pressure of argon was maintained inside the furnace throughout each experiment.

CHAPTER 4

EXPERIMENTAL RESULTS

The aims of this research were the following:

1) To determine the PTT curves for the precipitation of Nb(CN) and VN under dynamic conditions.
2) To determine the effects of Mn, Mo and V addition on the dynamic precipitation kinetics of Nb(CN).
3) To determine the contributions of these elements to the high temperature yield stress.
4) To prepare a dynamic recrystallization-time-temperature (RTT) curve for a selected strain rate condition for comparison with static RTT curves.

4.1 Experimental Conditions

Six steels were tested; a reference plain carbon and five HSLA steels containing V, Nb, high Mn-Nb, Mo-Nb and Nb-V. To obtain data for objectives 1 to 3 above, compression tests were conducted isothermally at 875, 900 and 925°C. These tests were carried out in the strain rate range 3.2×10^{-5} to $0.74\ s^{-1}$.

In order to produce the RTT curves, a series of tests was performed at a strain rate of $3.7 \times 10^{-2} s^{-1}$ at 975, 1025 and 1075°C in addition to the above three temperatures. These tests also provided yield stress information at these temperatures.

To attain high peak strains, torsion tests were carried out at strain rates from 2×10^{-2} to 3 s^{-1} on the Nb-bearing steels only. Most of these experiments were conducted at 875°C. However, a few were also performed at 925°C.

4.2 Flow Curves in Compression

Typical sets of compression flow curves are presented in Figures 4.1 through 4.3. They include the whole range of strain rates and temperatures employed for each type of steel. These curves are given as plotted by the computer. The shape of these curves is typical of materials that recrystallize dynamically. After the macroscopic yield is attained, the material work hardens. As the rate of recovery increases with strain (stress), the rate of work hardening decreases with strain. Finally, dynamic recrystallization is initiated just before the peak strain is attained, and the subsequent drop in peak stress is due to the progress of dynamic recrystallization. This softening process involves nucleation and growth, and therefore requires time. The higher the strain rate, the shorter is the time required to reach a given strain; thus higher peak strains are necessary to initiate recrystallization at higher strain rates. (Note that the time, t, to reach a selected strain, ε, at a given constant strain rate, $\dot{\varepsilon}$, is $t = \varepsilon/\dot{\varepsilon}$.)

In Fig. 4.1(a) are depicted the flow curves observed for the plain carbon steel. As the strain rate is increased

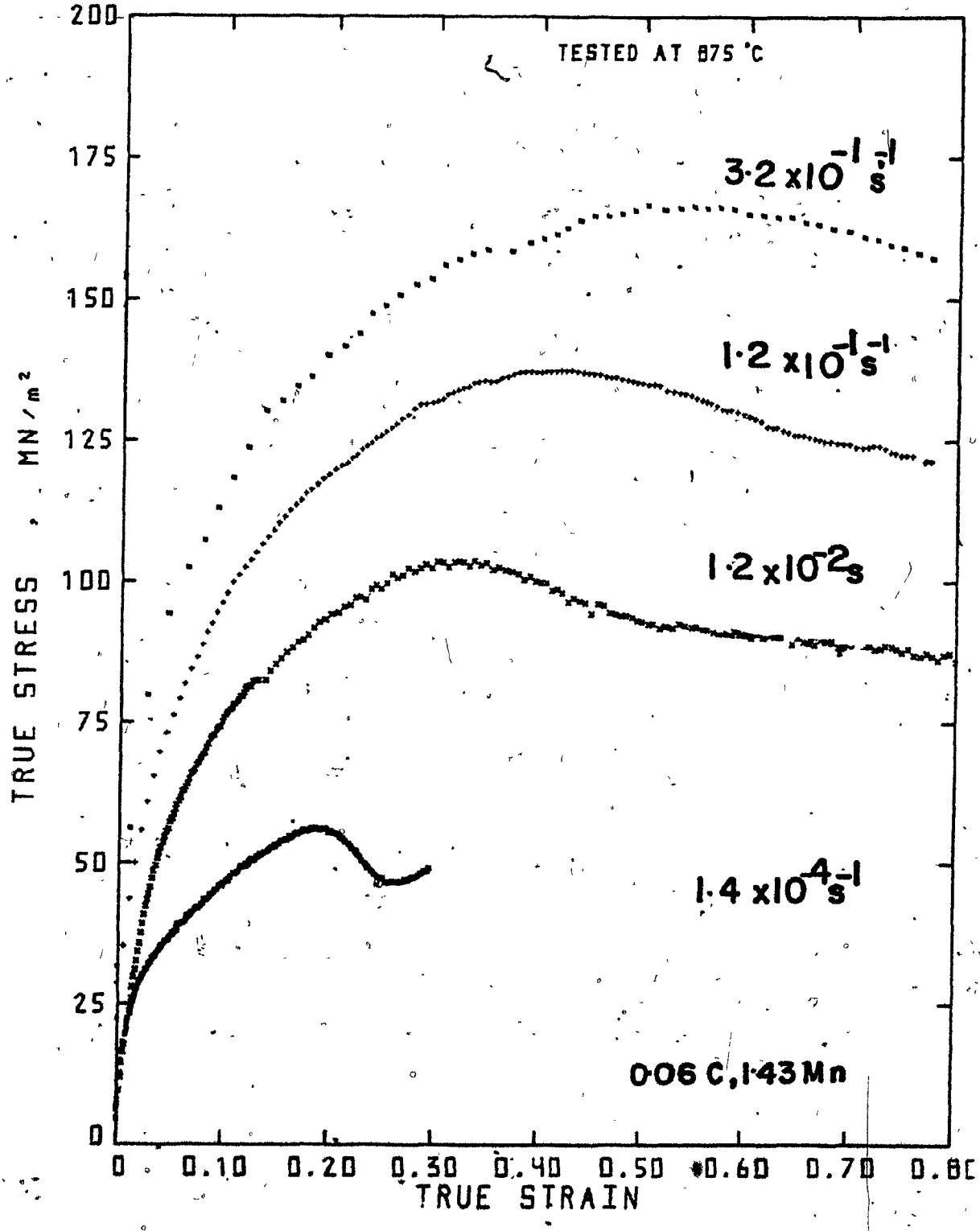

Figure 4.1 (a) Flow curves for the plain C steel at 875°C over the range of strain rates investigated.

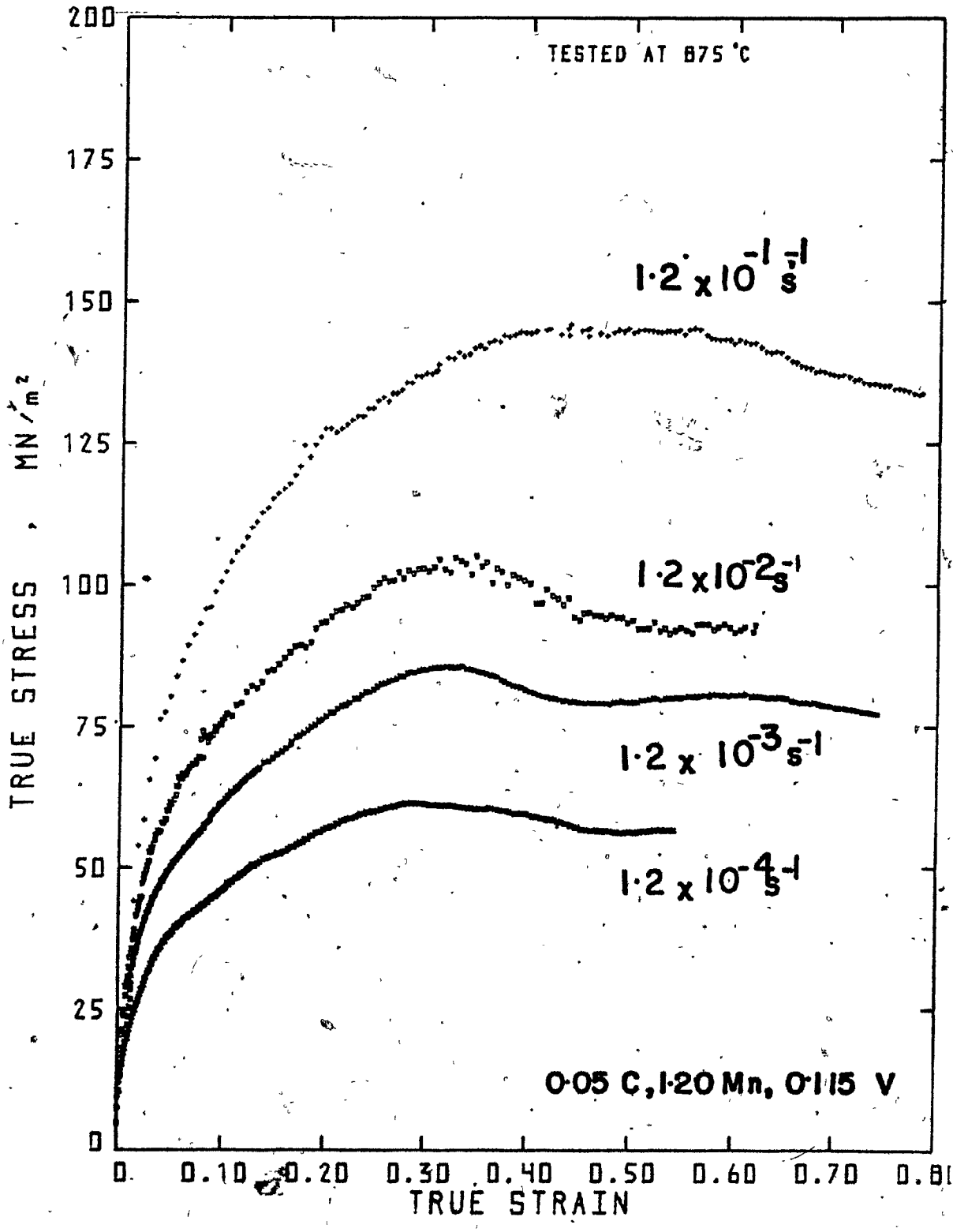

Figure 4.1 (b) Flow curves for the 0.115% V steel at 875°C over the range of strain rates investigated.

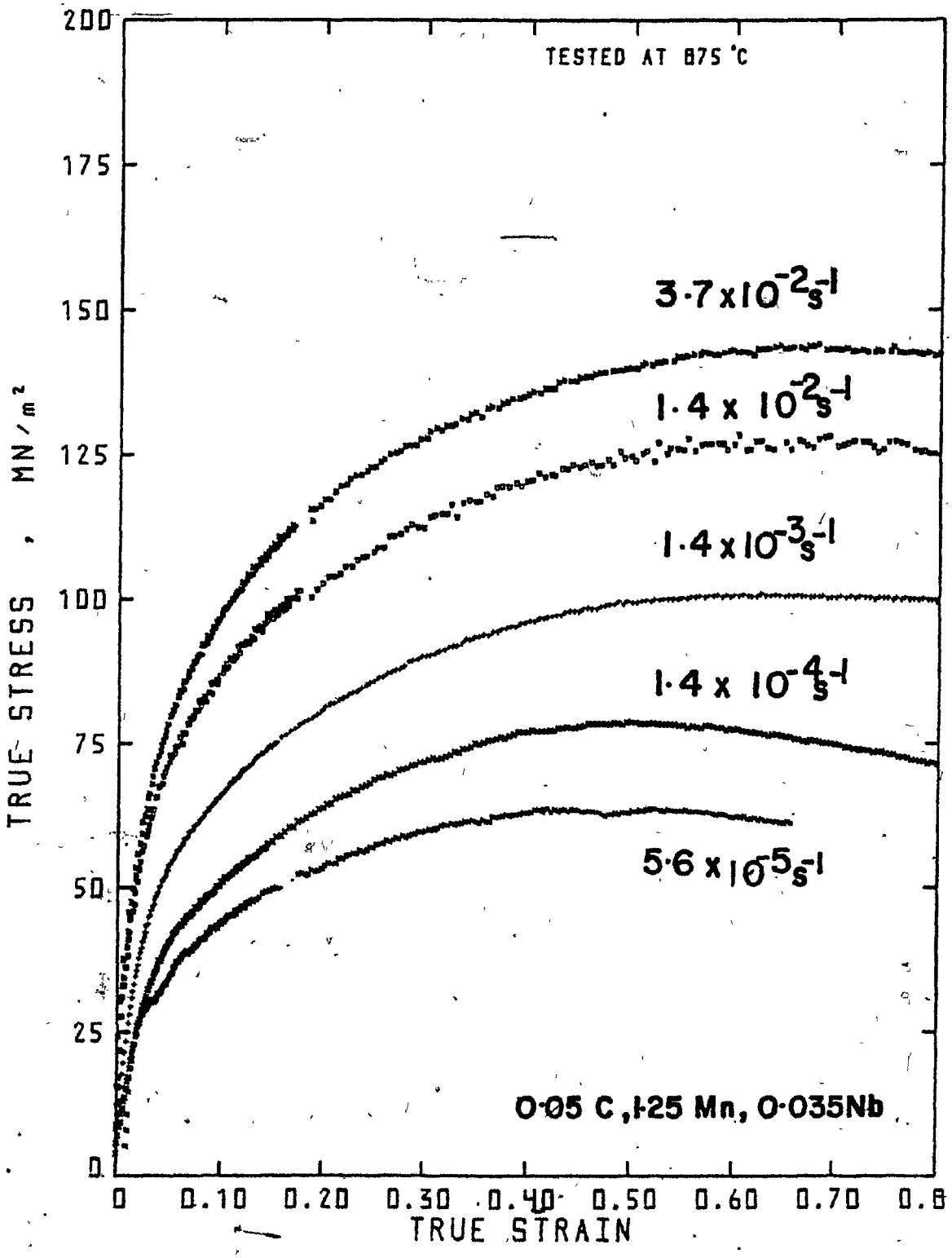

Figure 4.1 (c) Flow curves for the 1.25% Mn, 0.035% Nb steel at 875°C over the range of strain rates investigated.

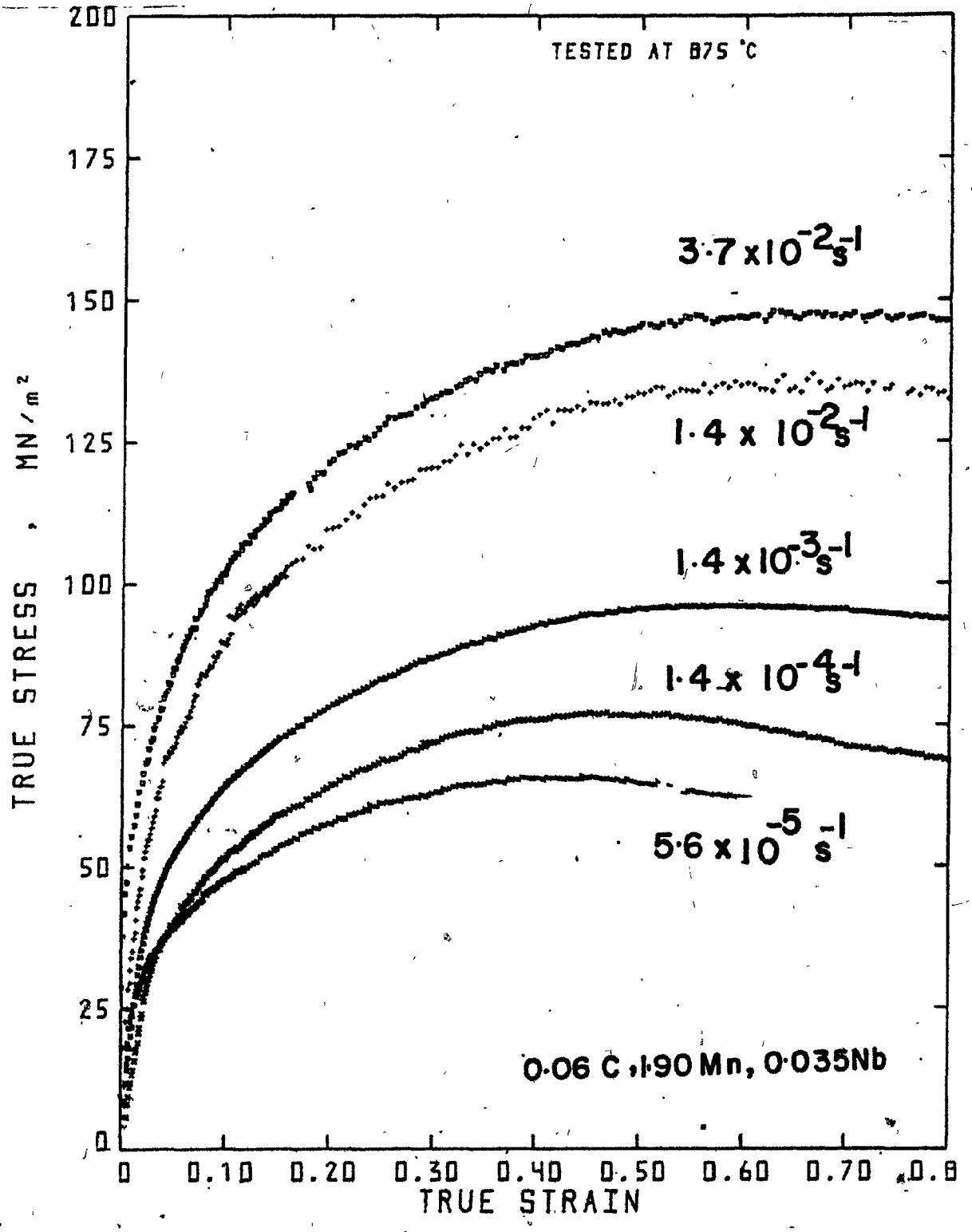

Figure 4.1 (d) Flow curves for the 1.90% Mn, 0.035% Nb steel at 875°C over the range of strain rates investigated.

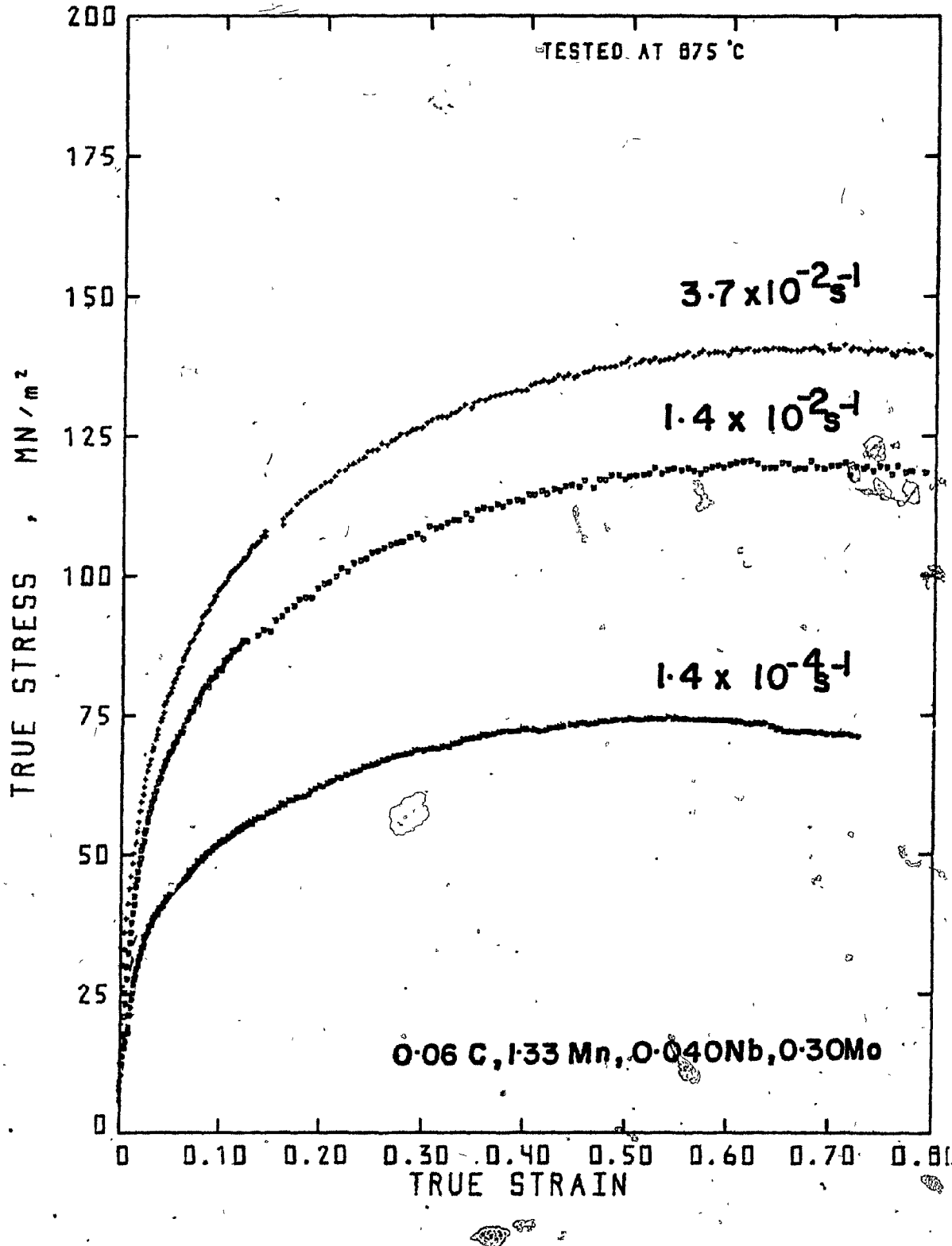

Figure 4.1 (e) Flow curves for the 0.30% Mo, 0.035% Nb steel at 875°C over the range of strain rates investigated.

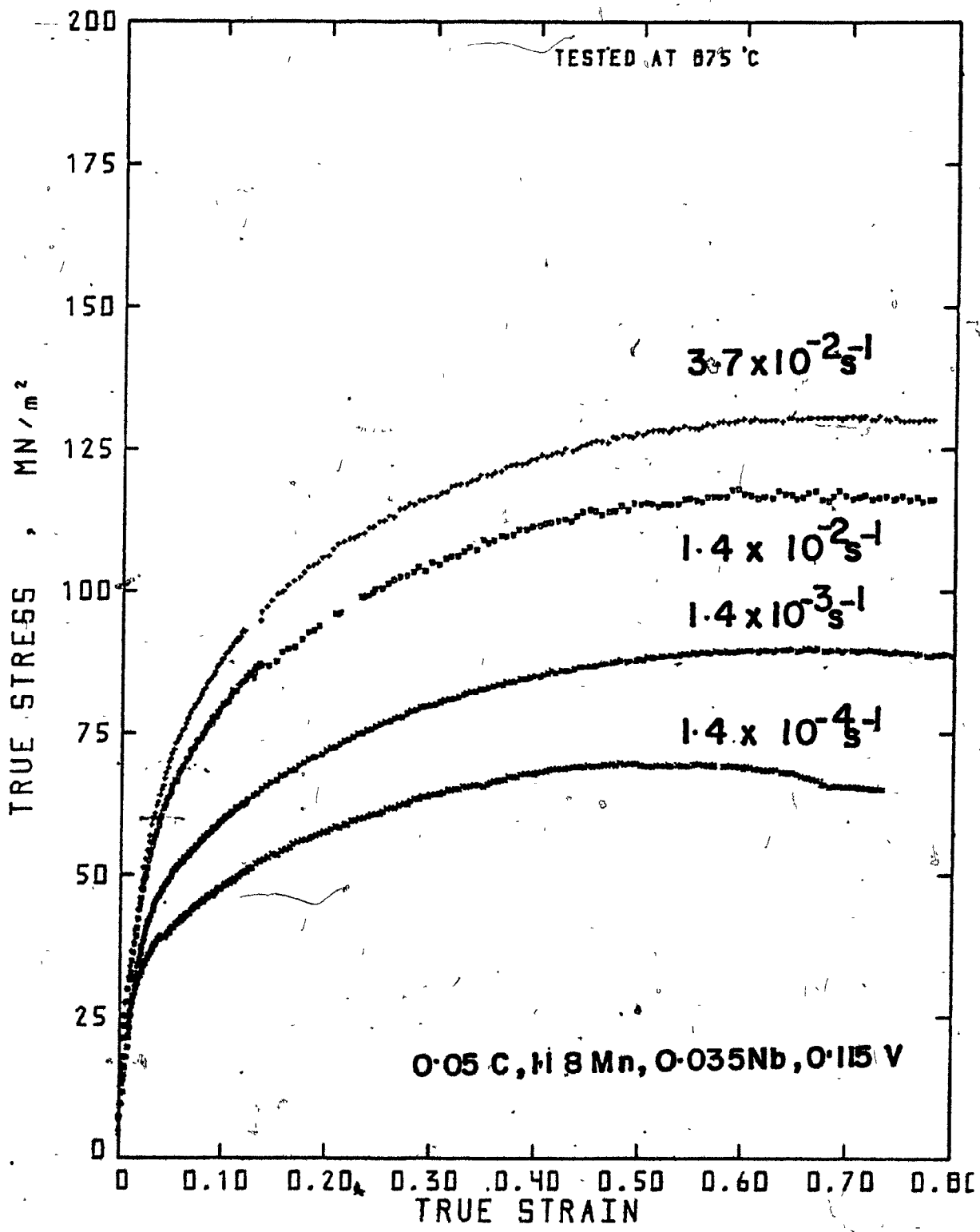

Figure 4.1 (f) Flow curves for the 0.115% V, 0.035% Nb steel at 875°C over the range of strain rates investigated.

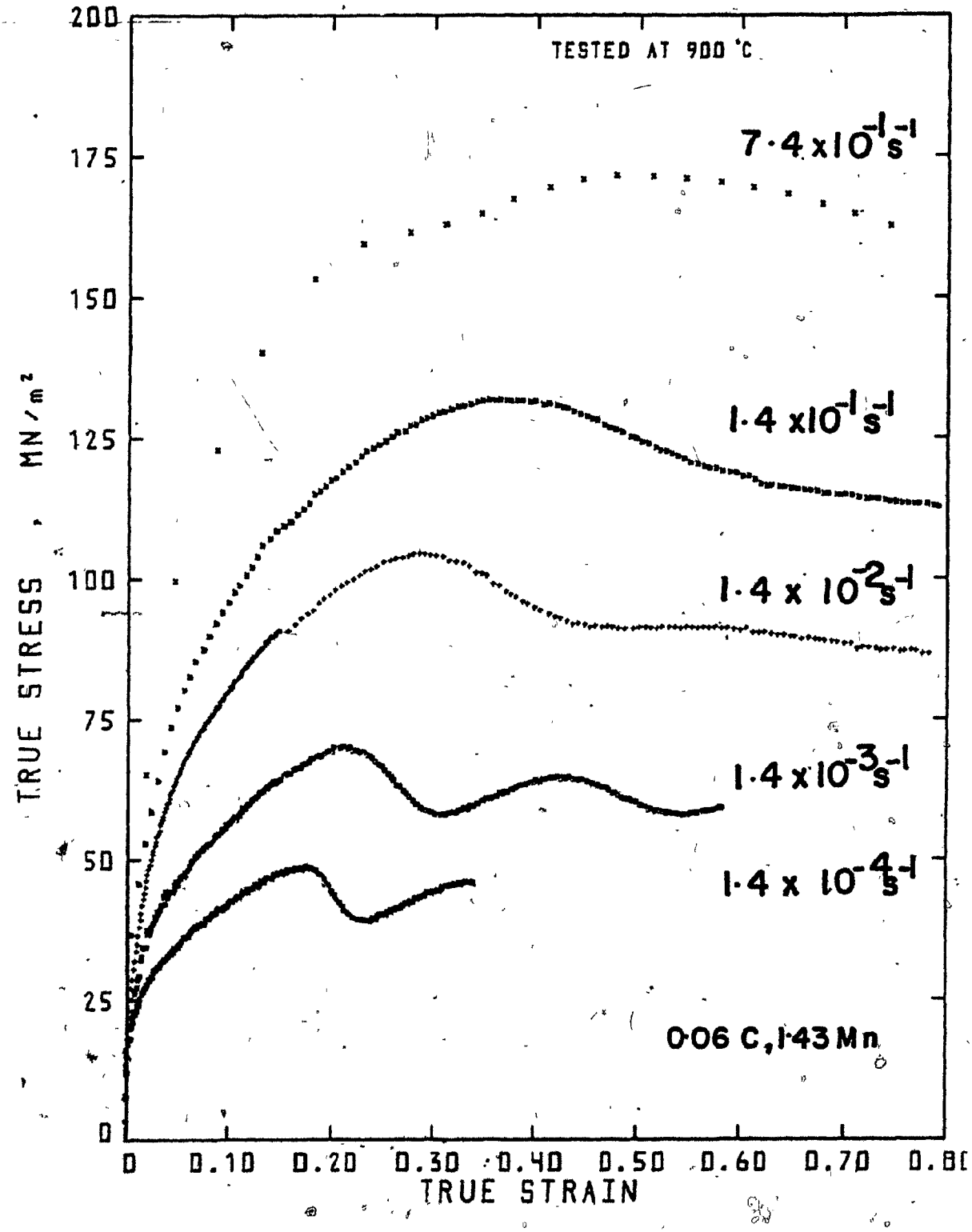

Figure 4.2 (a) Flow curves for the plain C steel at 900°C over the range of strain rates investigated.

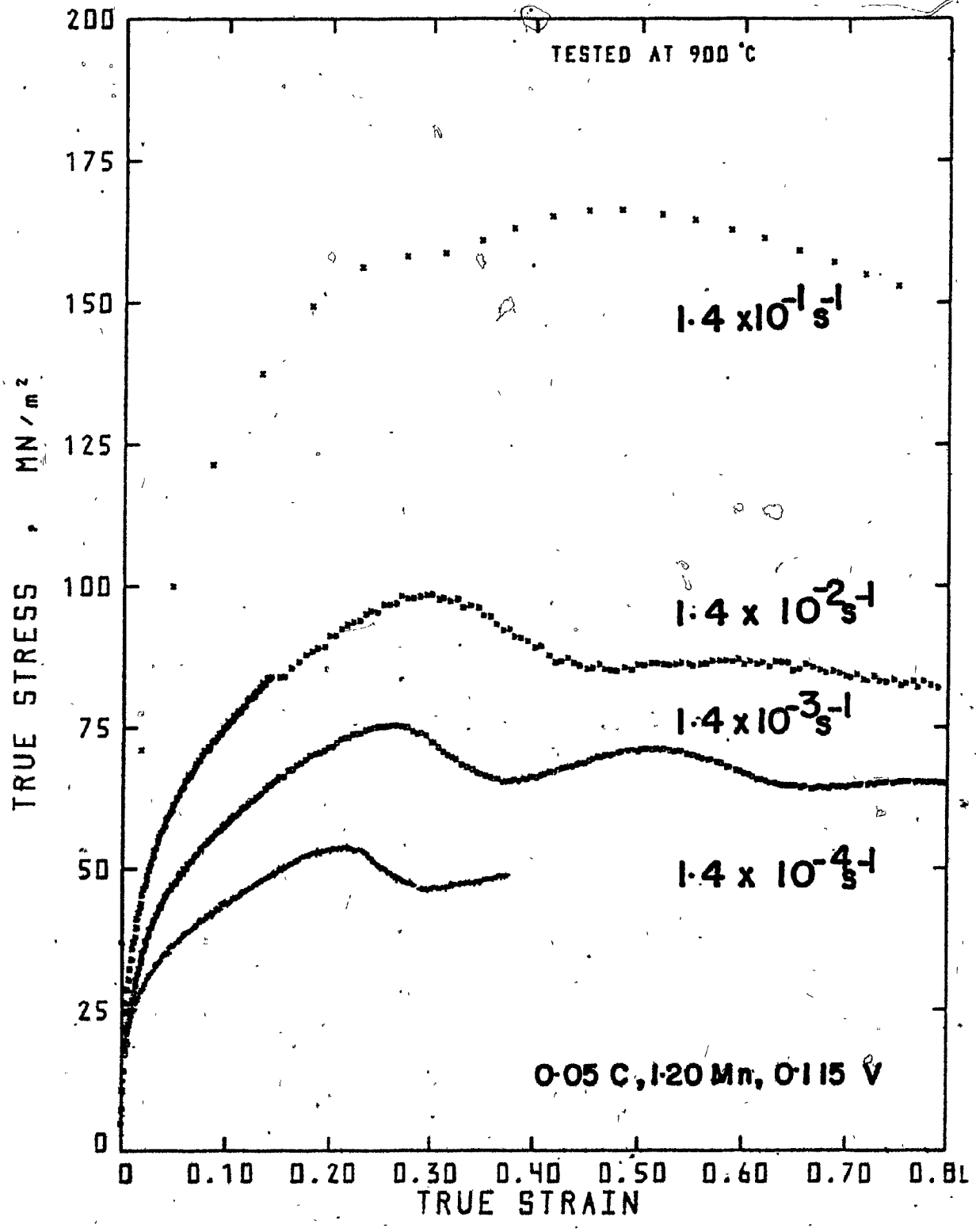

Figure 4.2 (b) Flow curves for the 0.115% V steel at 900°C over the range of strain rates investigated.

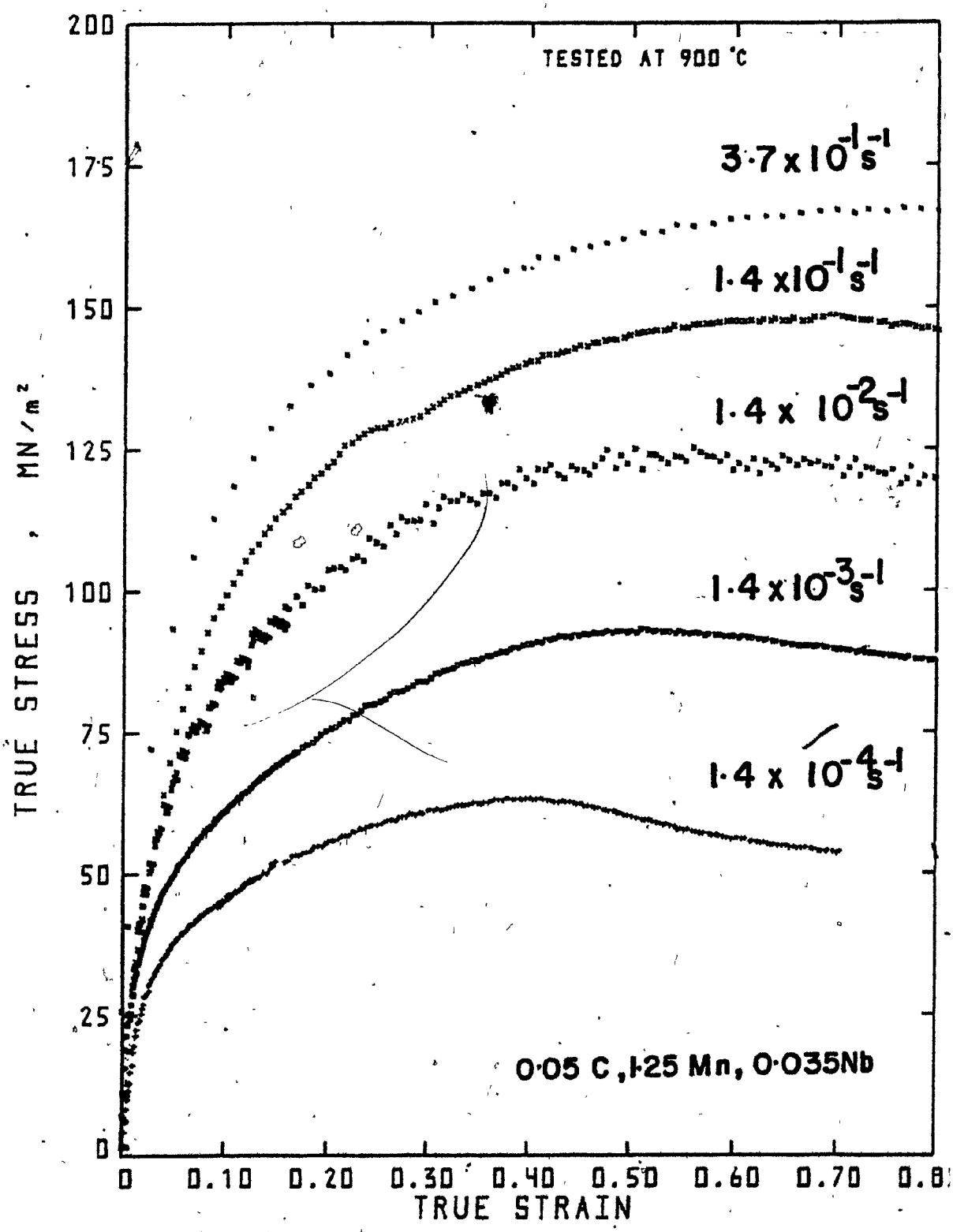

Figure 4.2 (c) Flow curves for the 1.25% Mn, 0.035% Nb steel at 900°C over the range of strain rates investigated.

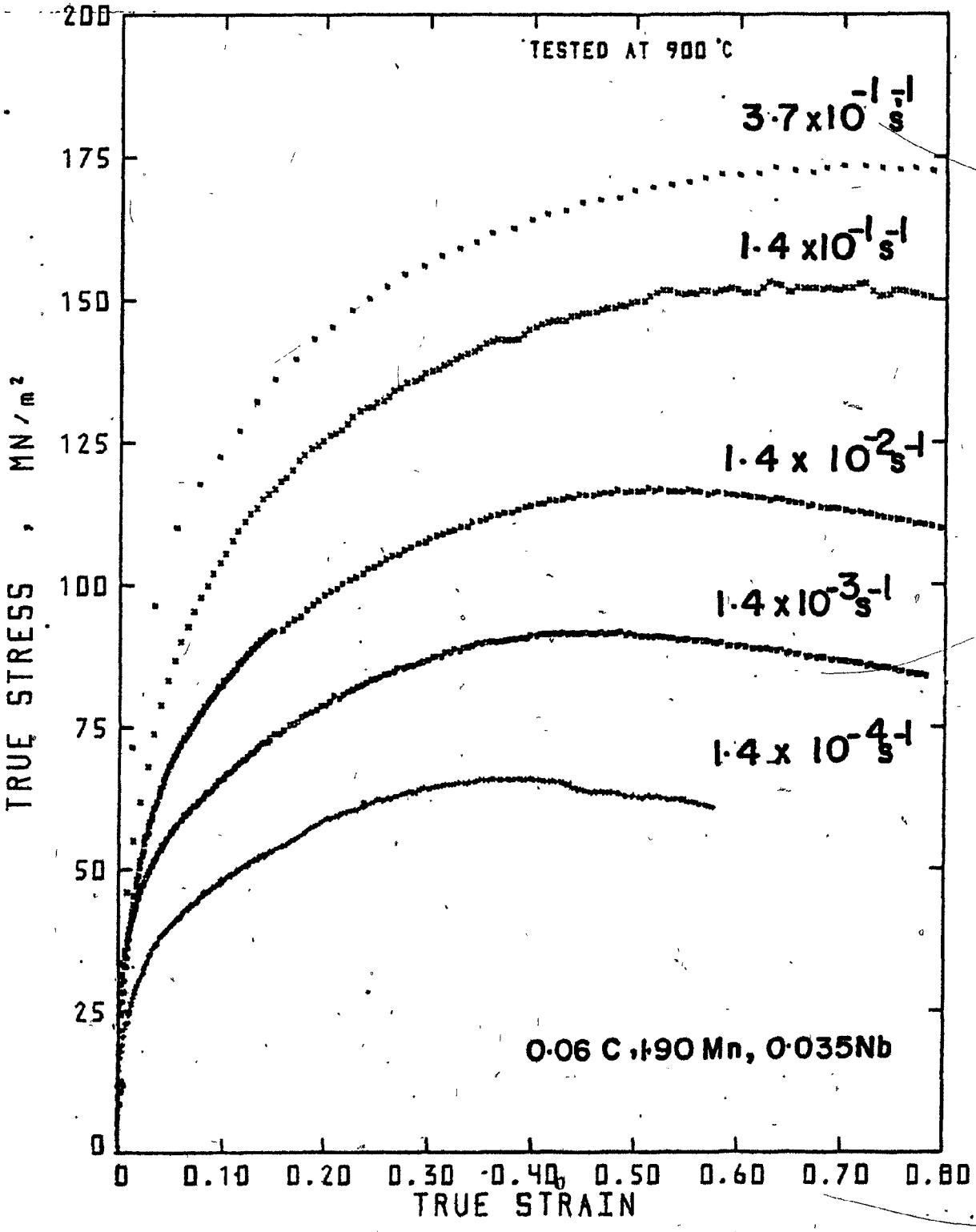

Figure 4.2 (d) Flow curves for the 1.90% Mn, 0.035% Nb steel at 900°C over the range of strain rates investigated.

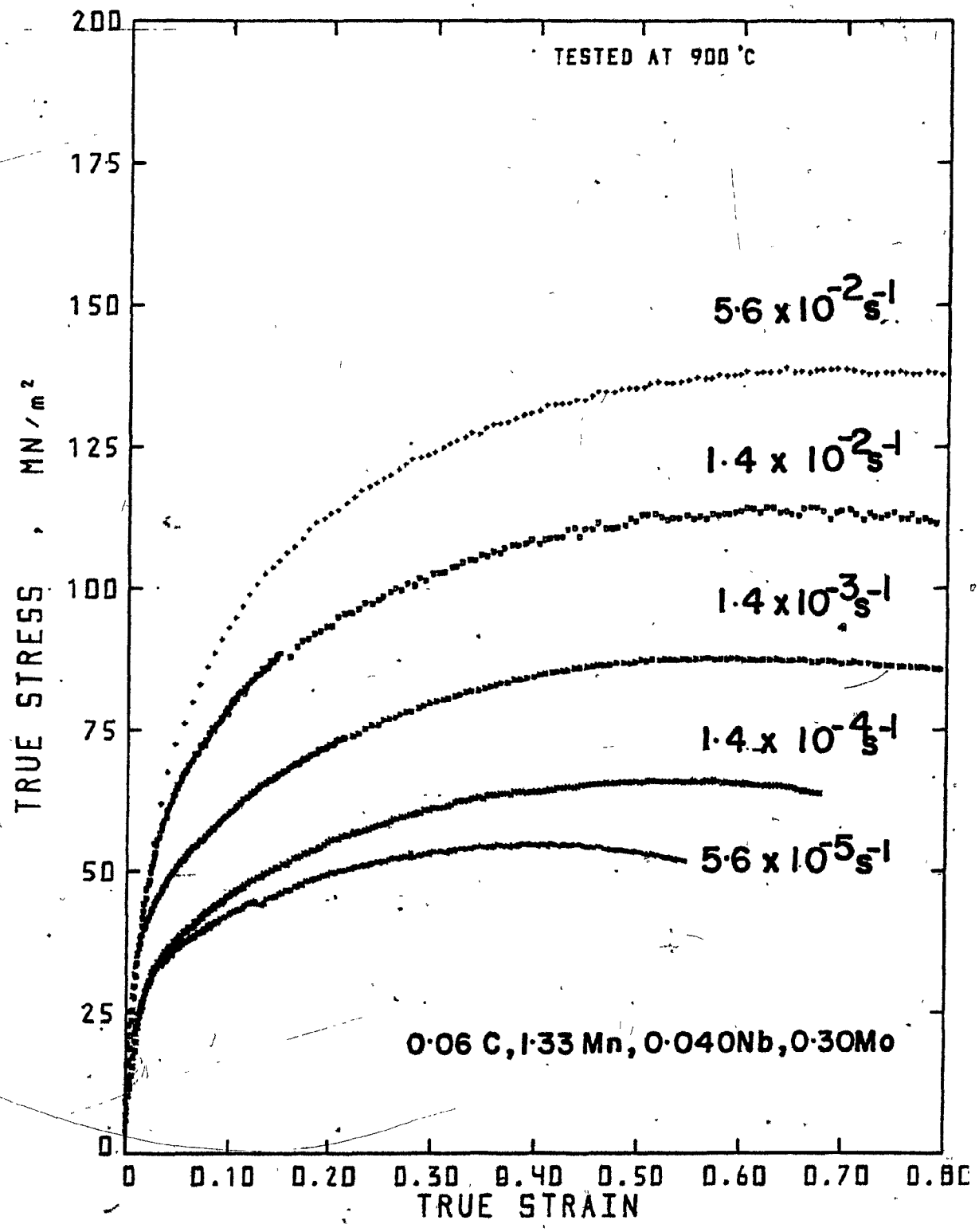

Figure 4.2 (e) Flow curves for the 0.30% Mo, 0.035% Nb steel at 900°C over the range of strain rates investigated.

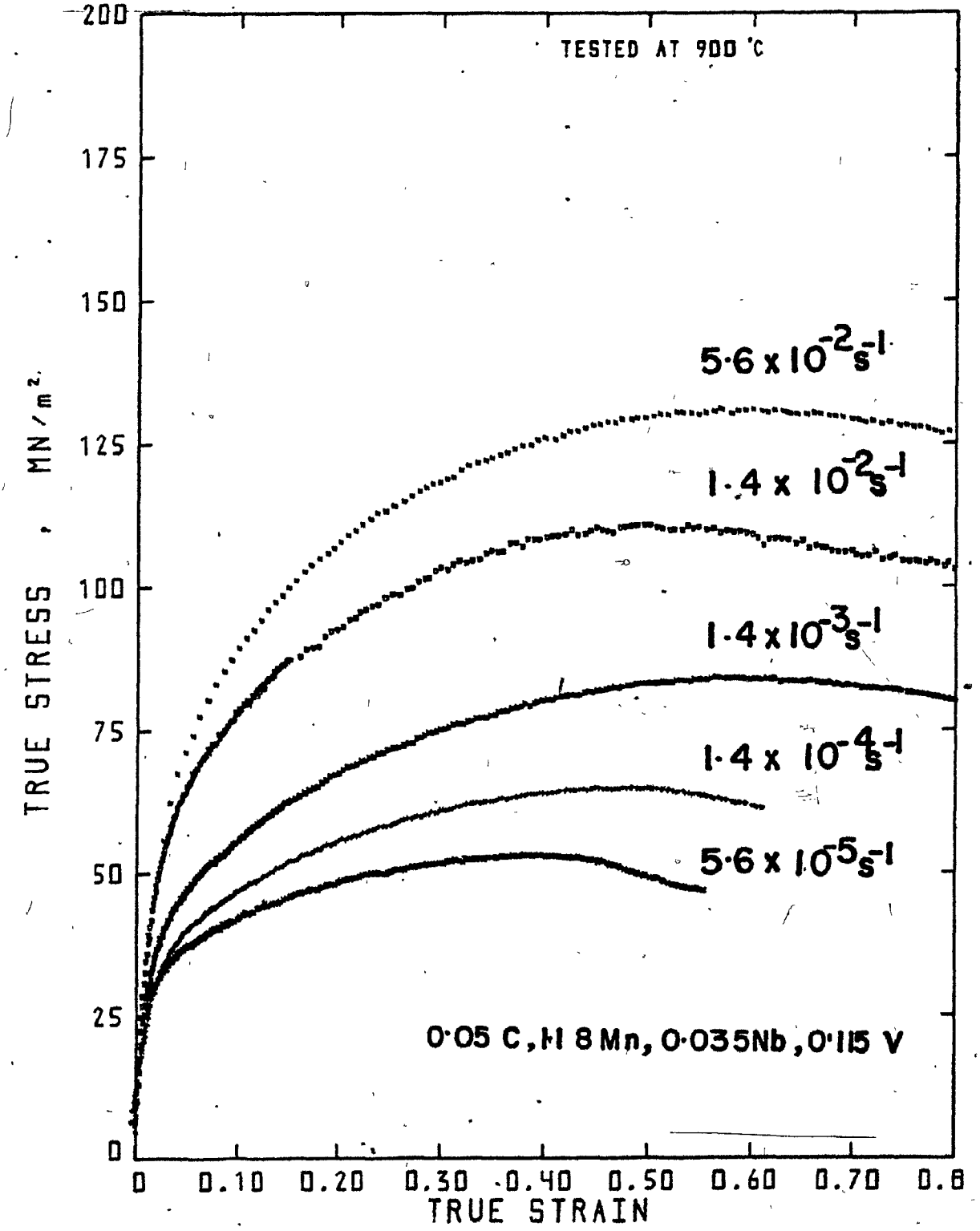

Figure 4.2 (f) Flow curves for the 0.115% V, 0.035% Nb steel at 900°C over the range of strain rates investigated.

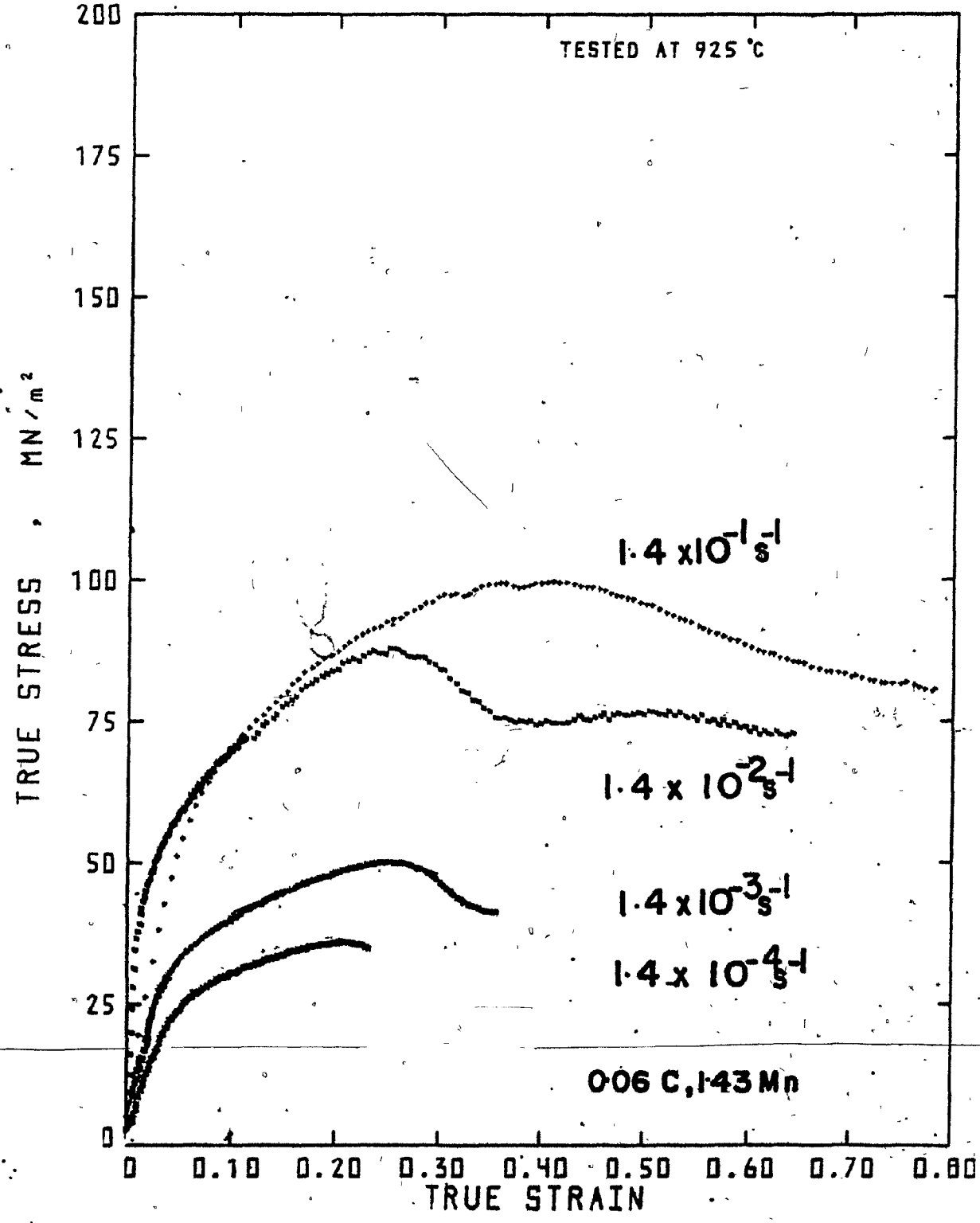

Figure 4.3 (a) Flow curves for the plain C steel at 925°C over the range of strain rates investigated.

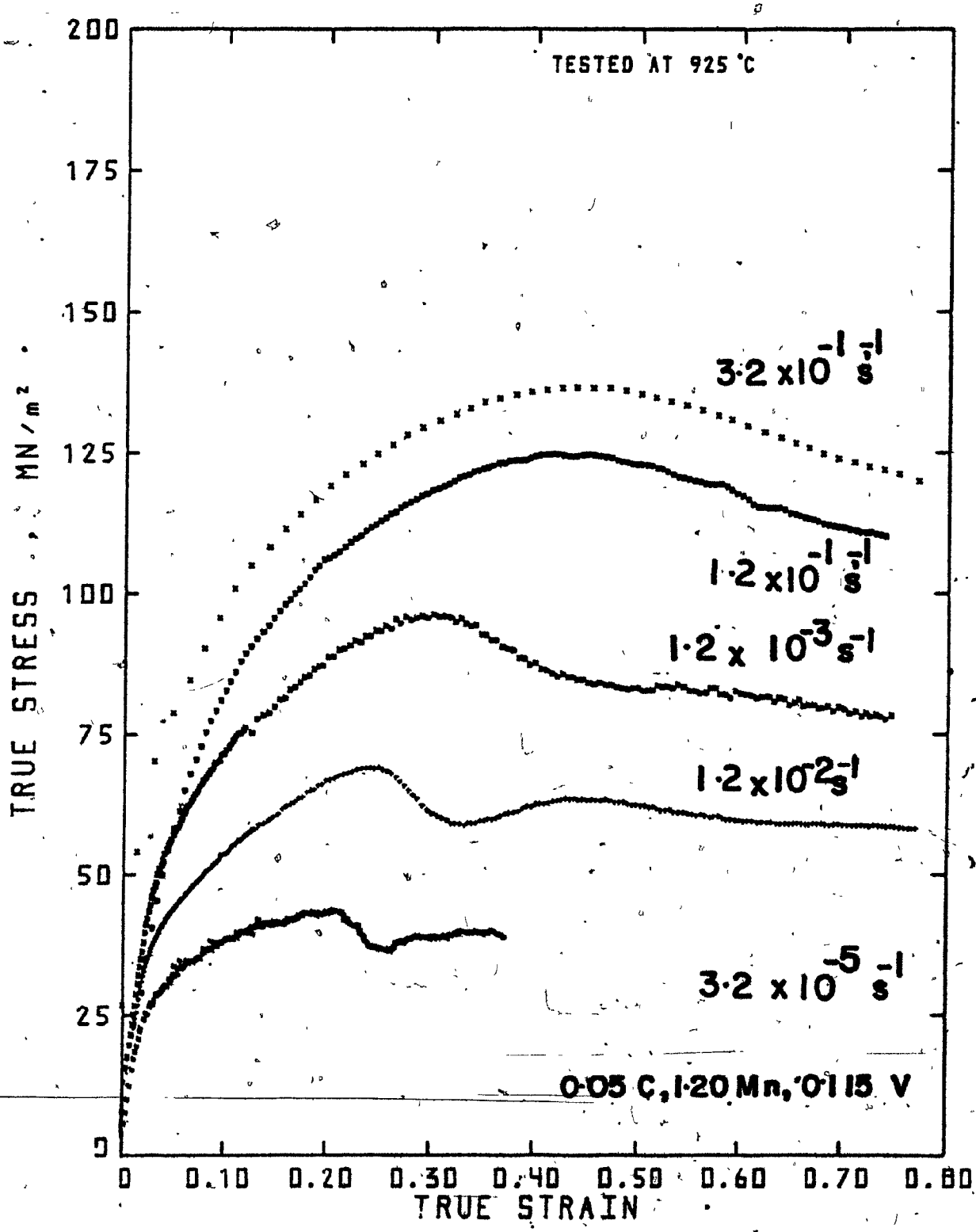

Figure 4.3 (b) Flow curves for the 0.115% V steel at 925°C over the range of strain rates investigated.

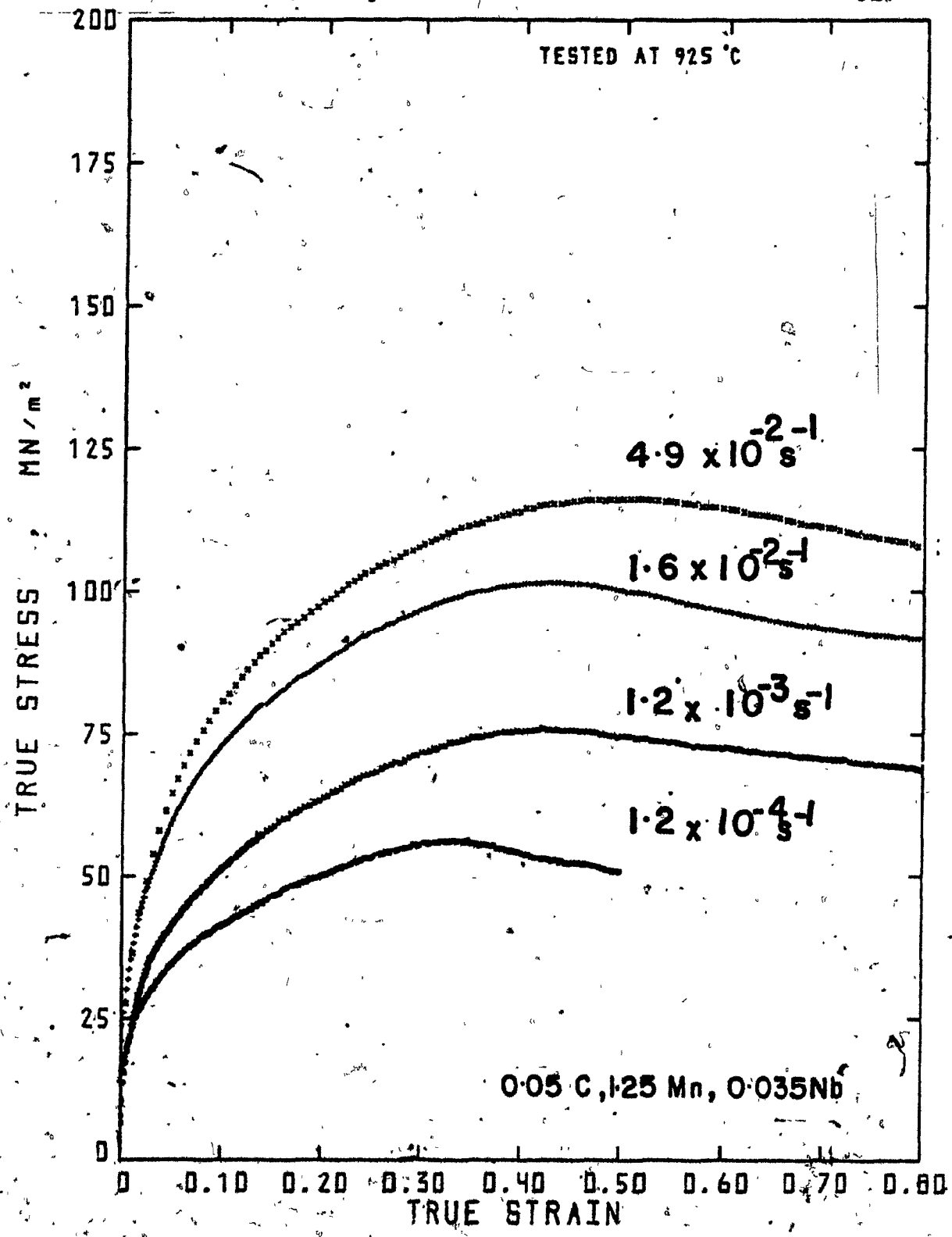

Figure 4.3 (a) Flow curves for the 1.25% Mn, 0.035% Nb steel at 925°C over the range of strain rates investigated.

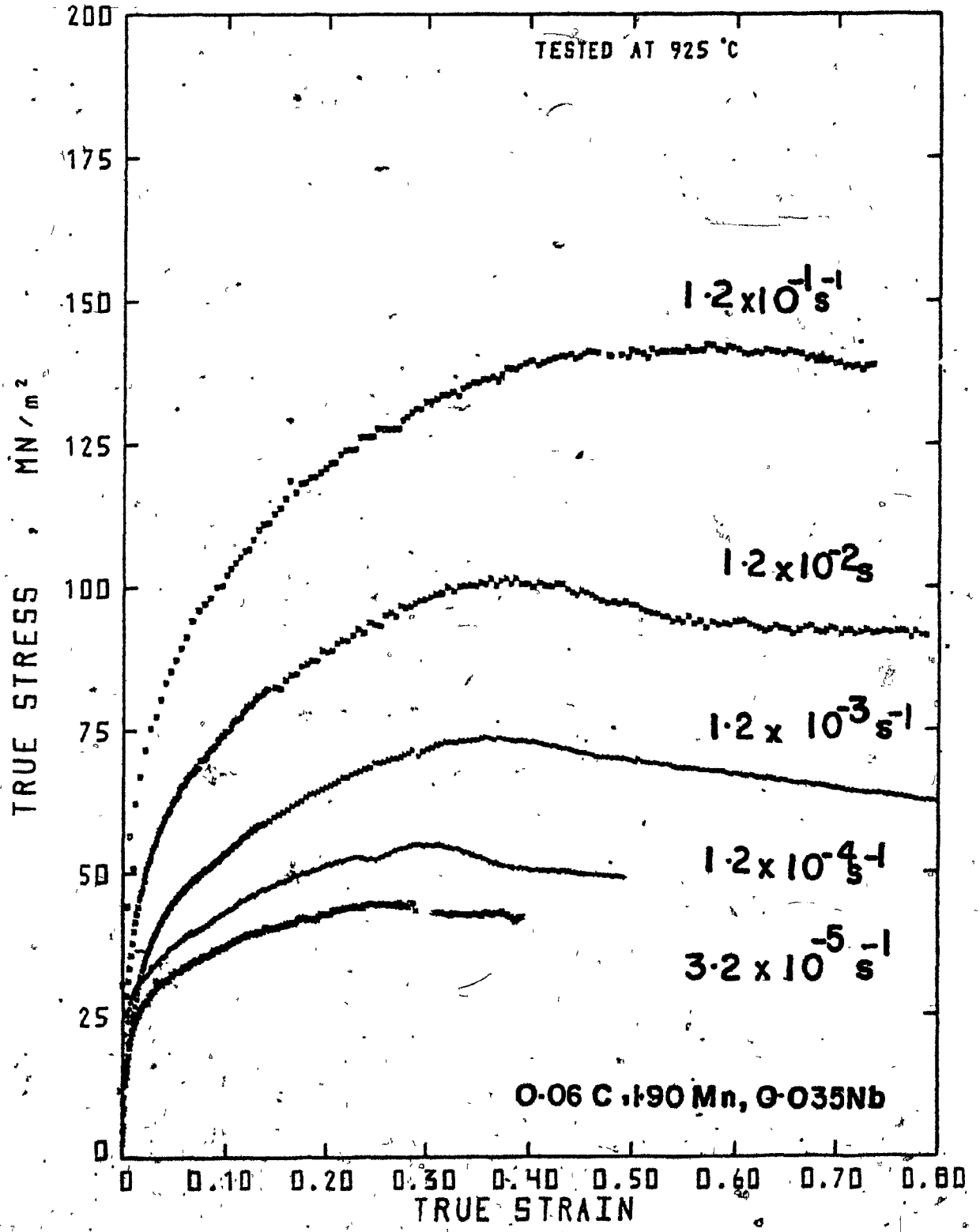

Figure 4.3 (d) Flow curves for the 1.90% Mn, 0.035% Nb steel at 925°C over the range of strain rates investigated.

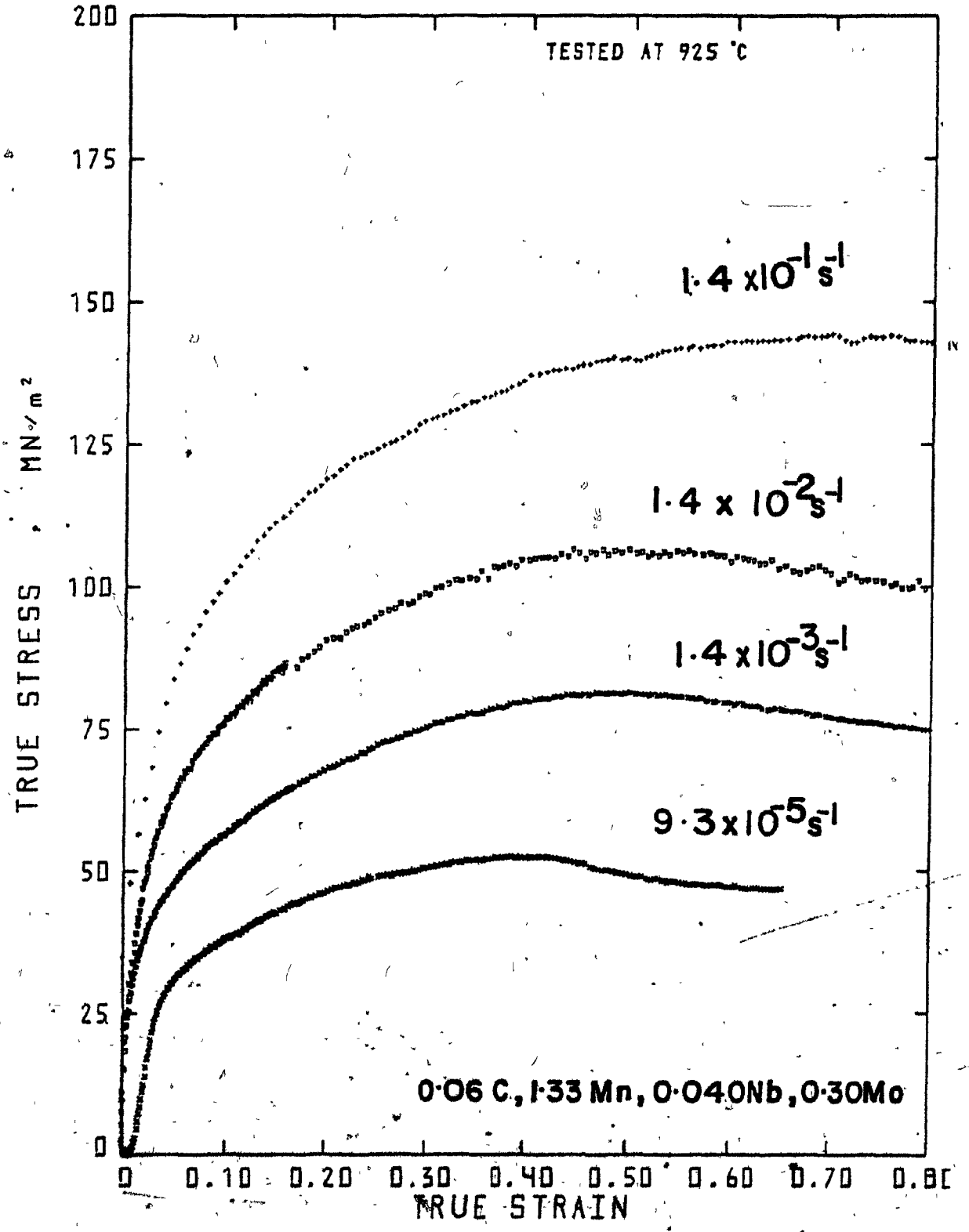

Figure 4.3 (e) Flow curves for the 0.30% Mo, 0.035% Nb steel at 925°C over the range of strain rates investigated.

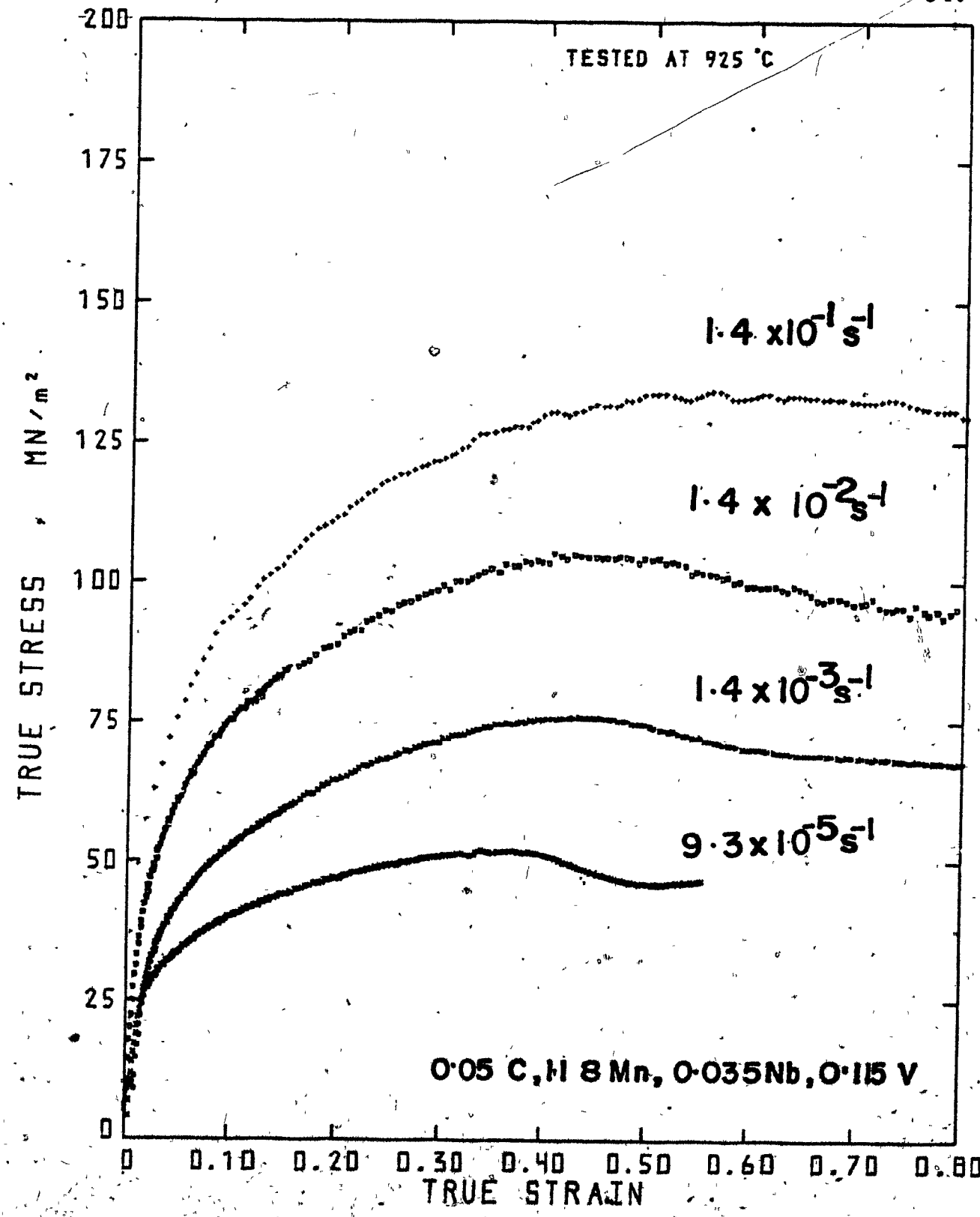

Figure 4.3 (f) Flow curves for the 0.11$ V, 0.035$ Nb steel at 925°C over the range of strain rates investigated.

by three orders of magnitude from 1.4×10^{-4} to $1.2 \times 10^{-1} s^{-1}$, the peak strain increases by a factor of more than two (2.55). In the case of the V-steel, Fig. 4.1(b), the same change in strain rate leads to an increase in the peak strain by a factor of only 1.4. The considerably smaller effect of increasing the strain rate in the V-steel is due to the dynamic precipitation of VN during work hardening at the lower strain rates. Under these conditions, recrystallization is delayed because the fine precipitates that form on dislocations during deformation hinder their motion. Thus the highly recovered substructure required for the nucleation of recrystallization cannot form. The influence of dynamic precipitation during testing is particularly evident when the two sets of flow curves in Figs. 4.1(a) and 4.1(b) determined at strain rates of 1.2×10^{-4} and 1.2×10^{-3} s^{-1} are compared.

The Nb steel, as shown in Fig. 4.1(c), shows broader peaks than the plain carbon steel, even at low strain rates such as $1.4/1.9 \times 10^{-4}$. This broadening of the peak is associated with both precipitate and solute effects (to be discussed in more detail below), and is seen in all of the Nb bearing steels (Figs. 4.1(c) to (f)). It is also evident, to a lesser extent, in the V-steel (Fig. 4.1(b)). The higher peak stress and strain in the Nb-steel is partially due to dynamic precipitation during the rising part of the flow curve, with a further contribution from the solute retardation of recrystallization due to Nb addition. These two effects will be examined much more closely in the sections that follow. The flow curves

for the Nb-bearing steels are qualitatively similar; the relative differences in their peak strains and stresses will be discussed in Sections 4.5 and 4.6, respectively.

4.3 Flow Curves in Torsion

The experimentally determined torque vs. equivalent strain curves are shown in Figs. 4.4 and 4.5. These tests were carried out only on the Nb-bearing steels because, in these materials, the peak strain could not be attained in compression. The equivalent strains are proportional to the measured angle of twist θ, as given by

$$\varepsilon_{eq} = \varepsilon = \frac{R\theta}{\sqrt{3}L} \qquad (4.1)$$

where R and L are the radius and length of the sample, respectively.

The increase in the peak strain and maximum torque with increasing strain rate is illustrated in Fig. 4.4(a) for the Nb-steel. Due to the flatness of the torque vs. strain curves, the strains at peak torque are not easily determined at 875°C (Fig. 4.4(a)). At the next higher temperature (Fig. 4.5(a)), where recovery rates are faster and recrystallization starts sooner, this problem is considerably reduced. The addition of high levels of Mn to a Nb steel does not seem to affect the peak torque (compare, for example, the curves for deformation at a strain rate of 3 s^{-1} in Figs. 4.4(a) and (b)), although the peak strains are somewhat higher.

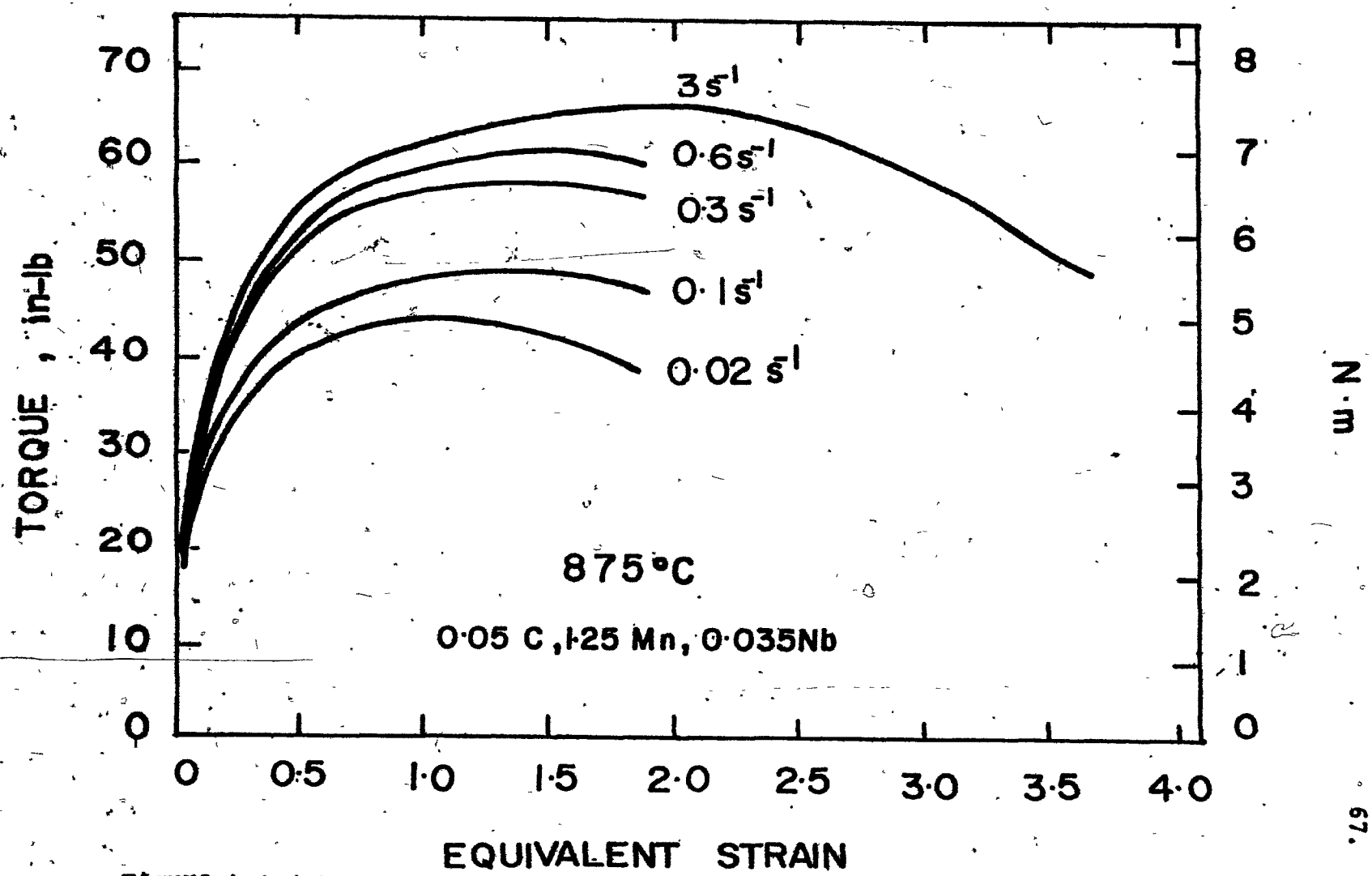

Figure 4.4 (a) Flow curves for the 1.25% Mn, 0.035% Nb steel in torsion at 875°C. The results are displayed in terms of torque vs. equivalent surface strain.

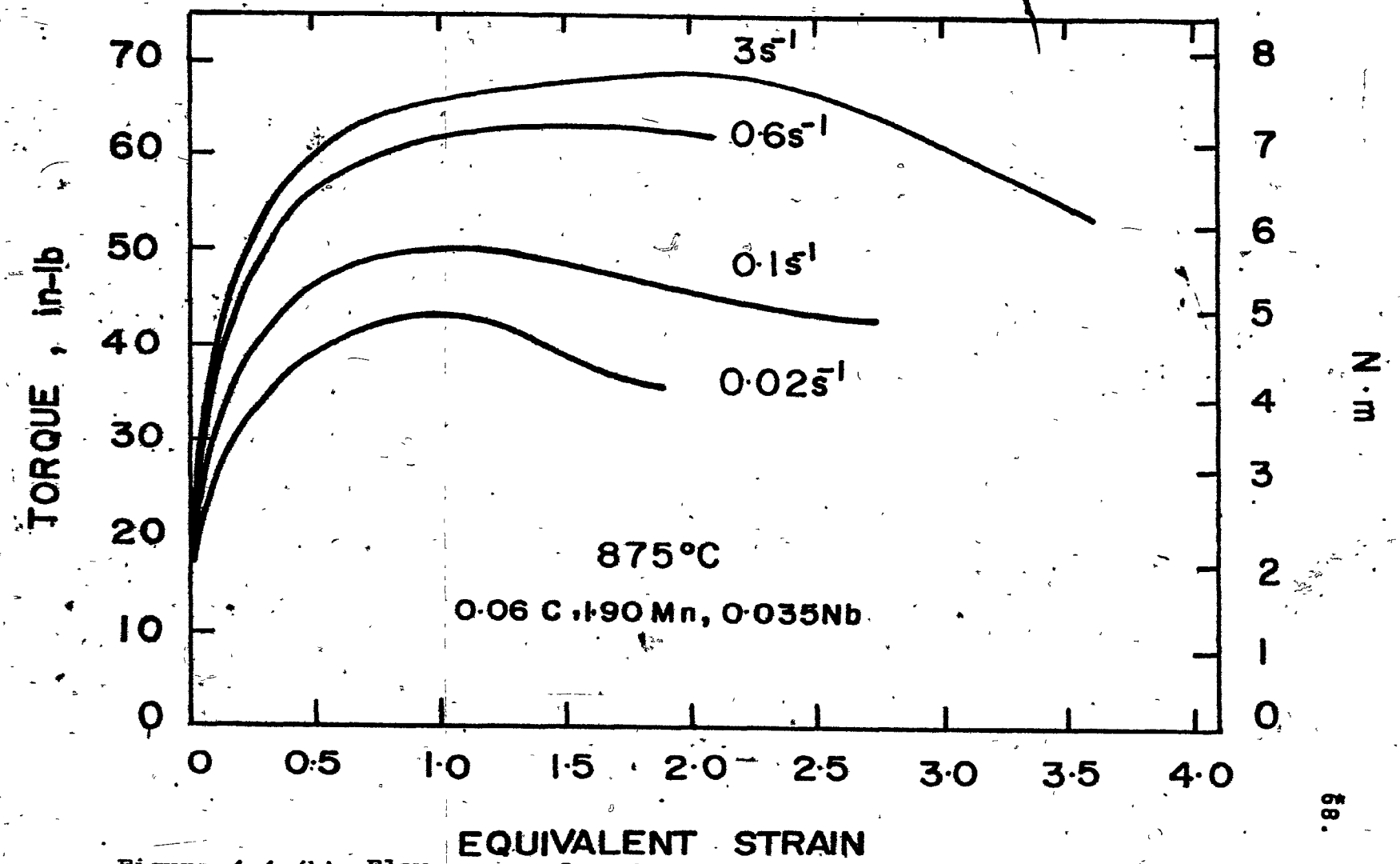

Figure 4.4 (b) Flow curves for the 1.90% Mn, 0.035% Nb steel in torsion at 875°C. The results are displayed in terms of torque vs. equivalent surface strain.

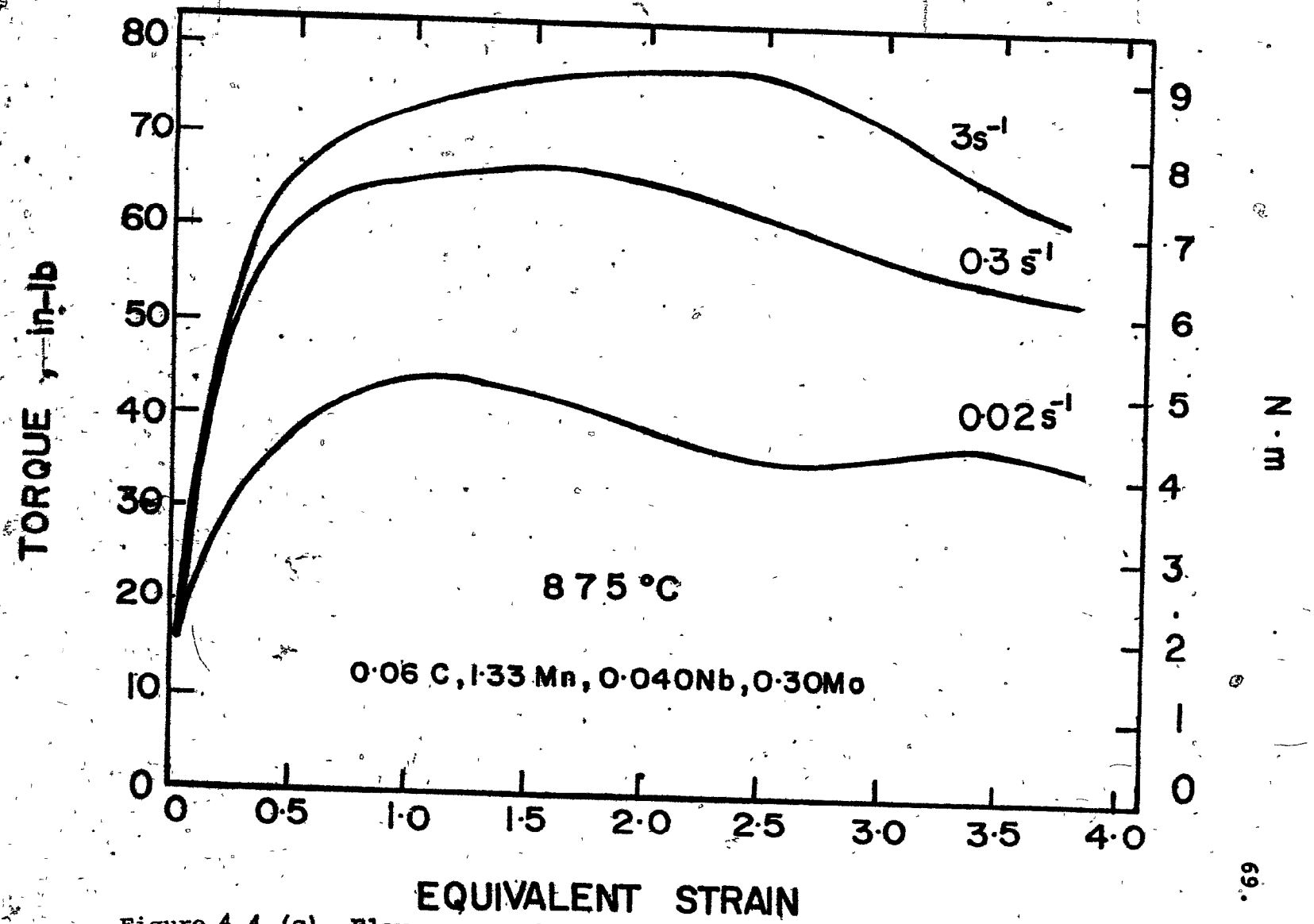

Figure 4.4 (c) Flow curves for the 0.30% Mo, 0.035% Nb steel in torsion at 875°C. The results are displayed in terms of torque vs. equivalent surface strain.

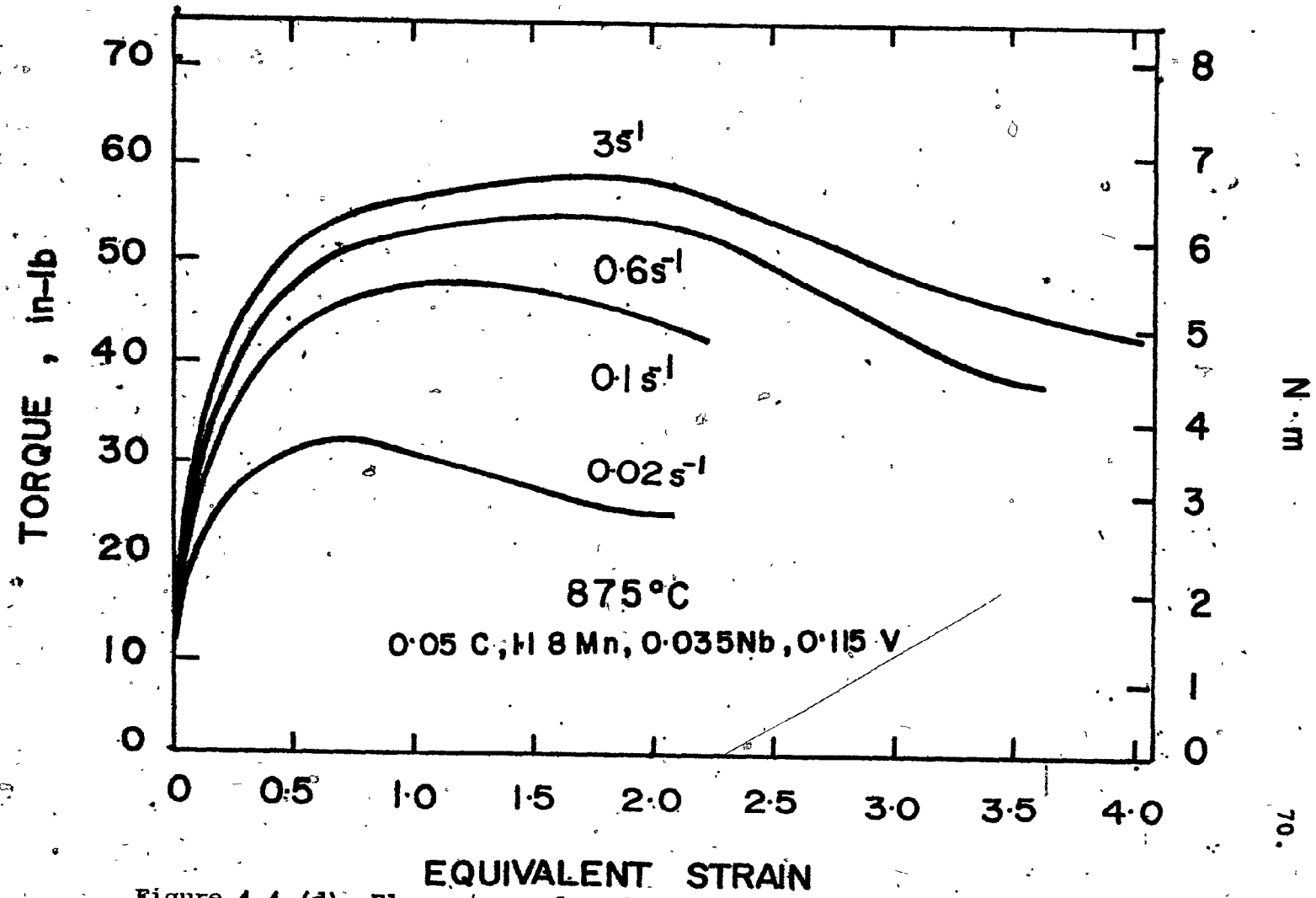

Figure 4.4 (d) Flow curves for the 0.115% V, 0.035% Nb steel in torsion at 875°C. The results are displayed in terms of torque ve. equivalent surface strain.

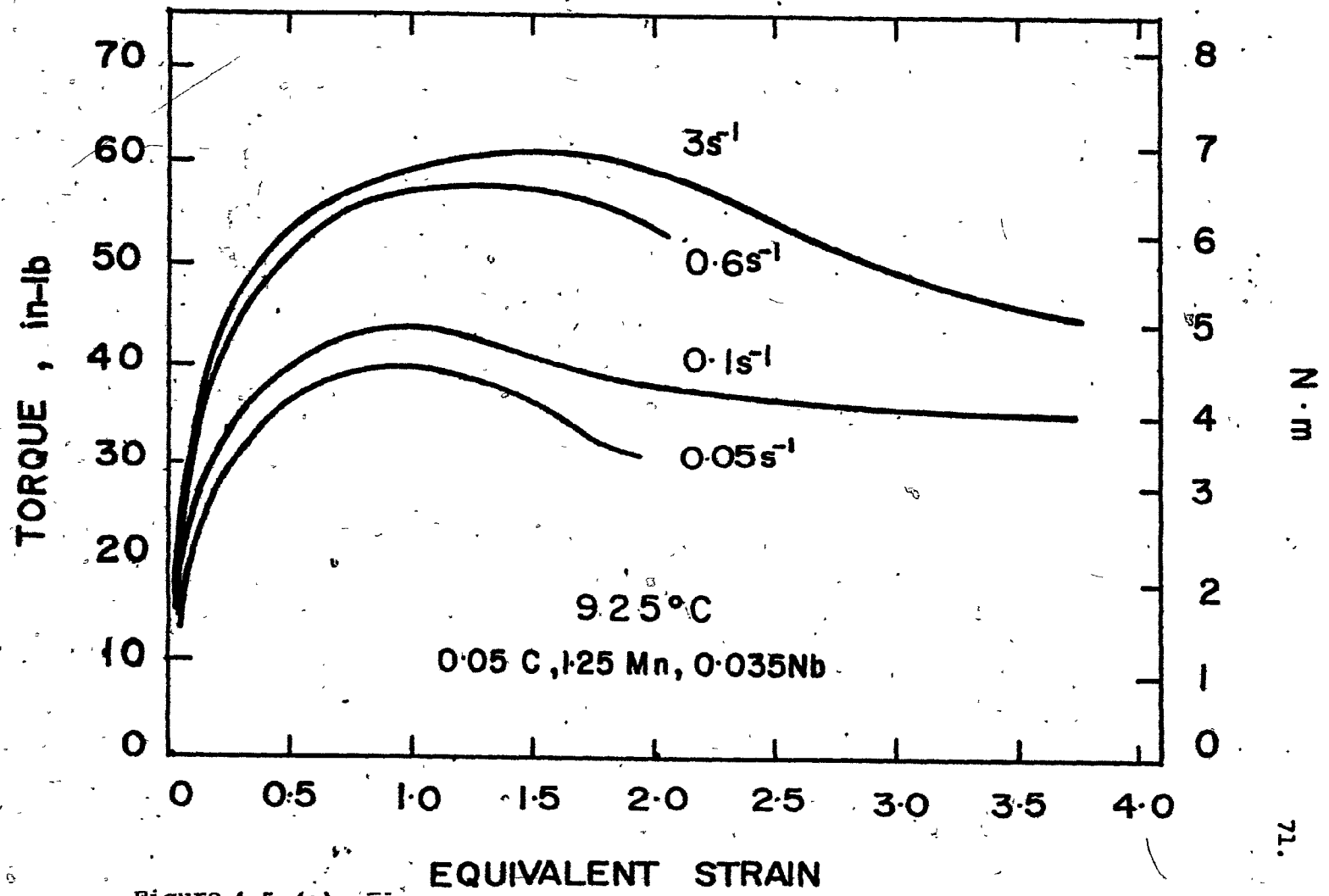

Figure 4.5 (a) Flow curves for the 1.25% Mn, 0.035% Nb steel in torsion at 925°C. The results are displayed in terms of torque vs. equivalent strain.

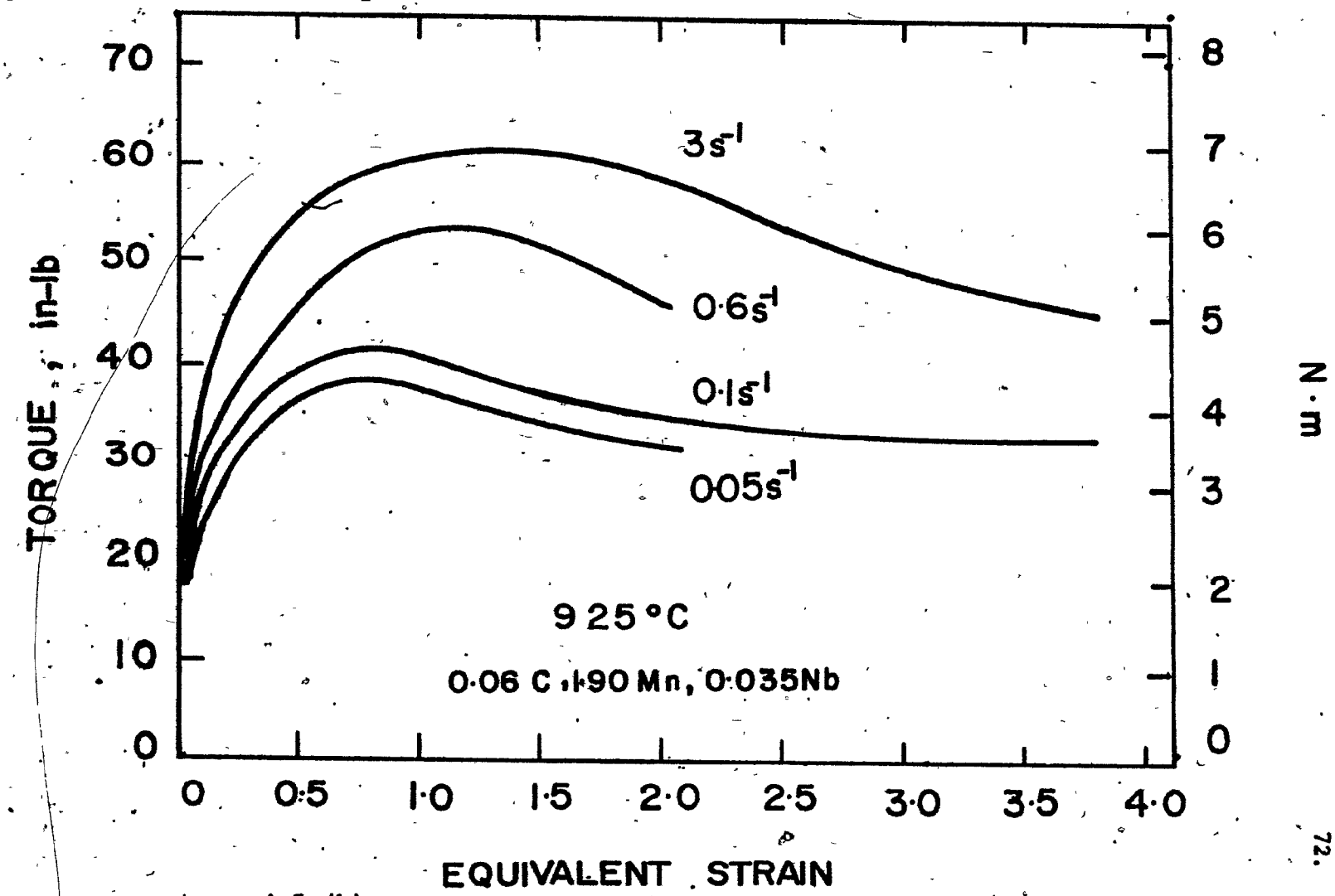

Figure 4.5 (b) Flow curves for the 1.90% Mn, 0.035% Nb steel in torsion at 925°C., The results are displayed in terms of torque vs. equivalent surface strain.

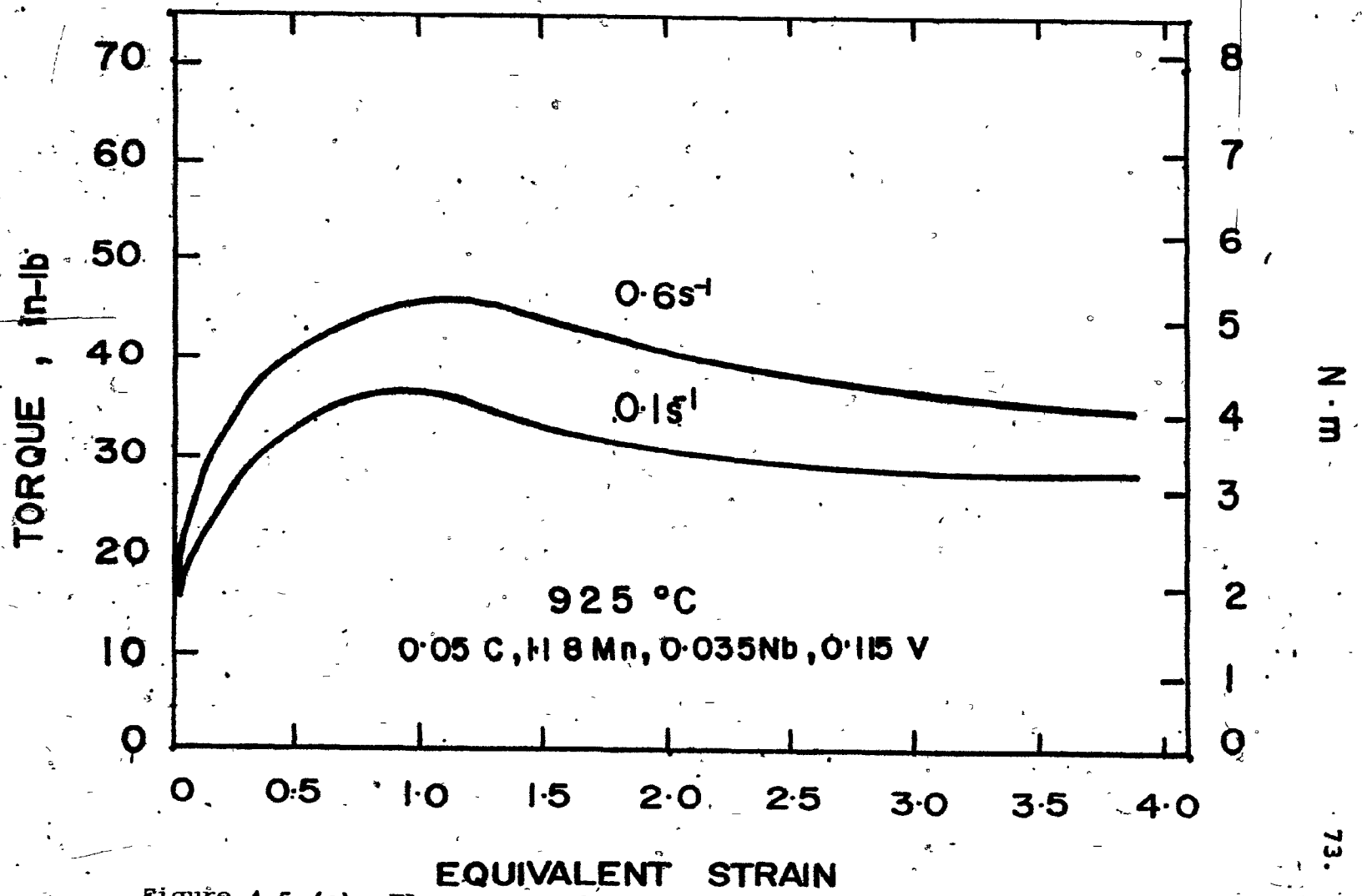

Figure 4.5 (c) Flow curves for the 0.115% V, 0.035% Nb steel in torsion at 925°C. The results are displayed in terms of torque vs. equivalent strain.

The peak torque values for the Nb-V steel (Figs. 4.4(d) and 4.5(c)) are consistently lower than in the Nb-steel (Figs. 4.4(a) and 4.5(a), respectively). The peak strains are slightly lower in the Nb-V steels. On the other hand, Mo in a Nb steel (Fig. 4.4(c)) led to higher peak torques than observed in the Nb-steel and also to higher peak strains.

4.4 Correlation between the Compression and Torsion Flow Data

True stress-true strain curves are readily calculated from the load/displacement data of compression tests. In torsion, however, where torques and rotations are measured, the conversion to stress and strain is not as easily accomplished. The equivalent strain at the surface is determined with no difficulty from Eq. 4.1 above. The equivalent stress at the surface is usually evaluated from the experimental torque, T, via the relation proposed by Fields and Backofen (60), namely:

$$\sigma_{eq} = \sigma = \frac{\sqrt{3}T}{2R^3}(3 + m + n) \qquad (4.2)$$

Here, m is the strain rate sensitivity of the torque and n is the work hardening coefficient derived from the torque. These two coefficients are defined as follows:

$$m = \left(\frac{\partial \ln T}{\partial \ln \dot{\varepsilon}}\right)_{\varepsilon} \qquad (4.3)$$

and

$$n = \left(\frac{\partial \ln T}{\partial \ln \varepsilon}\right)_{\dot{\varepsilon}} \qquad (4.4)$$

The (torque-based) work hardening coefficient can be determined from a log T - log ε plot, as shown in Fig. 4.6. The (torque-based) strain rate coefficient can, in principle, be calculated from two tests carried out at different strain rates; e.g. from the relation $\log(T_2/T_1)_\varepsilon / \log(\dot{\varepsilon}_2/\dot{\varepsilon}_1)_\varepsilon$. Because of the dependence of m on σ, the difficulty with this method is that the numerical value of m depends on the strain rates used.

This difficulty is illustrated in Table 4.1, where it can be seen that the value of m at a given strain approximately doubles in going from $\dot{\varepsilon}_2/\dot{\varepsilon}_1$ ratios of 2 to 6, or 2 to 3. By contrast, there is little change in m in the $\dot{\varepsilon}_2/\dot{\varepsilon}_1$ range from 3 to 6. However, as the overall range of m is restricted to the interval 0.1 to 0.2, this variation is of little consequence in the (3 + m + n) term of Eq. (4.2).

The instantaneous values of n vary from ∿ 0.5 in the initial work hardening region to - 0.7 beyond the maximum torque. Using the instantaneous values for n and an average value for m, the equivalent stress can always be calculated to produce a stress/strain curve, although it can sometimes be a lengthy and tedious process. The peak strain determined in this way should be comparable with that obtained from compression data. Unfortunately this has not been found to be the case (32,61), and the torsion σ_p values are consistently higher than those determined from compression testing.

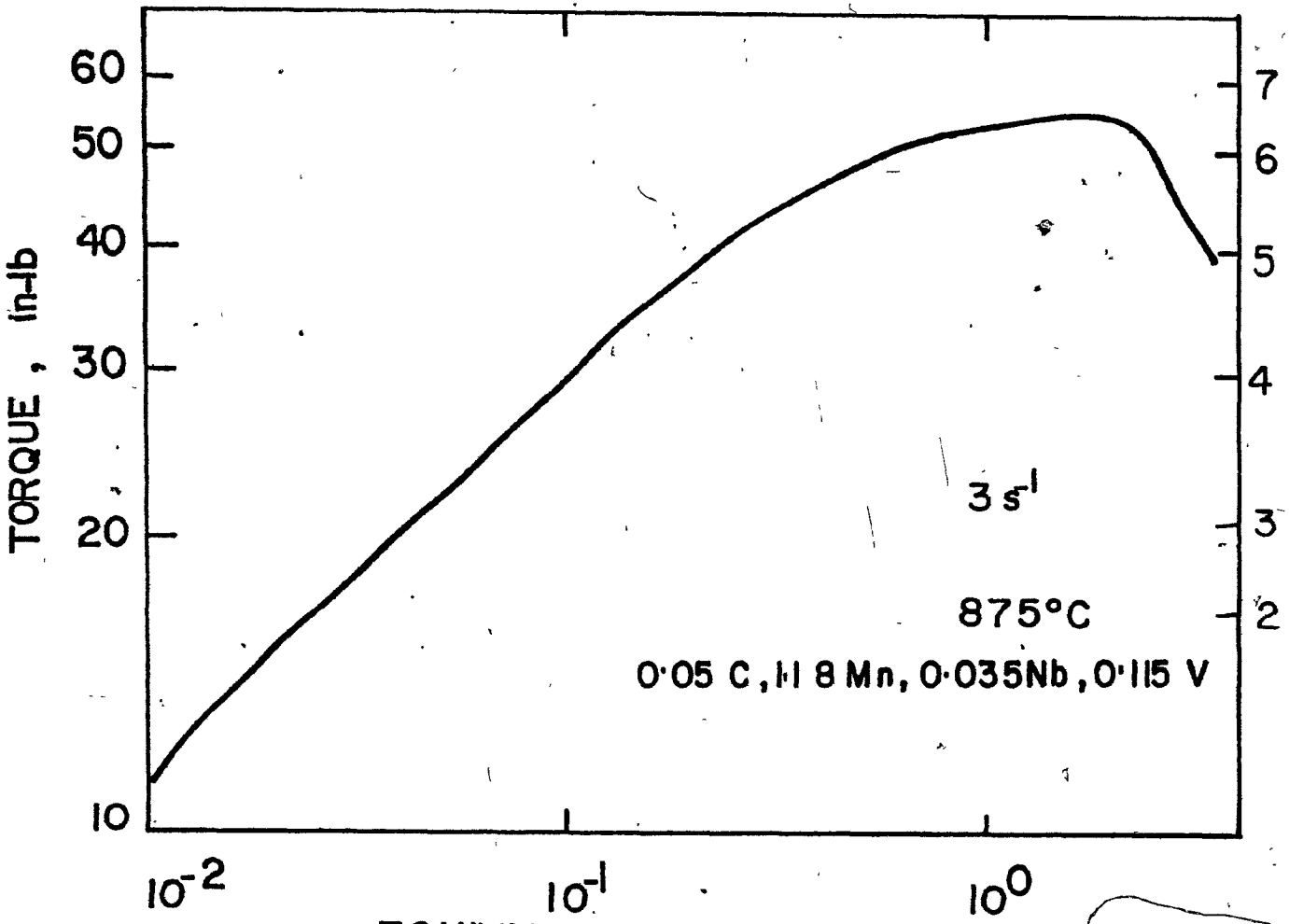

Figure 4.6 Flow curve for the 0.115% V, 0.035% Nb steel tested in torsion at an equivalent strain rate of 3 s^{-1} at 875°C, plotted on a full log scale for purposes of determining the strain sensitivity of the torque.

TABLE 4.1

Strain Rate Sensitivity (m) of the Torque in the 1.2% Mn, 0.035% Nb Steel at 875°C

m	ϵ	$\dot{\epsilon}_1/\dot{\epsilon}_2$	$\dot{\epsilon}_1$	$\dot{\epsilon}_2$
0.080	0.2	2	0.6	0.3
0.086	0.5	2	0.6	0.3
0.080	1.0	2	0.6	0.3
0.084	1.5	2	0.6	0.3
0.074	2.0	2	0.6	0.3
0.13	0.2	3	0.3	0.1
0.13	0.5	3	0.3	0.1
0.16	1.0	3	0.3	0.1
0.17	1.5	3	0.3	0.1
0.18	2.0	3	0.3	0.1
0.11	0.2	6	0.6	0.1
0.12	0.5	6	0.6	0.1
0.14	1.0	6	0.6	0.1
0.14	2.0	6	0.6	0.1

This point is illustrated in Fig. 4.7, where the test results are compared at 925°C and an equivalent $\dot{\varepsilon}$ of $5x10^{-2}s^{-1}$. It is evident that the torsion peak stress is lower than the compression ε_p, and the same relative positions were observed at other temperatures and strain rates. Canova et al. (62) have recently proposed an explanation for this difference; in torsion there are two planes of maximum shear stress whereas in axisymmetric compression there are an infinite number of them. Also, only one of these two planes is particularly active in torsion. Thus, in torsion, with essentially a single slip system operative, the work hardening rates are lower than in compression, where there are numerous slip systems, so that the work hardening rates are also higher.

This explanation may be extended to account for the considerably higher peak strains observed in torsion than in compression. The nucleation of recrystallization is dependent on achieving a critical dislocation density as well as on the development of a substructure containing certain minimum misorientations. The differences in the two work hardening rates and in the number and geometry of the operative slip systems, as described very briefly above, could mean that larger (equivalent) strains are required in torsion than in compression (or tension) to accumulate either the critical dislocation density or the minimum misorientation. Thus the very particular slip geometry associated with torsion and simple shear may be directly responsible for the higher strains to initiate recrystallization in torsion than in axisymmetric testing.

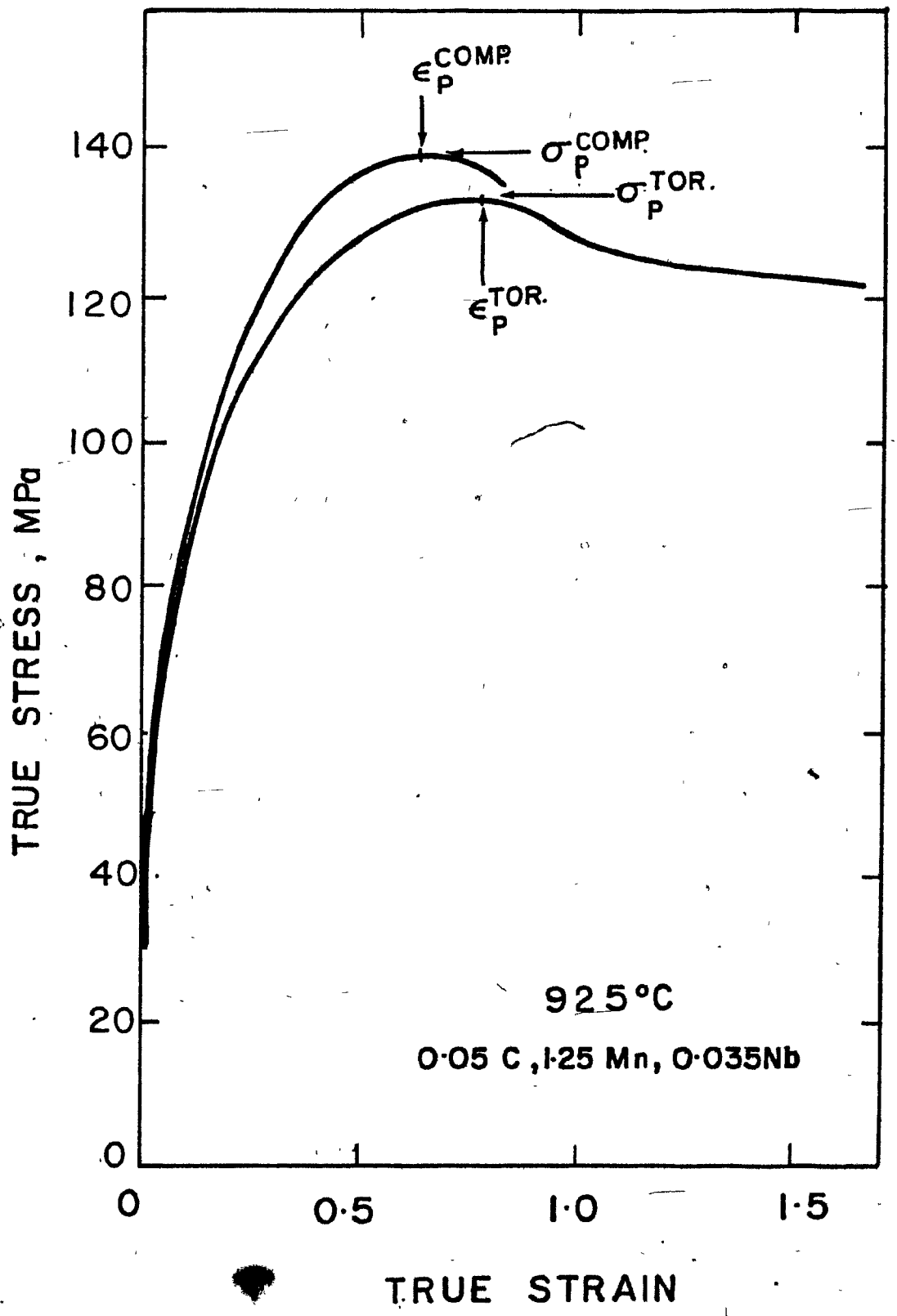

Figure 4.7 Comparison of the flow curves for the 1.25% Mn, 0.035% Nb steel as determined in compression and as calculated from the torsion data by the method of Fields and Backofen (60).

Although the above qualitative explanation can account for the differences between torsion and compression flow curves, it does not lead to quantitative conversion factors for passing back and forth between the two types of data. For the present purpose, it was therefore decided to use a simple 'calibration' procedure instead. Additional torsion tests were carried out at strain rates and temperatures similar to those of the compression tests. From these data, the mean value of the ratio $R_1 = \varepsilon_p^{comp}/\varepsilon_p^{tor}$ was determined. This was used to calculate the compression equivalent peak strain values from the ε_p^{tor} data over the entire experimental range. A similar ratio $R_2 = \sigma_p/T_p$ was employed for conversion of the peak torques to peak equivalent stresses. Because the sample length and radius were the same for all the torsion specimens, this simple procedure eliminated the necessity of first converting the torque to equivalent (torsion) stress before making the conversion to equivalent (compression) stress.

4.5 Strain Rate Dependence of the Peak Strain

The dependence of the peak strain on alloy composition and on strain rate is shown in Fig. 4.8 for the plain carbon, V and Nb steels. The ε_p values increase smoothly with strain rate for the plain carbon steel. By way of contrast, there are two things to note about the microalloyed steels: (i) the shift in the overall curve to higher peak strains over the whole range of strain rates; i.e. the general

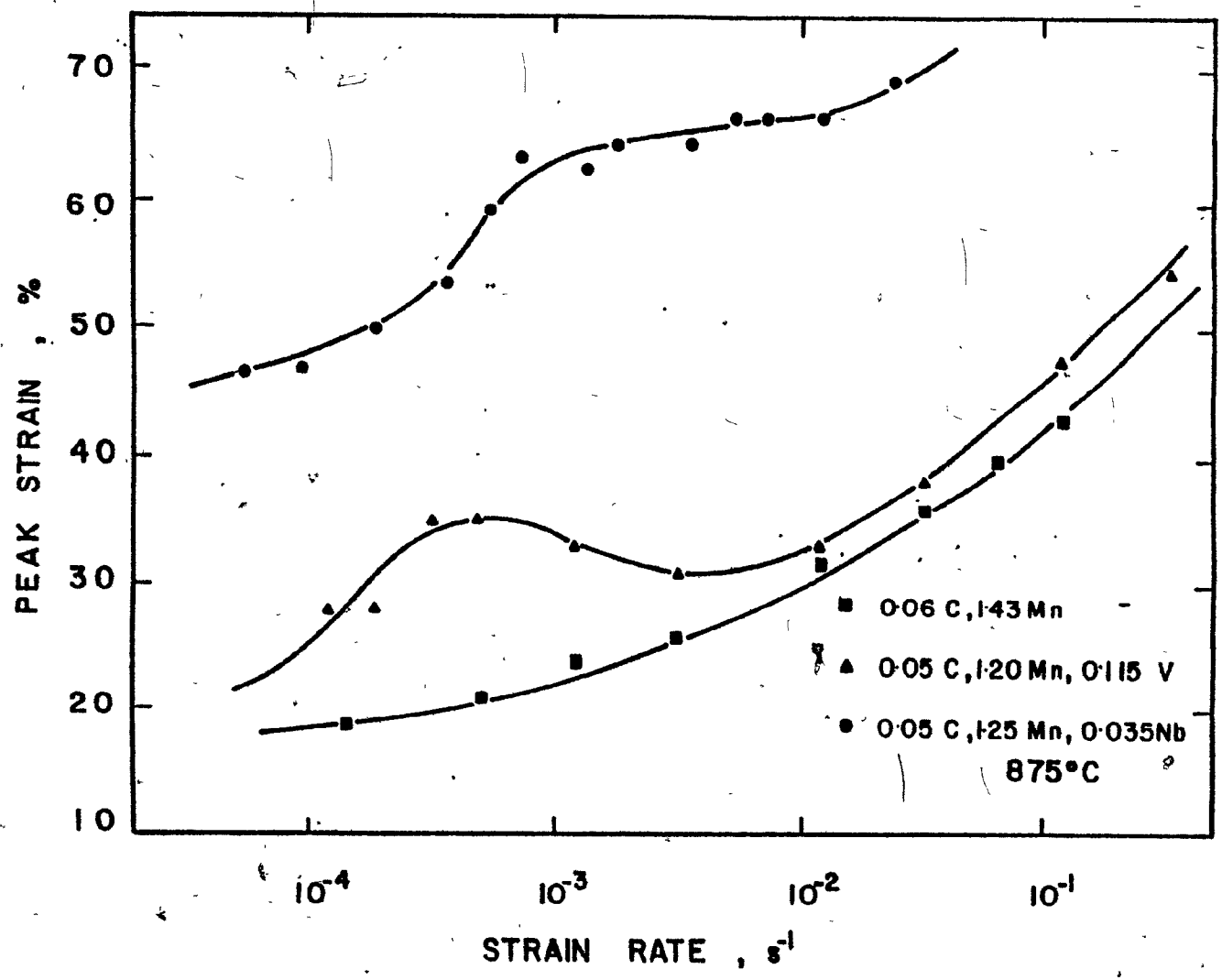

Figure 4.8 (a) Dependence of the peak strain on the strain rate at 875°C in the plain C, 0.115% V and 1.25% Mn, 0.035% Nb steels.

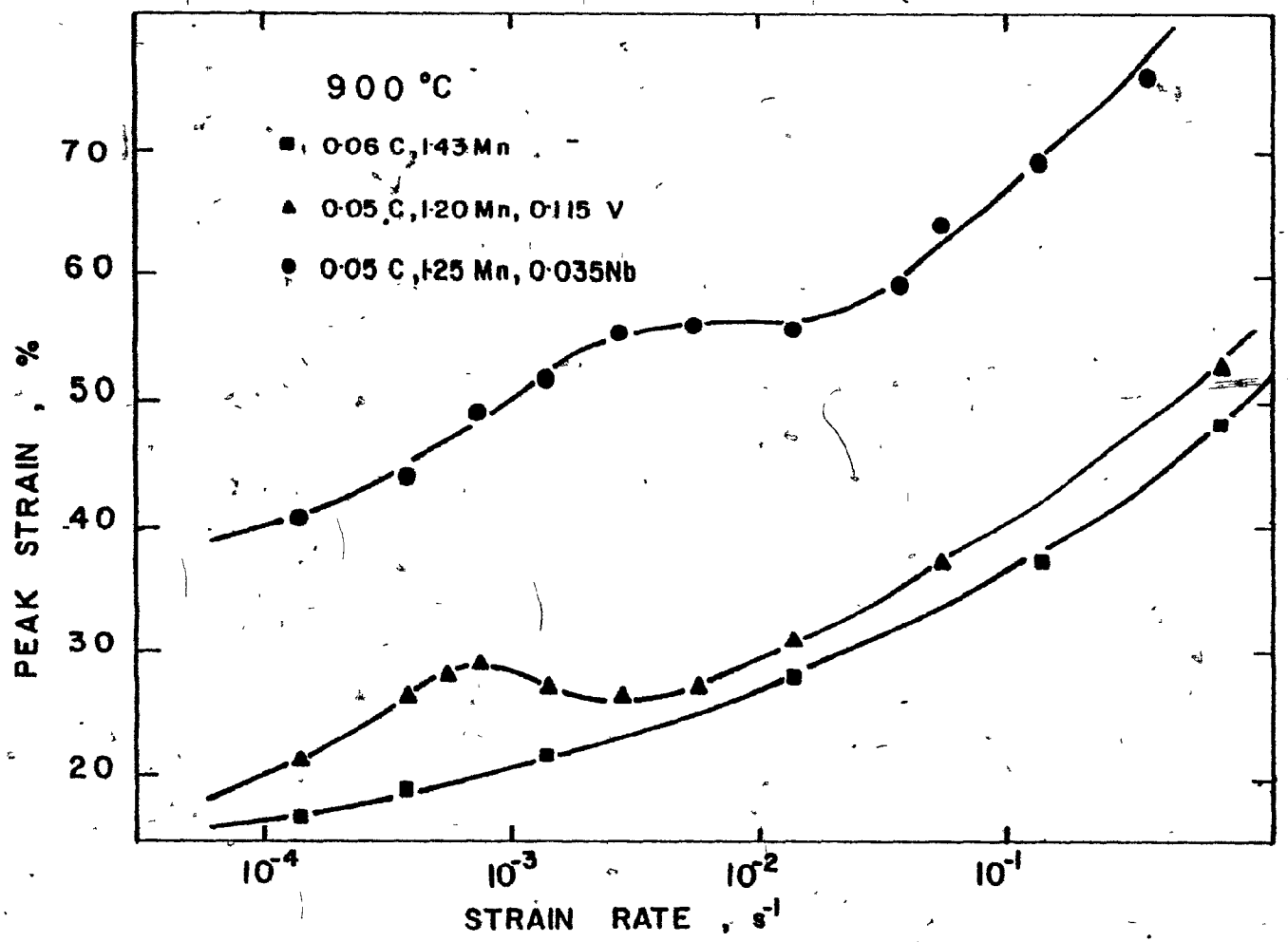

Figure 4.8 (b) Dependence of the peak strain on the strain rate at 900°C in the plain C, 0.115% V and 1.25% Mn, 0.035% Nb steels.

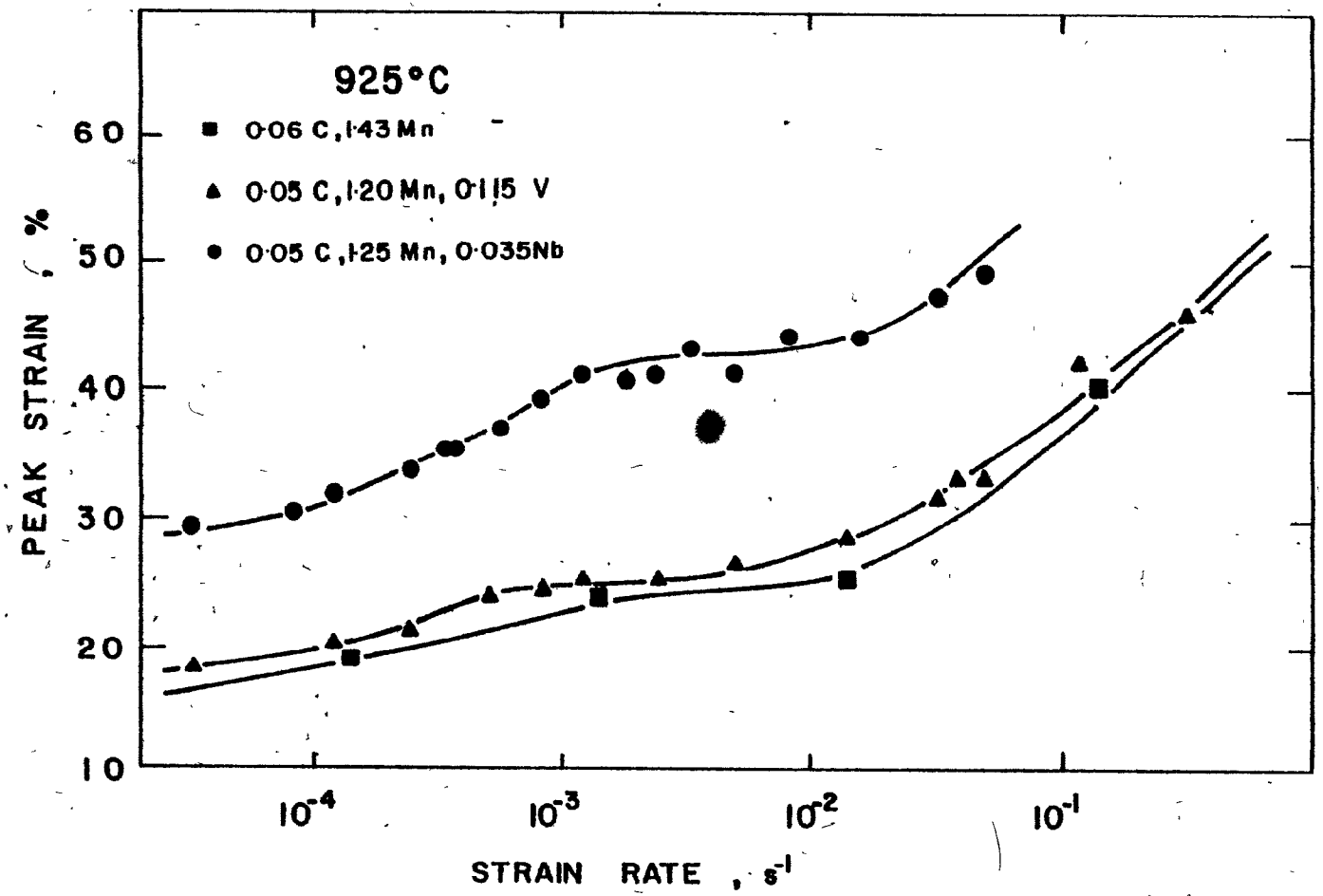

Figure 4.8 (c) Dependence of the peak strain on the strain rate at 925°C in the plain C, 0.115% V and 1.25% Mn, 0.035% Nb steels.

retardation of the onset of dynamic recrystallization; and (ii) the localized humps in these curves over a particular strain rate range.

The overall shift in the curves, ((i) above) is due, as will be discussed in more detail below, to the retardation of recrystallization by the influence of Nb and V in solution. At the high strain rate end of these diagrams, the whole test is completed within 10 seconds or less, and as will be shown in Section 5.1.3, this time is insufficient for any significant dynamic precipitation to occur.

The location of the humps, in the intermediate strain rate range, is associated with the dynamic precipitation of Nb(CN) and VN in the course of the test (21,29,30). At these strain rates, there is sufficient time for dynamic precipitation to take place before the onset of recrystallization. This precipitation leads to a component of retardation beyond that due to the solute effect alone. The precipitation of Nb(CN) and VN during deformation hinders the rearrangement and recovery of dislocations. In this way, the substructural rearrangements required for the nucleation of new grains cannot take place or they occur more slowly. This effect reaches a maximum when precipitation starts at relatively small strains and continues until the peak strain is reached. At even lower strain rates, to the left of the hump, precipitation starts very early during straining and ends a little later, but still early in the work hardening region, and well before the peak strain is reached. In this region,

there is deformation enhanced precipitate coarsening (21,29, 30). The lower the strain rate, the greater is its extent. The retarding effect of these coarse precipitates on dynamic recrystallization is limited, however, so that the retardation observed in the low strain rate range is largely due to the solutes that have not yet precipitated.

It is of interest that the overall shapes of the Nb and V steel curves are similar in that both materials exhibit a hump. The size of the humps, however, decreases with temperature (compare Figs. 4.8 (a), (b) and (c)). By contrast, the solute retarding effect of V, as judged by the overall height of the curves, is much smaller than for Nb. The reasons for this difference will be considered more closely in the Discussion chapter.

The strain rate dependence of the peak strain for the four Nb-bearing steels, taken as a group, is shown in Fig. 4.9. The relative magnitude of the solute effect in each steel is indicated by the value of the peak strain outside the hump region. The largest peak strains (and therefore the greatest retardations of recrystallization) are observed in the Mo-Nb steel, then in the Nb-steel. Slightly lower peak strains are noted in the Nb-V steel at 875°C (Fig. 4.9(a)), and depending on the strain rate range, at 900°C (Fig. 4.9(b)). At 925°C, however, this steel exhibits peak strains larger than those of the Nb-steel. The onset of recrystallization is earliest in the Mn-Nb steel, which is a possible exception to the expected order in terms of the solute retarding effects.

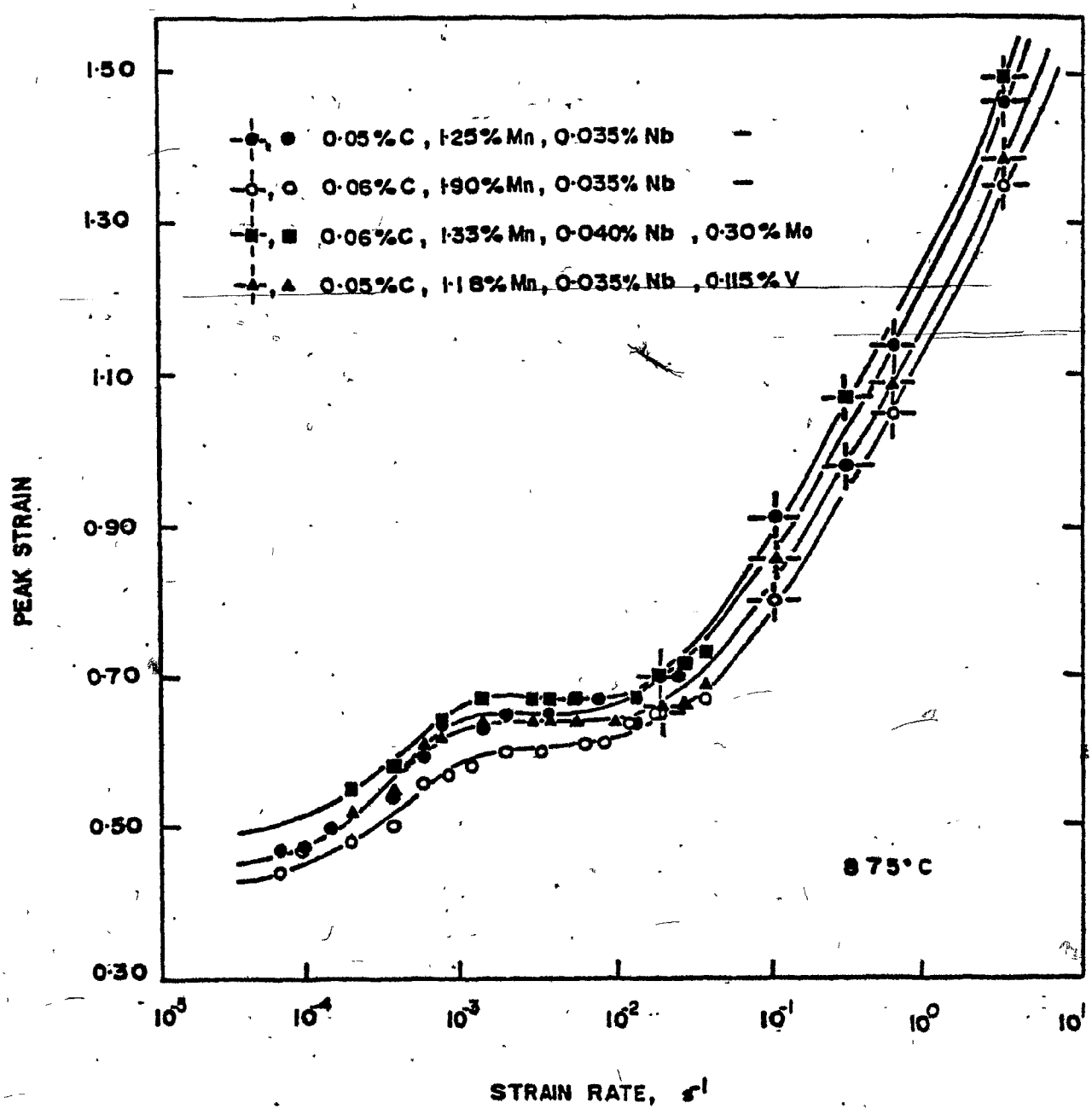

Figure 4.9 (a). Dependence of the peak strain on the strain rate at 875°C for the four Nb-bearing steels. (The peak strains at high strain rates represented by asterisks -⊹-, -⊹-, -⊹-, -⊹- were determined in torsion.)

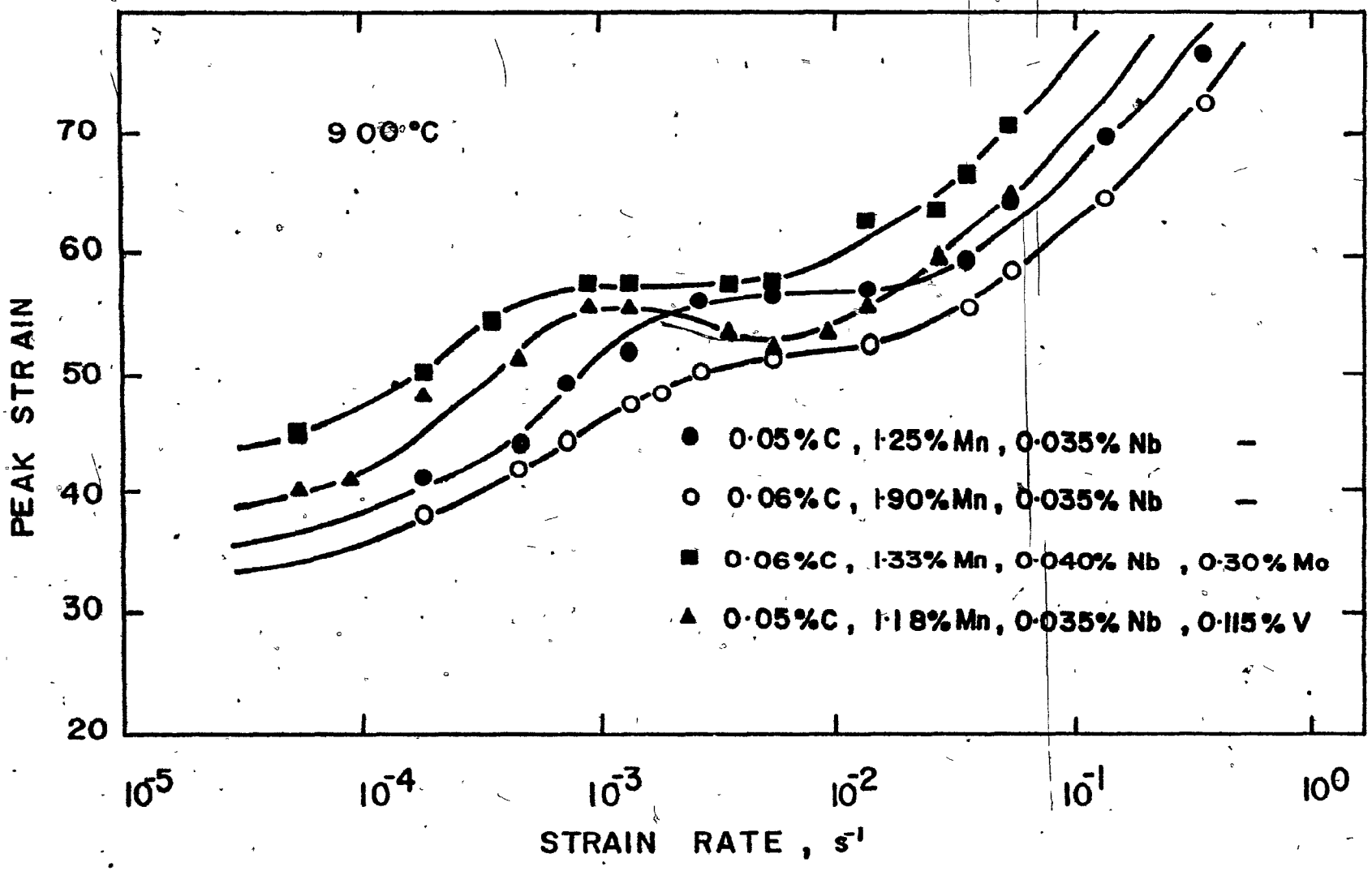

Figure 4.9 (b) Dependence of the peak strain on the strain rate at 900°C for the four Nb-bearing steels.

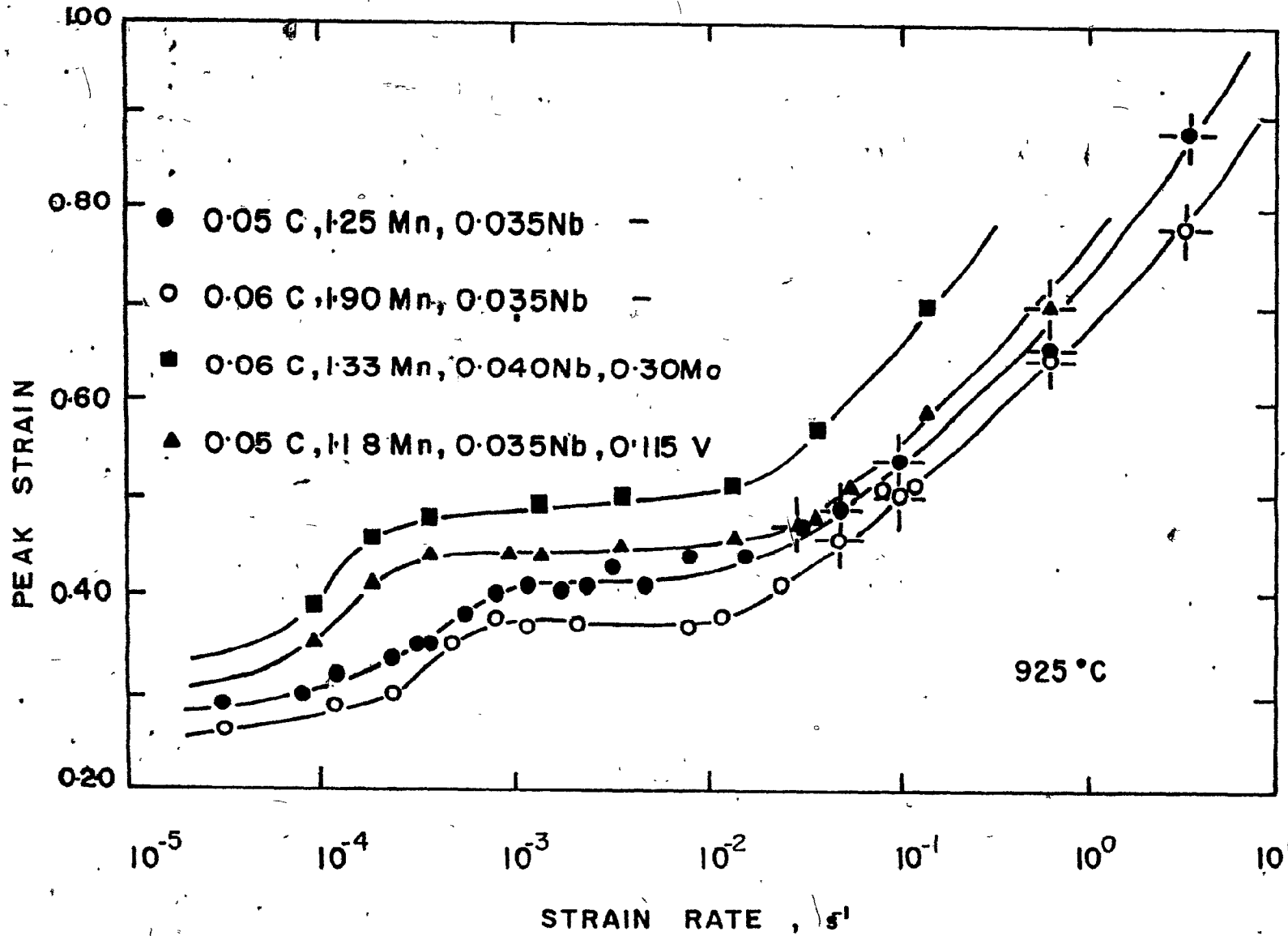

Figure 4.9(c) Dependence of the peak strain on the strain rate at 925°C for the four Nb-bearing steels. (The peak strains at high strain rates represented by asterisks -⊙-, -●-, -■-, -▲- were determined in torsion.)

This steel had a smaller initial grain size in comparison to the other steels (see Section 3.3). The smaller initial grain size may be responsible for the lower than expected peak strains. If this interpretation is correct, the smaller peak strains are due to the greater grain boundary area per unit volume available in the Mn-Nb steel for the nucleation of recrystallization. The smaller grain size probably did not affect the precipitation kinetics, however, for reasons that will also be discussed in the next chapter.

4.6 Strain Rate Sensitivity of the Peak Stress

The peak stresses attained in high temperature flow can be affected by alloy additions in one of several ways. With substitutional alloy additions such as Mn, Mo, Nb and V, there can be a direct increase in the yield stress, as well as a change in the work hardening behavior. For interstitial additions, e.g. N (32), the yield strength can be decreased, and the work hardening behavior can also be affected of course. Precipitates can have two kinds of effects: one is that fine precipitates can pin the dislocations and therefore increase the work hardening rate, leading to higher peak stresses. This is due, principally, to the associated decrease in the rate of dynamic recovery. The other effect is linked to the first in that the nucleation of dynamic recrystallization can be delayed or even prevented completely by the precipitates, again leading to higher peak stresses.

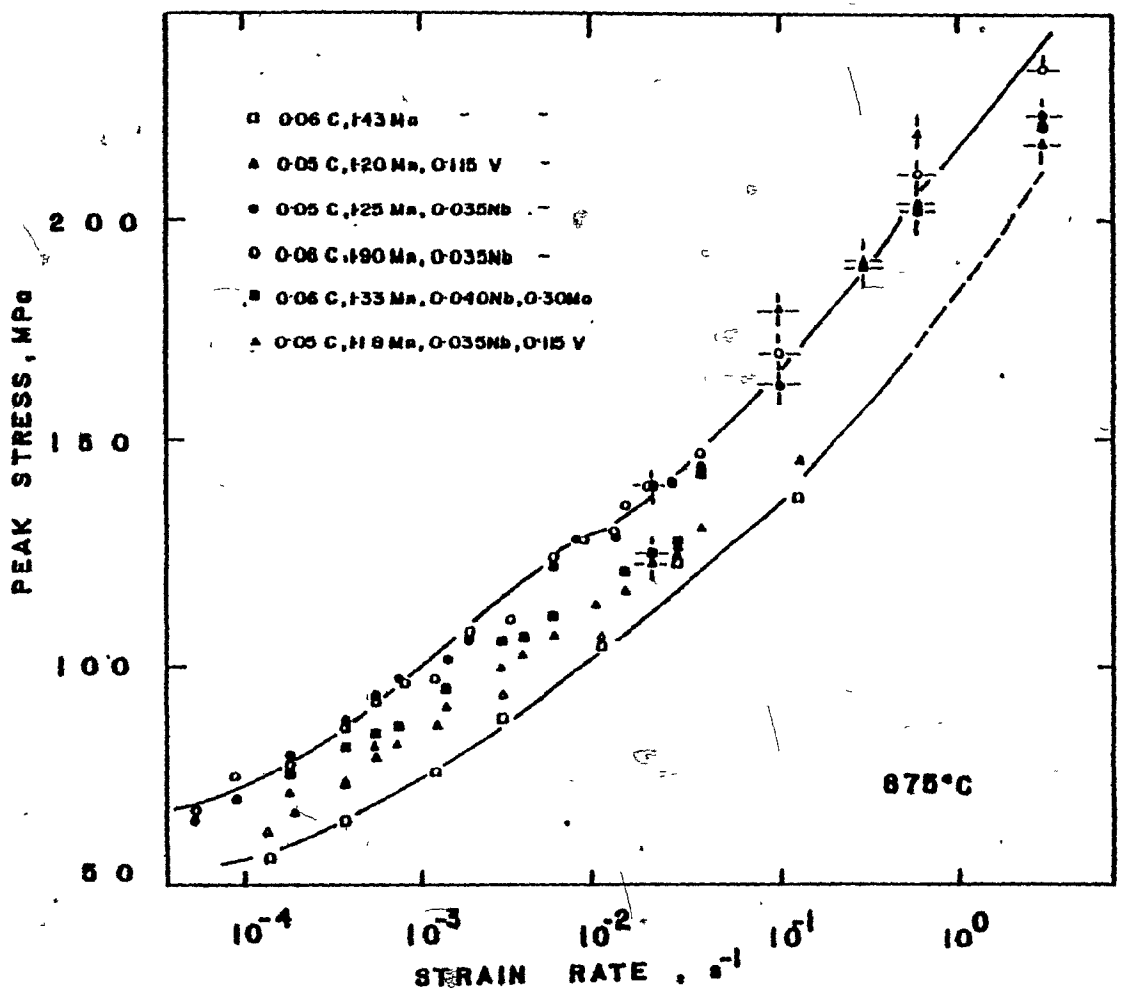

Figure 4.10 (a) Dependence of the peak stress on the strain rate at 875°C for the six steels. (The peak stresses at high strain rates for the Nb steels represented by asterisks -o-, -●-, -■-, -▲- were determined in torsion.)

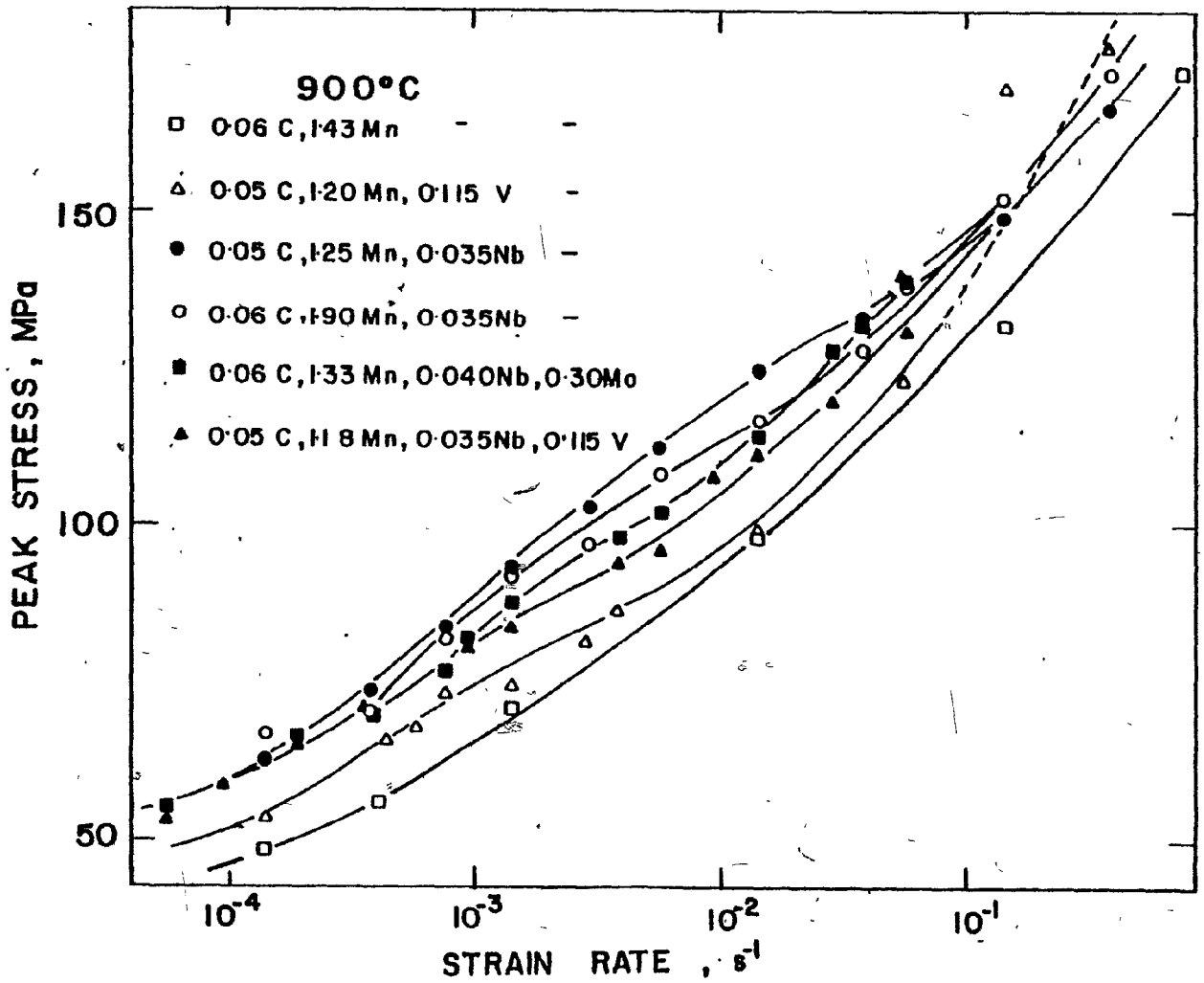

Figure 4.10 (b) Dependence of the peak stress on the strain rate at 900°C for the six steels.

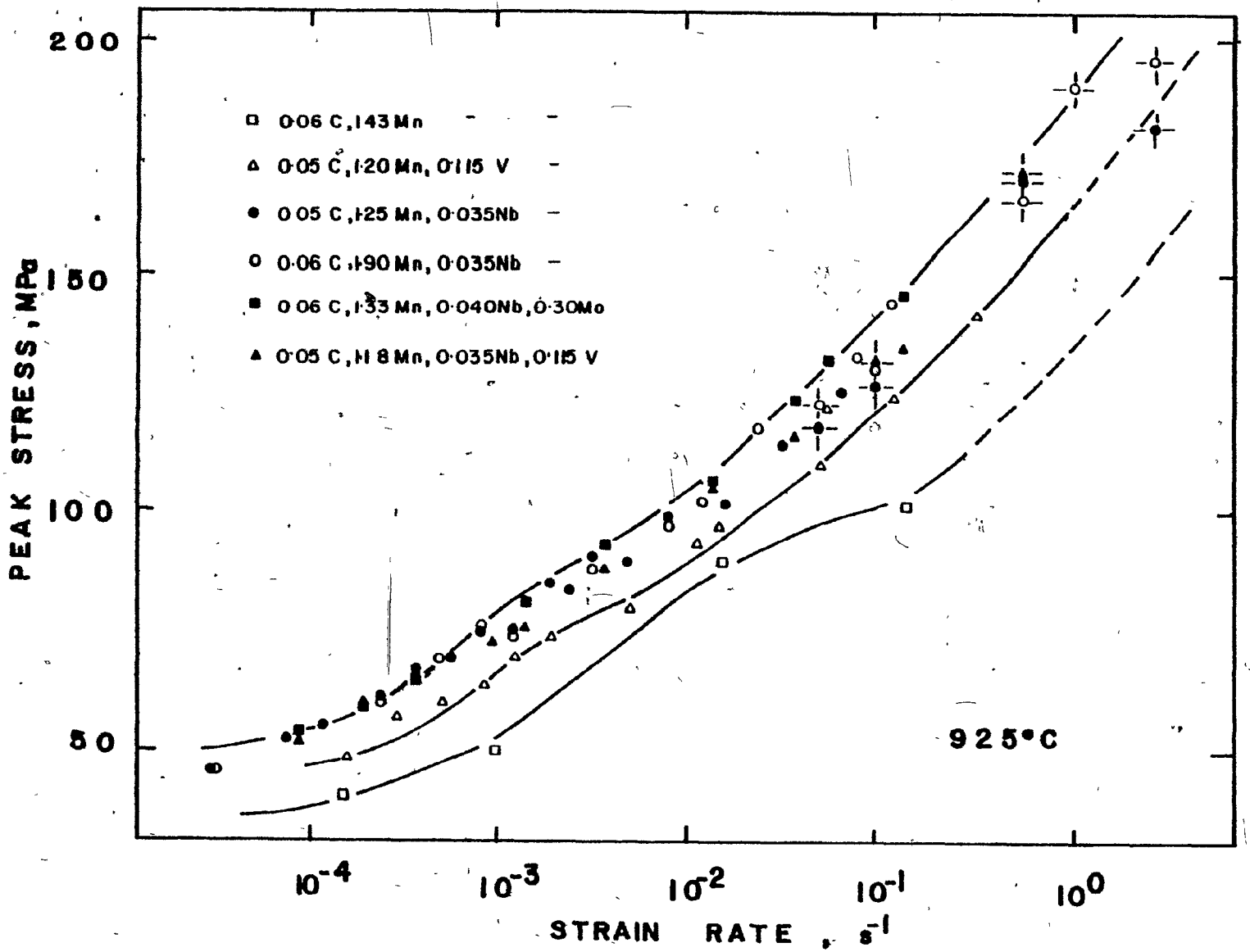

Figure 4.10 (c) Dependence of the peak stress on the strain rate at 925°C for the six steels. (The peak stresses at high strain rates for the Nb steels represented by asterisks -o-, -●-, -■-, -▲- were determined in torsion.)

The strain rate dependence of the peak stress is shown in Fig. 4.10 for the plain carbon, V and Nb-bearing steels. The peak stresses for the plain carbon steel, as expected, are the lowest, followed by those for the V steel. There is a small contribution of the precipitates when present to these values; for example in the V steel, in the strain rate range $5x10^{-4}$ to $10^{-2}s^{-1}$, at 875°C (Fig. 4.10(a)). This effect is much less noticeable in the Nb bearing steels and is almost lost in the experimental scatter. A comparison of Figs. 4.10(a),(b),(c) does not regrettably reveal a consistent pattern regarding the extent to which Mn or Mo alters the peak stress of the Nb bearing steels.

4.7 High Temperature Yield Stresses

The strain rate dependence of the yield stress for the six steels is shown in Fig. 4.11. At the low strains associated with macroscopic yielding, i.e. within the first 1-3%, there is insufficient time for precipitation to occur. The difference in the strength levels of the various steels can then be attributed to the alloy additions which are present in the form of solutes. (The torsion data are not included in Fig. 4.11 due to the difficulties encountered in data acquisition at low strains and high strain rates.)

The strengthening per 0.1 at.% of alloying addition relative to a plain carbon steel was evaluated from the following relation:

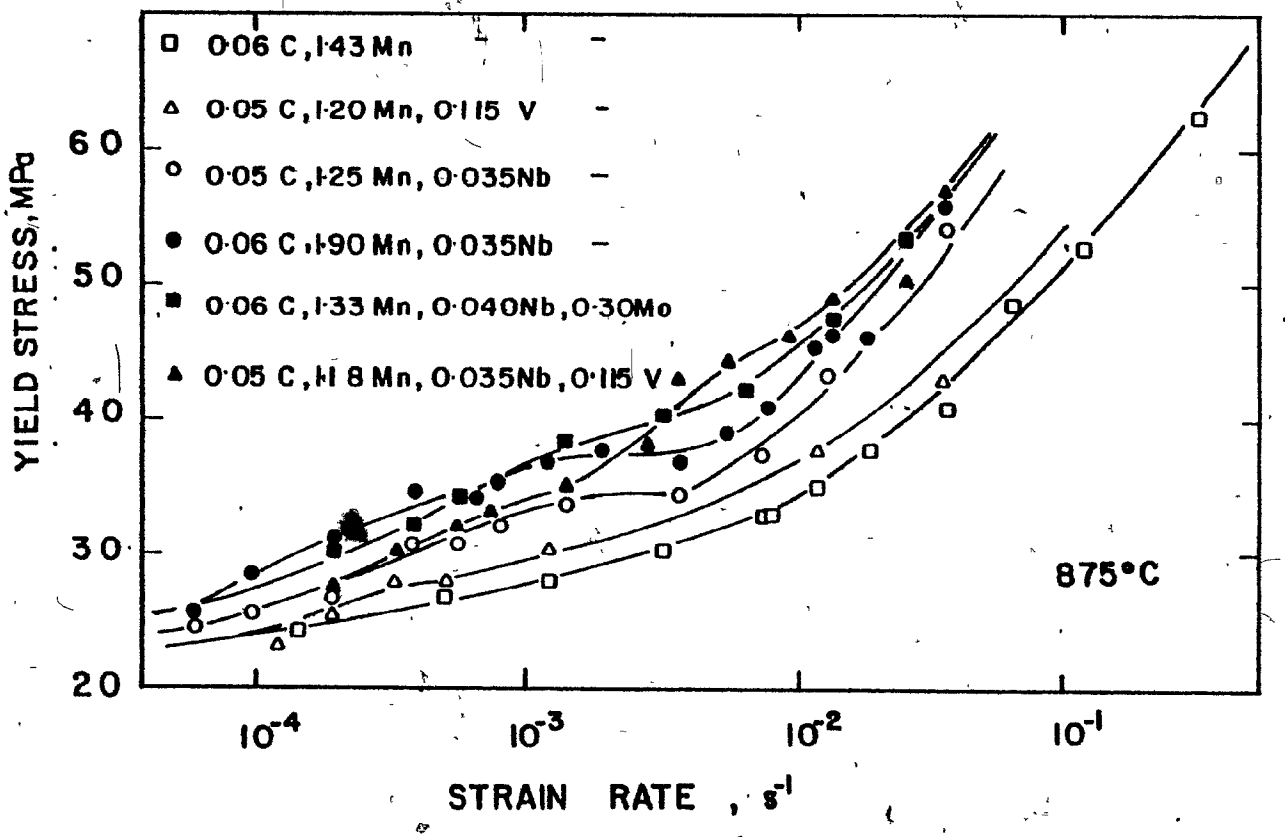

Figure 4.11 (a) Dependence of the yield stress on the strain rate at 875°C for the six steels.

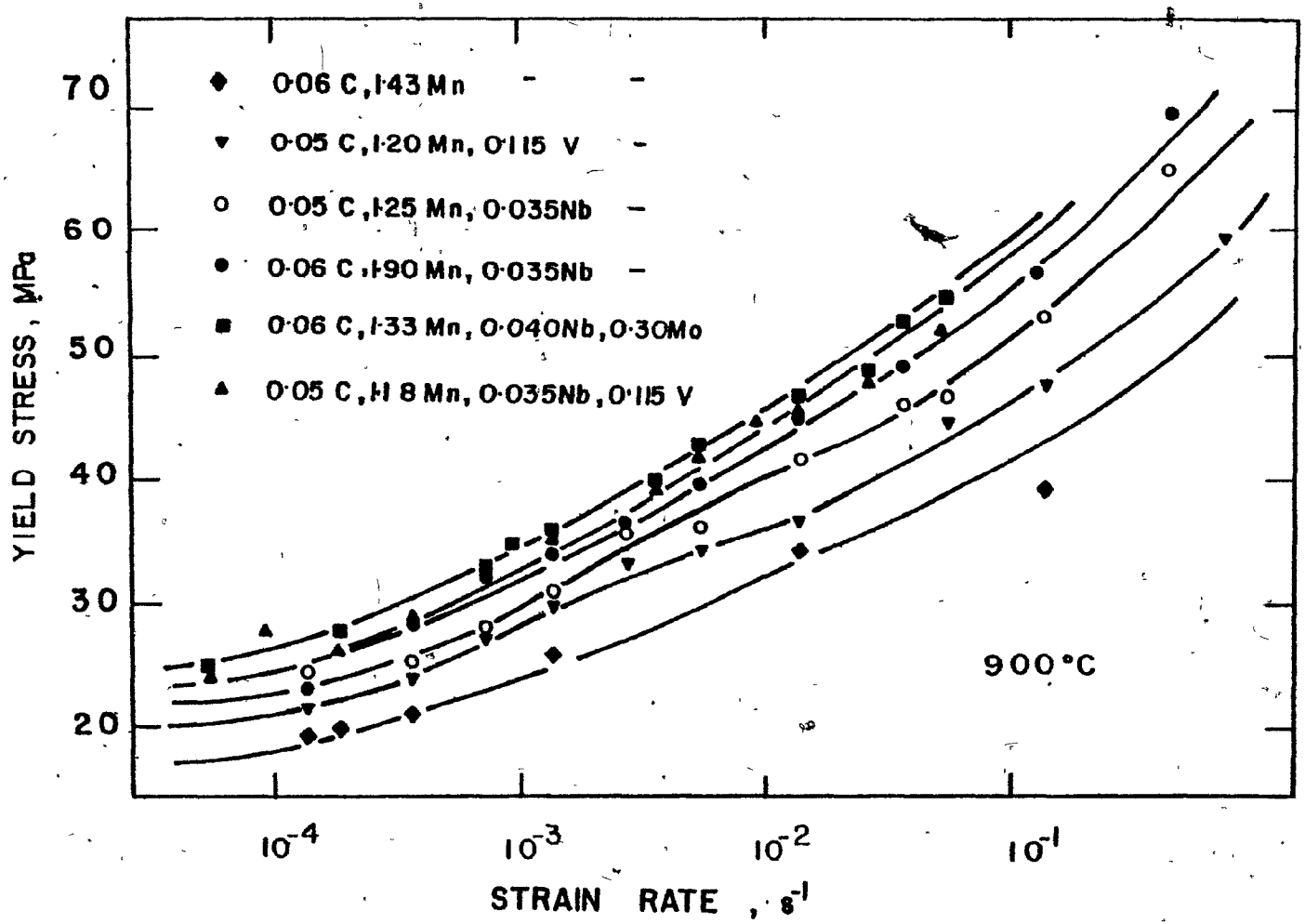

Figure 4.11 (b) Dependence of the yield stress on the strain rate at 900°C for the six steels.

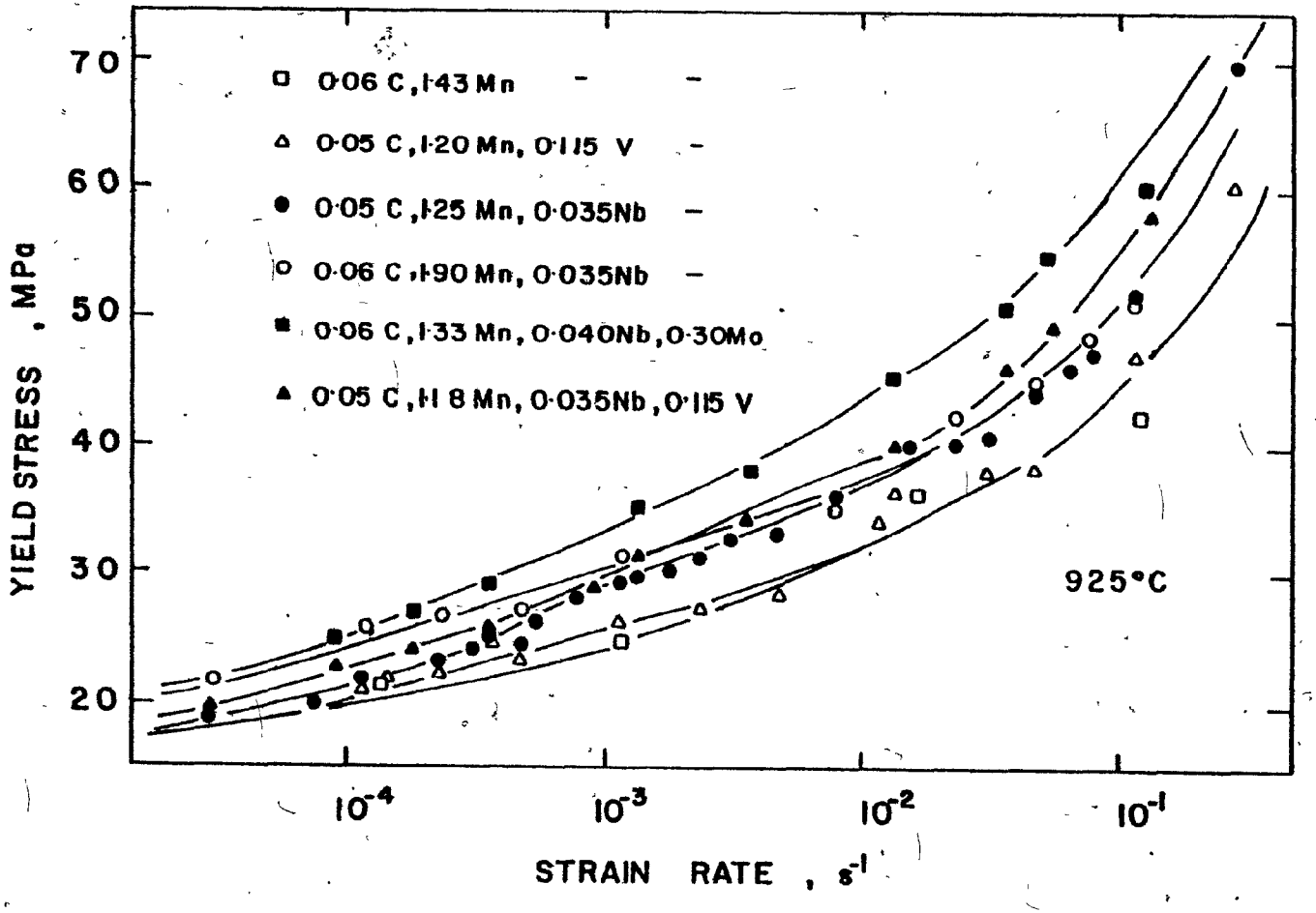

Figure 4.11 (c) Dependence of the yield stress on the strain rate at 925°C for the six steels.

$$\Delta S^{a} = \frac{\sigma_{YS} - \sigma_{YS}^{Pl.C}}{\sigma_{YS}^{Pl.C}} \times \frac{0.1}{at.\%s}$$

In a similar manner, the strengthening per 0.1 wt% of alloy addition was calculated from:

$$\Delta S^{w} = \frac{\sigma_{YS} - \sigma_{YS}^{Pl.C}}{\sigma_{YS}^{Pl.C}} \times \frac{0.1}{wt\%s}$$

s is the alloy addition assumed to be in solution. To estimate the incremental strengthening due to Mn, Mo or V addition over that due to Nb addition alone, σ_{YS}^{Nb} was used in place of $\sigma_{YS}^{Pl.C}$ in the expressions given above. For purposes of comparison, σ_{YS}^{V} was also substituted in these expressions and the strengthening due to the addition of Nb to a V steel was calculated in this way.

The results obtained using this method are presented in Tables 4.2(a) and (b). Table 4.2(a) is for 875, 900 and 925°C over the whole range of strain rates, and Table 4.2(b) is for a strain rate of $3.2/3.7 \times 10^{-2} s^{-1}$ over the temperature range 975-1075°C. (The flow curves for this last set of tests are shown in Appendix A.)

It is evident from the tables that Nb has the greatest effect, and leads to a strength increase of about 70% per 0.1 at % of addition. This influence is followed in magnitude by Mo and V, which have somewhat similar strengthening effects, 9% and 7% respectively per 0.1 at %. Mn has a very small effect, 1.3% for the same amount. The relative positions of

TABLE 4.2 (a)

Strengthening Due to Microalloy Additions at 875, 900 and 925°C

Solute Element (s)	Comparison Base	Δσy/σy (base) % at T°C*			Arithmetic Average	Δσy/σy (base) % per 0.1 at.% Solute (s)	Δσy/σy (base) % per 0.1 wt.% Solute (s)
		875	900	925			
V	Plain C	6.0 ± 3.0	15.0 ± 3.5	4.5 ± 5.3	8.5	7	7
Nb	Plain C	13.3 ± 10.2	22.6 ± 3.2	13.8 ± 5.8	17.0	70	49
Mn + Nb (in Mn-Nb steel)	Plain C	25.7 ± 7.5	32.6 ± 3.2	20.8 ± 4.8	26.5	5	5
Mn (in Mn-Nb steel)	Nb Steel	12.2 ± 13	8.4 ± 3.8	5.6 ± 7.5	8.7	1.3	1.3
Nb + V (in Nb-V steel)	Plain C	13.2 ± 27	38.5 ± 4.9	22.9 ± 8.0	24.9	17	17
V (in Nb-V steel)	Nb Steel	11.2 ± 13	12.0 ± 3.1	6.8 ± 4.3	10	8	9
Nb (in Nb-V steel)	V Steel	21.0 ± 13	20.0 ± 3.0	16.3 ± 4.9	19	80	56
Mo (in Mo-Nb steel)	Nb Steel	15.4 ± 6.3	14.5 ± 3.3	20.0 ± 3.7	16.6	10	5
Mo + Nb (in Mo-Nb steel)	Plain C	29.7 ± 9.4	40.8 ± 3.8	37.4 ± 7.3	36	18	10

*Limits shown are 1 standard deviation.

TABLE 4.2 (b)

Strengthening Due to Microalloy Additions at a Strain Rate of $3.2/3.7 \times 10^{-2} s^{-1}$ in the 875-1075°C Temperature Range

Solute Element (s)	Comparison Base	$\Delta\sigma y/\sigma y$ (base) % Per 0.1 at.% Solute (s)	$\Delta\sigma y/\sigma y$ (base) % Per 0.1 wt.% Solute (s)	Overall Average* Per 0.1 at.% Solute (s)	Overall Average* Per 0.1 wt.% Solute (s)
V	Plain C	3.3	3.3	7	6
Nb	Plain C	78	55	70	50
Mn + Nb (in Mn-Nb steel)	Plain C	5	5	5	5
Mn (in Mn-Nb steel)	Nb Steel	0.6	0.6	1.3	1.3
Nb + V (in Nb-V steel)	Plain C	18	18	19	19
V (in Nb-V steel)	Nb Steel	5	6	8	8
Nb (in Nb-V steel)	V Steel	80	56	80	56
Mo (in Mo-Nb steel)	Nb Steel	8	4	9	5
Mo + Nb (in Mo-Nb steel)	Plain C	17	10	18	10

*Includes data from Table 4.2 (a).

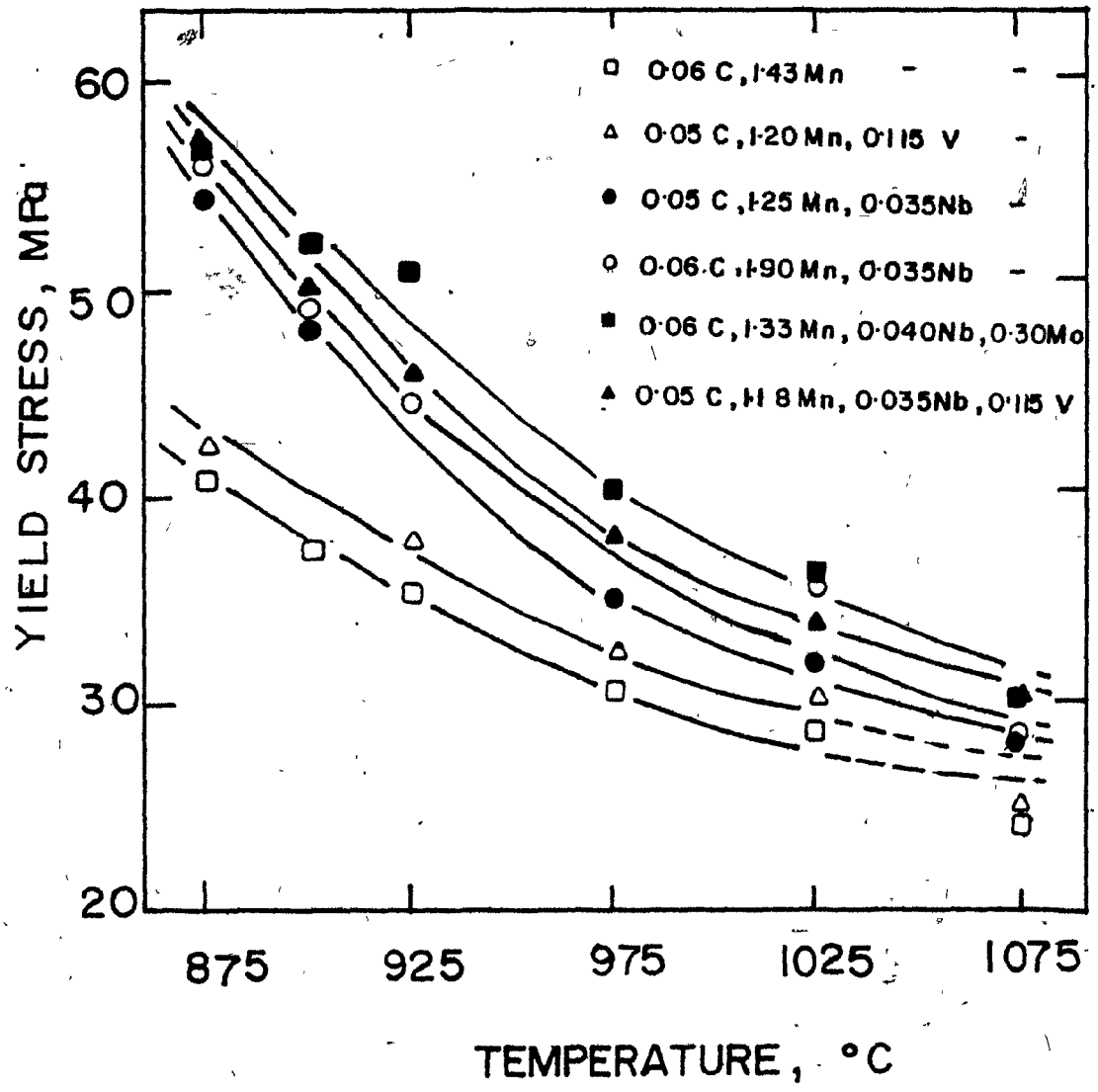

Figure 4.12 Dependence of the yield stress on temperature at $3.2/3.7 \times 10^{-2} s^{-1}$ strain rate.

each of these elements and the similar effects of Mo and V are unlikely to be coincidental, and some of the possible reasons will be discussed in the next chapter.

The temperature dependence of the yield stress at a strain rate of $3.2/3.7 \times 10^{-2} s^{-1}$ is shown in Fig. 4.12. It is interesting to note that the relative positions of the six curves are not strongly affected by the temperature; i.e. that the relative strengthening does not decrease markedly as the temperature is increased. The lower than expected yield stresses of the plain carbon and V-steels at 1075°C is most likely due to some grain growth that took place in these while the temperature was raised from 1030 and 1045°C respectively to the test temperature.

CHAPTER 5

DISCUSSION

5.1 Dynamic Precipitation in Austenite

There is considerable interest in being able to distinguish between the solute and precipitate retardation of recrystallization in austenite. One way of doing so would be to single out each effect, i.e. to determine the precipitation kinetics on the one hand, and to evaluate the relative solute effects of the different additions on the other. This is what has been attempted in the present study. In what follows, a description will first be given of the manner in which dynamic precipitation kinetics were determined. The results for Nb(CN) and VN will then be compared with those reported in the literature. The effects will then be considered of Mn, Mo and V addition on the kinetics of Nb(N) precipitation. Finally, in a separate section, the relative solute effects of Mn, Mo, Nb and V will be described and compared. A possible rationalization of the magnitudes of these effects will be presented and discussed.

5.1.1 Determining the Kinetics of Dynamic Precipitation

The precipitation start (P_s) and finish (P_f) times were determined from the ε_p vs. log $\dot{\varepsilon}$ data of the previous chapter. The method used in this study is basically that of I. Weiss (21,29,30) and involves the location of the hump in the ε_p vs log $\dot{\varepsilon}$ curve. Thus, a mechanical test method was

employed to determine P_s and P_f. The method of Weiss as originally developed, however, depends on a comparison of the slopes of the ε_p vs. log $\dot{\varepsilon}$ curves for the microalloyed steels (in which precipitation occurs) with those for a reference plain carbon steel (in which precipitation is absent). The present modified method, on the other hand, does not require a knowledge of the ε_p vs. log $\dot{\varepsilon}$ dependence for the plain carbon steel and is therefore somewhat simpler to use. For the sake of completeness, the method is described below.

In Fig. 5.1 a schematic ε_p vs. log $\dot{\varepsilon}$ curve is shown. The dashed line B is for the solute case, i.e. the expected behavior if there were only non-precipitating alloy additions. The point at which the two curves A and B diverge at the high strain rate end of the plot defines the strain rate at which precipitation starts, just prior to the peak strain ε_p. P_s is in turn determined from (21,29,30).

$$P_s = \varepsilon_p{}^s/\dot{\varepsilon}_s \qquad (5.1)$$

The curve marked C is parallel to B but shifted along the vertical axis until it is tangent to curve A. The precipitation finish time P_f is determined from the point of maximum divergence (point of tangency) as

$$P_f = \varepsilon_p{}^f/\dot{\varepsilon}_f \qquad (5.2)$$

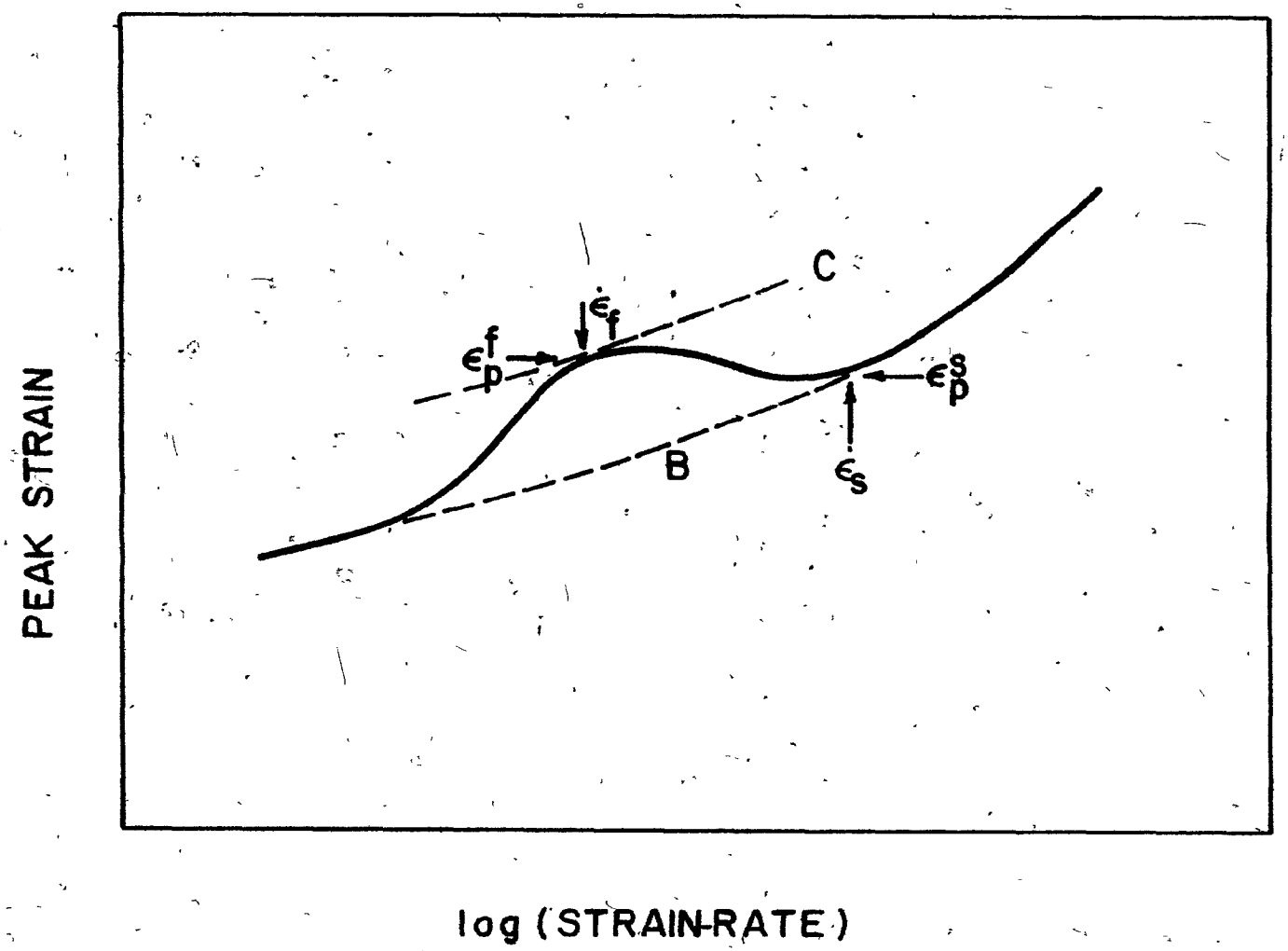

Figure 5.1 A schematic ϵ_p vs. log $\dot{\epsilon}$ curve to demonstrate the method of determining P_s and P_f times.

This represents the condition where precipitation starts early in the test and continues until the peak strain is attained.

5.1.2 Precipitation Kinetics of Nb(CN) in Austenite

The dynamic PTT curves of Nb(CN) in the four Nb bearing steels are shown in Fig. 5.2. Precipitation starts earliest in the base Nb-steel containing 1.25% Mn. Precipitation is delayed by the addition of 0.65% Mn (Mn-Nb steel), 0.30% Mo (Mo-Nb steel) or 0.115% V (Nb-V steel). In what follows, some of the reasons why the addition of these elements may retard the precipitation of Nb(CN) will be presented and the present results will be compared with those reported in the literature.

5.1.2.1 Effect of Mn on Precipitation of Nb(CN)

The dynamic PTT curves for the 1.25 and 1.90% Mn-Nb steels are compared with that for a 0.42% Mn steel in Fig. 5.3. All of these steels had a similar base chemistry and contained 0.05/6% C, and 0.035% Nb.* It is apparent that increasing the Mn concentration from 0.42 to 1.90% moves the PTT curve sharply to the right by more than an order of magni-

*The 0.42% Mn steel included 0.057% Al and 0.05% Si, whereas the higher Mn steels contained 0.025% Al and 0.24% Si. These differences in Al and Si concentration (+0.032 and - 0.19% respectively) are not considered to be significant with regard to the present discussion. This is because Al and Si are not transition elements and, therefore, have a relatively small electronic effect in γ-Fe (63) as will be discussed in more detail in Section 5.2

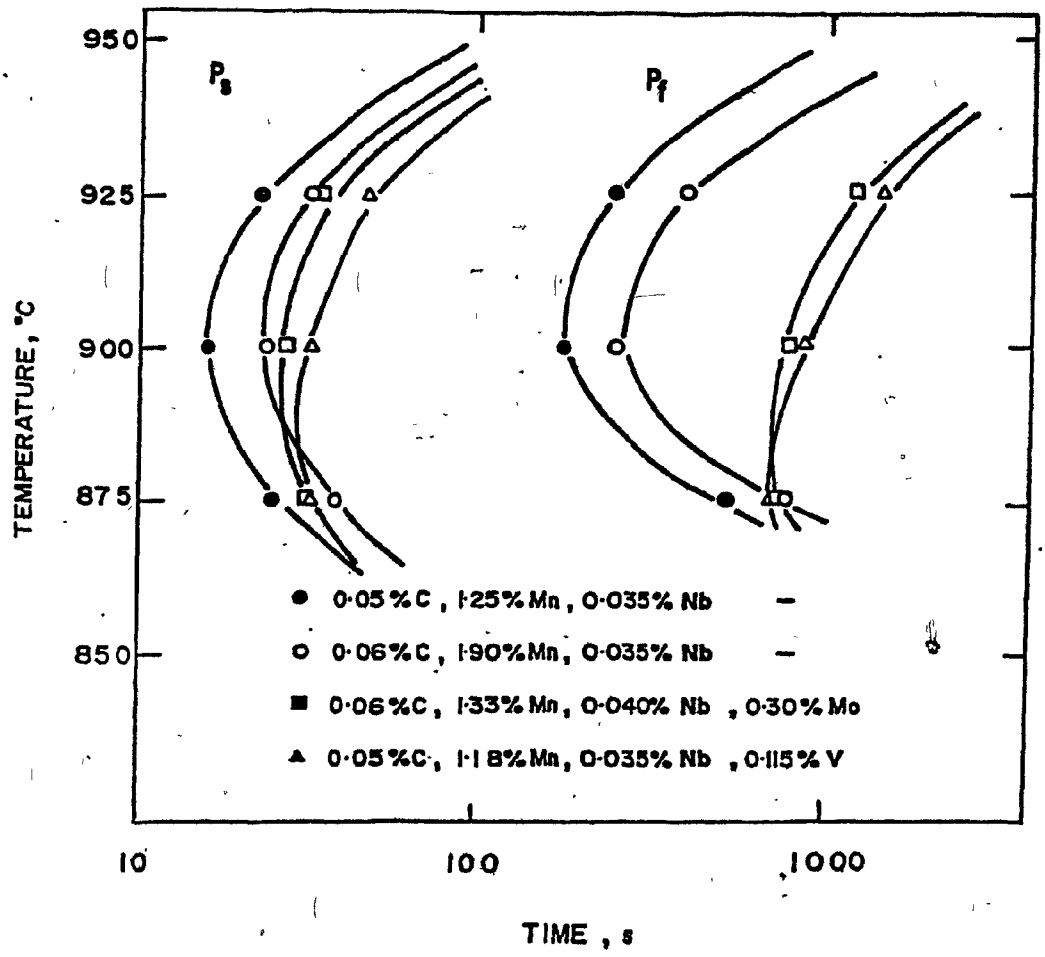

Figure 5.2 PTT curves for the dynamic precipitation of 'Nb(CN)' in the four Nb-bearing steels investigated in the present study.

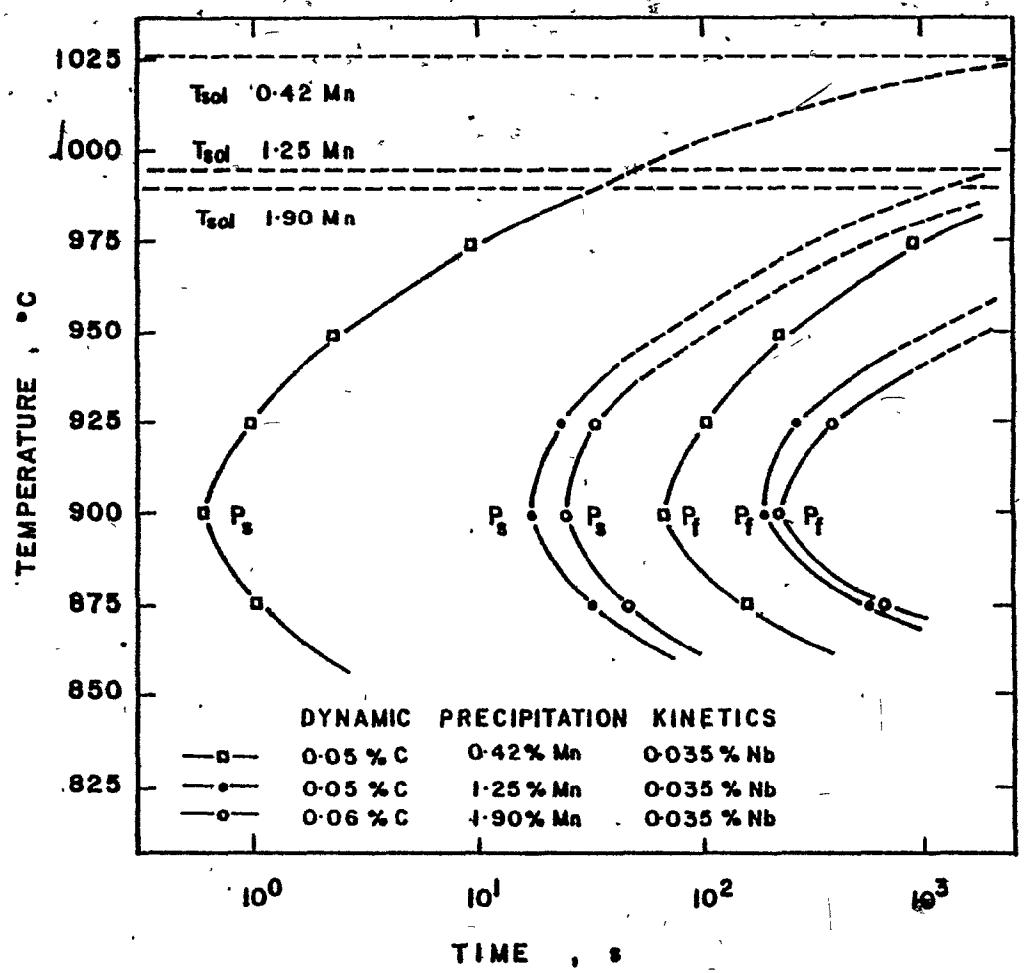

Figure 5.3 The effect of Mn on the dynamic precipitation kinetics of Nb(CN).

tude in time. That is, Mn decreases the rate of Nb(CN) precipitation. The reason for this delay is, in part, due to the effect that Mn has on the Nb(CN) solubility in austenite. The retardation observed in the present investigation is consistent with the observation of V.R. Golik et al. (64) that raising the Mn concentration from 0.75 to 1.20% increases the solubility of carbides in steels of 0.16% C with Nb concentrations of 0.08 to 0.29%. Similar observations have been reported by J. Woodhead (65) regarding the increased solubility of VN in austenite following the addition of Mn. A systematic study carried out by Koyama et al. (66) demonstrated that Mn increases the activity coefficient of Nb in austenite, but that it decreases the activity coefficient of C by a greater magnitude. This effect of Mn on the activity coefficient of C has also been reported by Wada et al. (67). The results of these two investigations are shown in Fig. 5.4. The physical significance of lowering the activity coefficient of an element in an alloy is that the material behaves as if there were less of that particular element present. Thus, lowering the activity coefficient of carbon in austenite by the addition of Mn makes the carbide more soluble because it is equivalent to having a lower concentration of C present. The net result is a decrease in the NbC solubility temperature. Koyama et al. (66) reported that the effect can be described by the following relation:

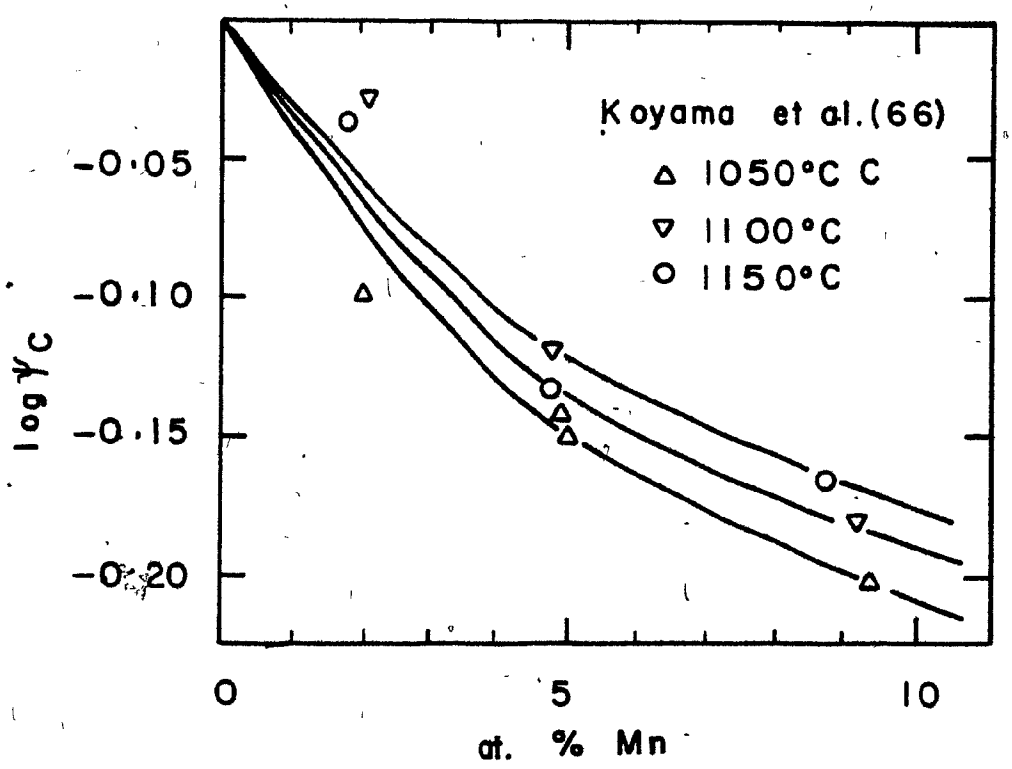

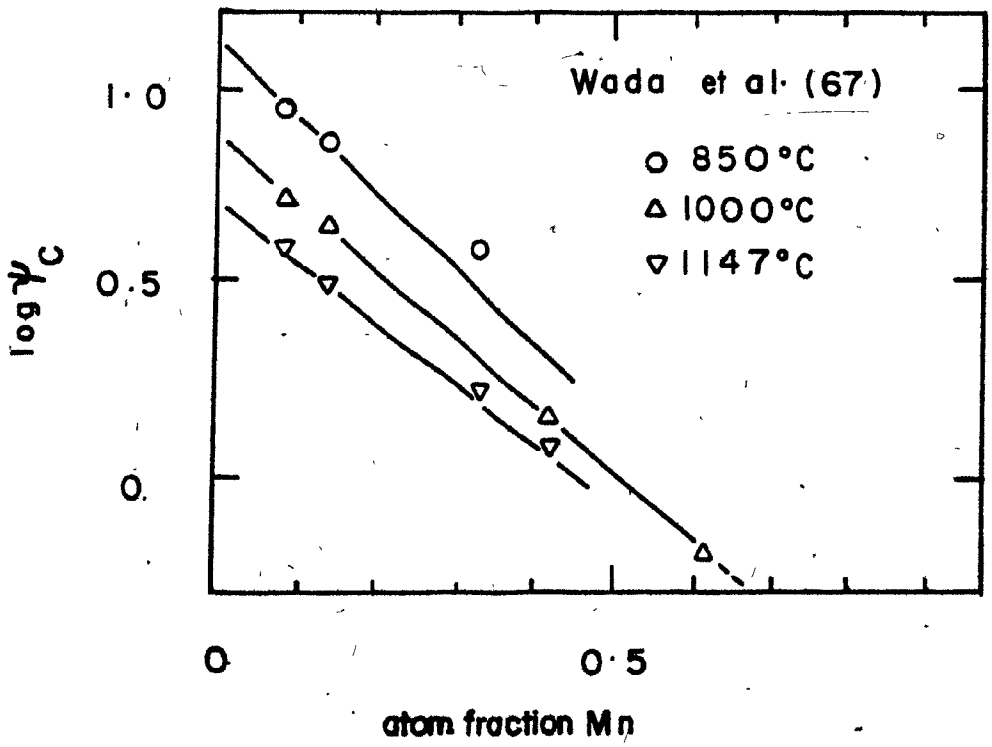

Figure 5.4 The effect of Mn addition on the activity coefficient of carbon as determined by Koyama et al. (66) and by Wada et al. (67).

$$\log(\%Nb)(\%C) = -\frac{7970}{T} + 3.31 + (\frac{1371}{T} - 0.900)(\%\ Mn) - (\frac{75}{T} - 0.0504)(\%Mn)^2 \quad ..(5.3)$$

This relationship leads to solution temperatures of 1027, 996 at 990°C for the 0.42, 1.25 and 1.90% Mn steels, as indicated on Fig. 5.3. The effect of temperature on the solubility of Nb(CN) in these steels is shown in Fig. 5.5. It is evident that, at a given temperature, there is a greater amount of supersaturation (with regard to Nb(CN) precipitation) in the lower Mn steels. The somewhat higher C level in the 1.90% Mn steel (0.06 vs. 0.05% in the other two steels), if accurately determined, may also accelerate the precipitation process due to the greater supersaturation of C.

The effect of Mn on some of the solubility equations for NbC reviewed by Nordberg & Aronsson (69) has been analyzed by the present author. A least squares fit through these data (Table 5.1) led to the following dependence of carbide solubility on the Mn concentration:

$$\log(C)(Nb) = -\frac{8266}{T} + 3.275 + (\frac{983}{T} - 0.59)(wt\%\ Mn) \quad .....(5.4)$$

According to this equation, the calculated solution temperatures for the 0.42, 1.25 and 1.90% Mn steels are 1086, 1059 and 1055°C respectively. (It should be noted that when the composition of the 1.90% Mn steel is adjusted to 0.05% C, this temperature is decreased to 1034°C). The solution temperatures given by

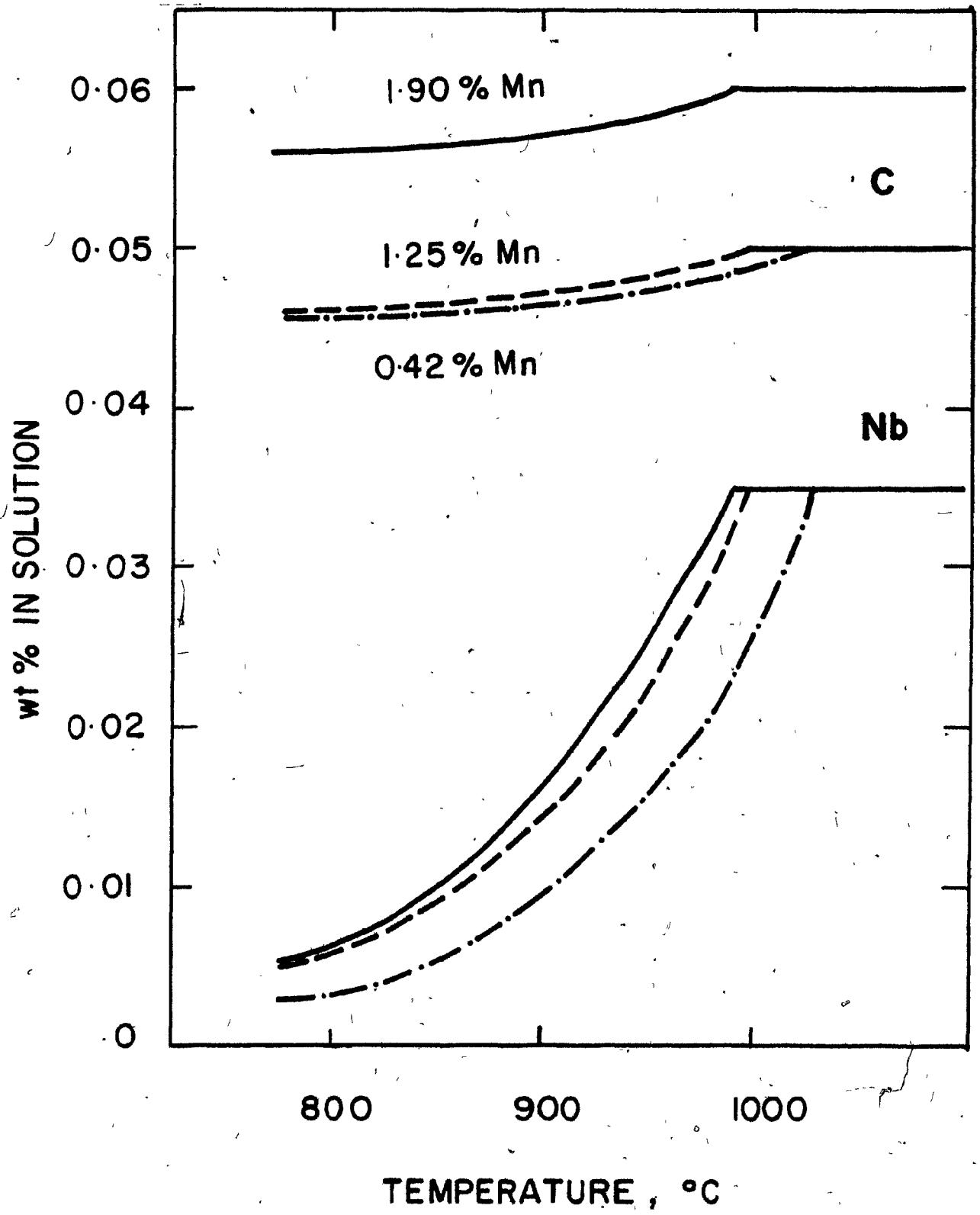

Figure 5.5 Calculated equilibrium solubility of Nb and C in three austenites containing 0.42, 1.25 and 1.90% Mn based on Eq. (5.3) due to Koyama et al. (66).

TABLE 5.1

Equilibrium Solubility Relationships for NbC in Austenites of Different Mn Levels*

% Mn	P	-Q	T°C Range	Nb Range	Method
0	3.7	9100	1000-1300	0-0.8	Equilibration with methane
0	2.26	6770	900-1300	0-0.08	Chemical techniques**
1.0	2.9	7500	900-1200	0.036	Hardness measurement
1.2	3.04	7290	900-1300	0-0.11	Isolation of precipitate
1.4	1.64	5832	880-1000	0.023	Isolation of precipitate
2.2	2.28	6815	880-950	0.019	Isolation of precipitate

*Based on results reported by Nordberg & Aronsson (69).

**See also reference #16.

$$P = 3.28 - 0.5981(\%\ Mn)$$

$$-Q = 8266 - 983(\%\ Mn)$$

$$\log(\%\ Nb)(\%\ C) = -\frac{8266}{T} + 3.28 + \left(\frac{983}{T} - 0.598\right)(\%\ Mn)$$

Eq. (5.4) are higher than those calculated from the Koyama et al. (66) relation. This suggests that the differences in the levels of the other alloying elements, e.g. Si, also affect the solution temperature.

The shapes of the PTT curves in Fig. 5.3 are also changed slightly by the increased Mn concentration. That is, the nose of each curve remains at approximately 900°C even though the location of the nucleation controlled branches of the C-curve is retarded by the decrease in the solution temperature. The observation that the temperature coordinate of the nose does not change indicates that Mn affects, not only the solubility of the carbo-nitride, but also the diffusion of the rate controlling species of the precipitation reaction. (The foregoing discussion is in terms of NbC precipitation alone. It is, nevertheless, likely that Mn has a similar effect on Nb(CN) solubility and similar results have been reported for the effect of Mn addition on the N activity coefficient (16,68). As the N concentration is much lower than the C concentration in these steels, no correction will be made for the influence of N in the discussion that follows.)

As already indicated, above the nose of the PTT curve, nucleation is the rate controlling process (Fig. 5.6(a)). The increased solubility of Nb(CN) is expected to result in a shift of the upper part of the PTT curve to the right, as illustrated in Fig. 5.6(b). If this were the only effect, it would shift the nose of the curve to a lower temperature. In

Opposite page 113

Figure 5.6(a) Illustration of the contributions of the nucleation and diffusion controlled branches of precipitation on the shape of the PTT curves and on the location of the nose time and temperature coordinates.

Figure 5.6 (b) Effect of decreased solubility temperature on the shape of the PTT curve and on the decrease in the nose temperature.

Figure 5.6 (c) Effect of both decreased solubility temperature and decreased diffusivity on shifting the nose of the PTT curve to longer times without changing the nose temperature.

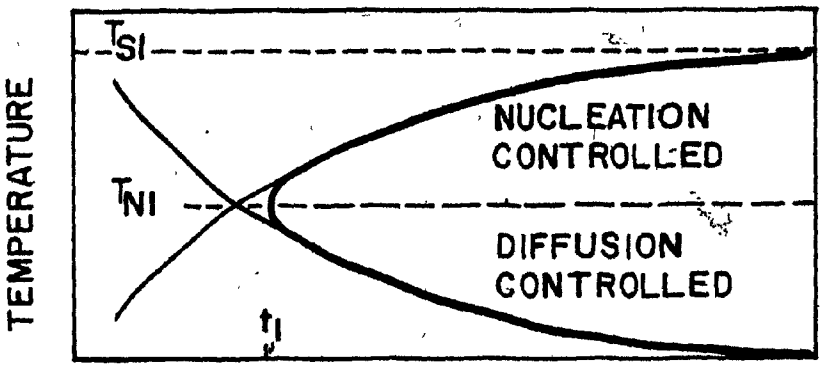
TEMPERATURE
T_{S1}
T_{N1}
NUCLEATION CONTROLLED
DIFFUSION CONTROLLED
t_1
log TIME

(a)

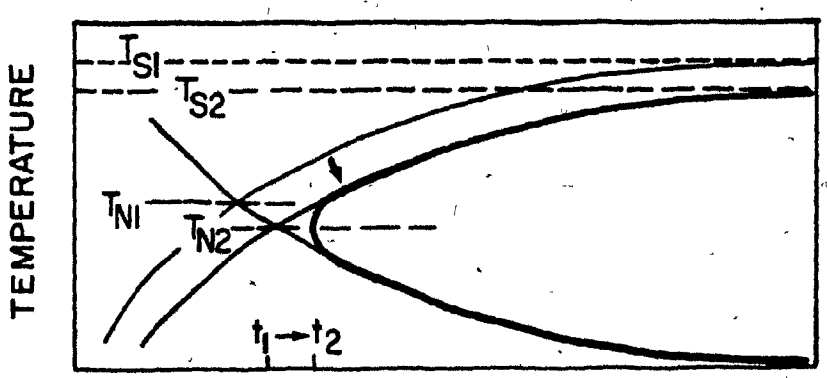
TEMPERATURE
T_{S1}
T_{S2}
T_{N1}
T_{N2}
$t_1 \rightarrow t_2$
log TIME

(b)

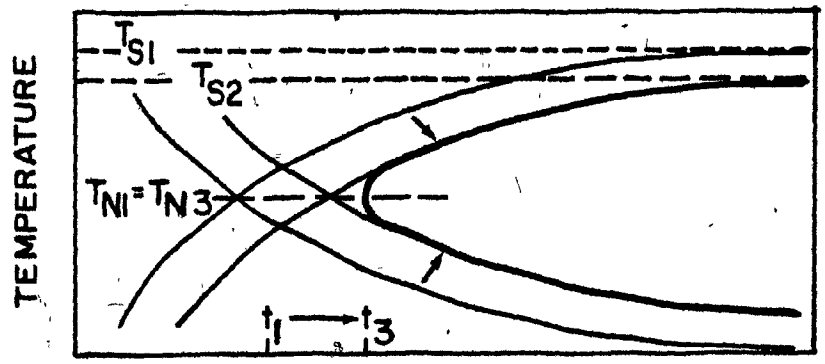
TEMPERATURE
T_{S1}
T_{S2}
$T_{N1} = T_{N3}$
$t_1 \rightarrow t_3$
log TIME

(c)

the present case, however, the lower part of the PTT curve, i.e. the portion below the nose, is also shifted to longer times. In this region, precipitation is growth or diffusion controlled. When both nucleation and growth controlled branches of the PTT curves are shifted to the right by approximately the same amount (Fig. 5.6(c)), the nose of the curve remains at the same temperature. It is, therefore, possible that Mn addition decreases the diffusion rate of Nb while it raises the activity coefficient. The specific reasons for this are not known, but both effects could be linked, for example, to the formation of Nb-Mn complexes.

Comparison with Other Results Reported in Literature

The P_s times for the two current Nb steels are presented together with the results from five other investigations in Fig. 5.7. At 900°C, precipitation starts in the range 0.6 (curve #1) to approximately 45 seconds (curve #5). This disparity (in time) can be attributed to two major factors: (i) differences in the prior heat treatment and state of deformation of each steel; and (ii) different alloy chemistries. The effect of Mn addition on the rate of dynamic precipitation under the same processing conditions (curves #1,6,7) has already been discussed above. This is also evident in curves 4 and 5 below 900°C, where an increase in Mn level from 0.99 to 1.35% retards precipitation. That these two curves cross over at about 915°C is probably due to the

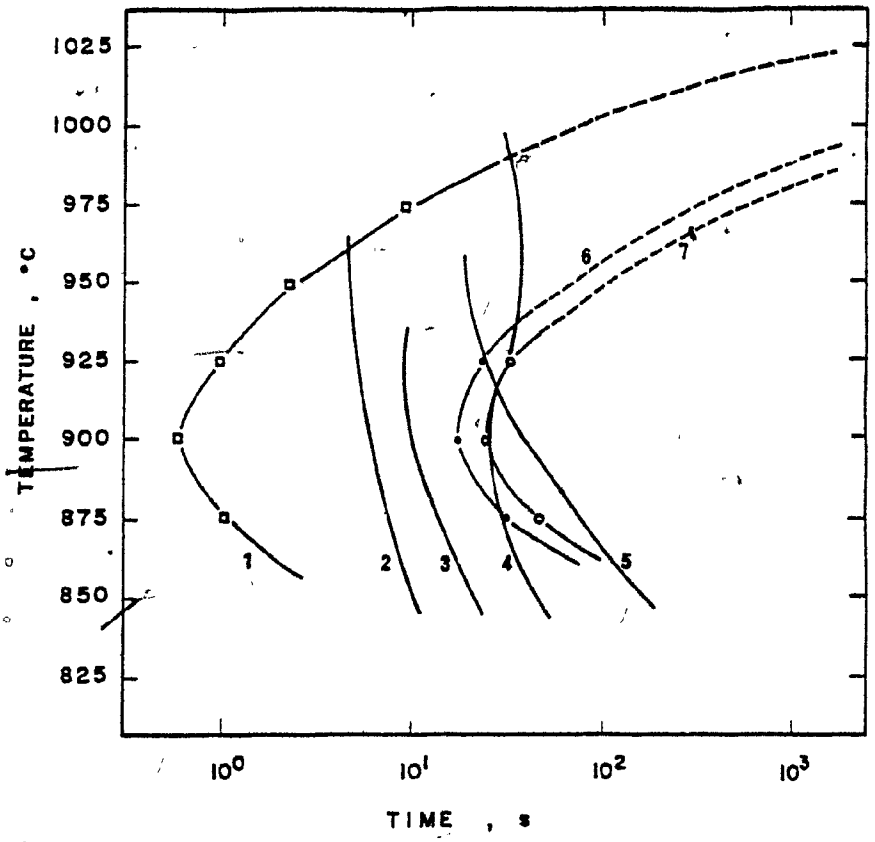

Figure 5.7 Comparison of the precipitation start time for Nb(CN) determined in the present study with some of the results reported in the literature.

LEGEND

Steel #	Composition (wt%) C	Mn	N	Nb	Condition	T_{soln} °C	Reference
1	0.05	0.42	0.004	0.035	deforming	1027	Weiss and Jonas (21)
2	0.17	1.35	0.011	0.040	1.3 ε at 3.6 s^{-1} at 900°C	1165	Le Bon et al.(28)
3	0.06	1.71	0.006	0.084	0.3 ε at 980°C (ε not given)	1113	Watanabe et al.(43)
4	0.1	0.99	0.008	0.04	0.5 ε at temperature (ε not given)	1110	Hoogendorn et al.(57)
5	0.11	1.35	0.01	0.031	0.5 ε at 2.6 s^{-1} at 950°C	1071	Hansen et al.(13)
6	0.05	1.25	0.006	0.035	deforming	996	present
7	0.06	1.90	0.006	0.035	deforming	990	present

somewhat different deformation histories. In the Hansen et al. (13) work (curve #5), the steel was given 50% pre-strain at 950°C at an average strain rate of $2.6\ s^{-1}$; then the temperature was decreased to make the precipitation measurements By contrast, in the Hoogendorn and Spanraft (57) work (curve #4), the material was pre-strained (the strain rate was not reported) at the temperature at which the precipitation kinetics measurements were made. It is, therefore, likely that at the higher temperatures, dynamic, post-dynamic, or classical recrystallization occurred, thus slowing down the precipitation process. At the lower temperatures, on the other hand, pre-cipitation occured in a deformed (or deforming) matrix and is, therefore, strain-induced or 'strain-enhanced'.

Curves #4 and #5 are in good agreement with those determined in this investigation. The higher C concentrations in the steels in curves #4 and #5 (0.10 and 0.11% respectively) are consistent with the noses of these curves being situated at higher temperatures. (Davenport et al. (44) reported that they expected the nose of the PTT curve for a similar steel to be at $\sim$ 950°C. As their results did not permit a full PTT curve to be defined, they were not included in Fig. 5.7). At the lower temperatures, on the other hand, precipitation occurs in a deformed (or deforming) matrix, and is therefore strain induced or 'strain-enhanced'.

The precipitation kinetics reported in curve #2 (Watanabe et al. (43)) are faster than the present work, despite the higher Mn and lower C levels. This is probably due to the considerably higher Nb concentration used by these workers (0.08 vs. 0.035%). In a similar vein, the Le Bon et al. data depicted as curve #2 are for a larger pre-strain (1.3) at a higher strain rate (3.6 s^{-1}). The comparatively short P_s times in their steel are probably due to (i) the higher dislocation density associated with the larger pre-strain, (ii) the higher C concentration in their material (0.17 vs. 0.1% in curves #4 and #5 and 0.06% in curve #3; and (iii) the lower deformation temperature that they used (900°C for all the samples).

In summary, Mn addition retards the precipitation of Nb(CN). This effect is attributed principally to the decrease in the activity coefficients of C and N associated with the increased Mn levels. The kinetics results obtained in this investigation are in broad agreement with those reported in literature, the differences being largely consistent with the different processing methods and starting materials used by the other authors.

5.1.2.2 Effect of Mo Addition on the Precipitation of Nb(CN)

The addition of Mo results in a retardation of Nb(CN) precipitation similar to that produced by the high Mn levels discussed above. The dynamic precipitation kinetics in the Nb and Nb-Mo steels are shown with the PTT curves reported by Watanabe et al. (43) in Fig. 5.8. When the P_s times for the present Nb-Mo steel are compared with those for the base steel, a slight delay is apparent, and the nose seems to drop to a somewhat lower temperature. The changes produced by the addition of Mo are more evident in the P_f times, where the delay is considerably longer. Parallel conclusions can be drawn from the Watanabe et al. (43) data. In their case, Mo accelerates the start of Nb(CN) precipitation by a very small amount; however, by the time precipitation is 85% complete, the retarding effect of Mo addition becomes predominant over a wide temperature range. The P_s times they observed are shorter than the present ones; once again, this is probably due to their higher Nb concentration (0.084% vs. 0.035%). The later completion of precipitation in their steels is probably due to the different deformation histories. The PTT curves from this investigation are for dynamic precipitation; while theirs are for a pre-strain of 30% imposed at 980°C (and therefore for static precipitation). In agreement with the findings of Jonas and Weiss (21), dynamic precipitation not only starts earlier than precipitation in a pre-strained material, it is also completed in a shorter time frame. This is because, when precipitation occurs concurrently with deforma-

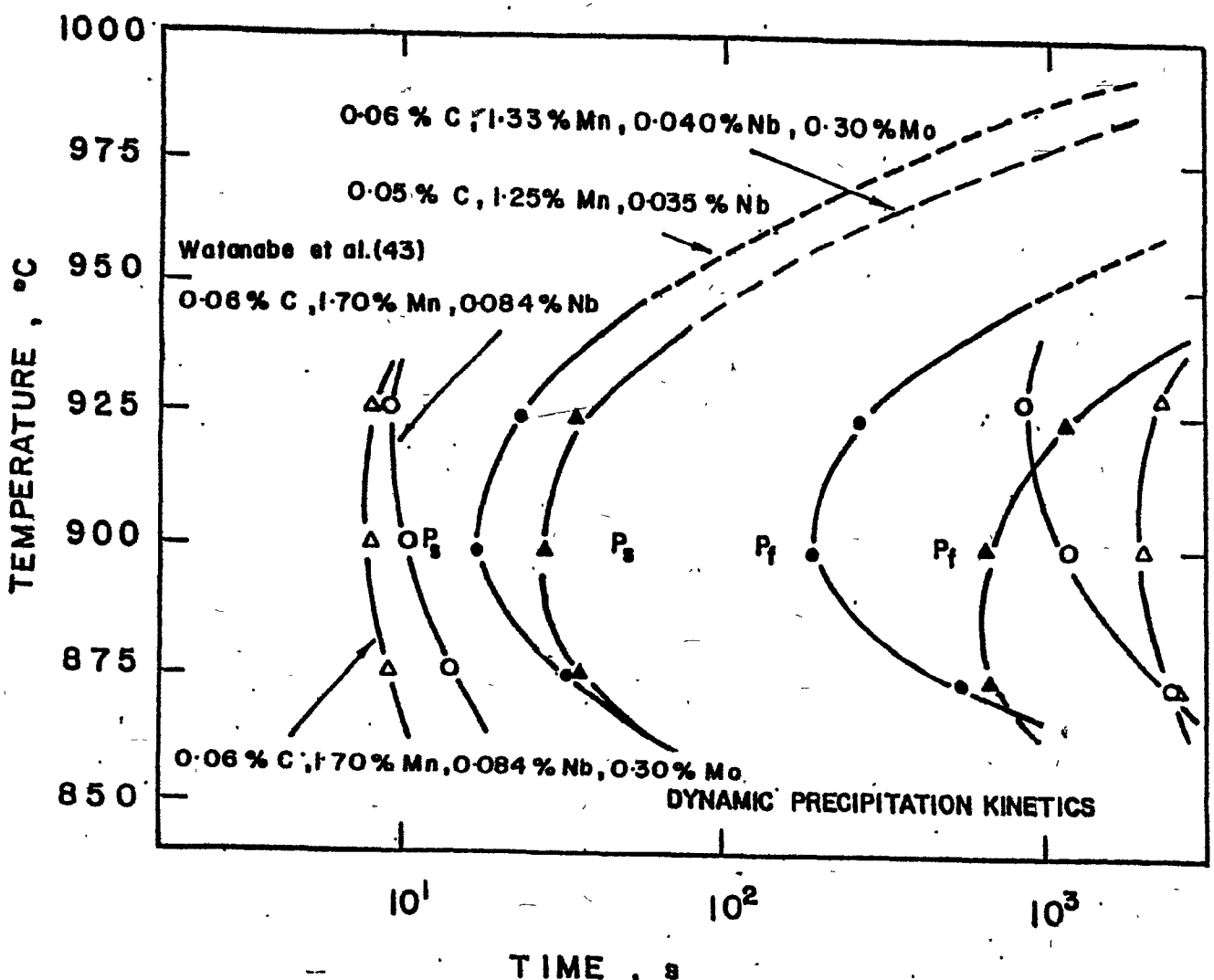

Figure 5.8 Effect of Mo addition on the precipitation kinetics of Nb(CN).

tion, new dislocations and vacancies are constantly being produced, making the rate of diffusion faster, and the progress of precipitation easier. Furthermore, in the pre-strained material, when the critical strain for static or metadynamic recrystallization is exceeded and recrystallization occurs, elimination of the dislocations can lead to a considerable delay in the progress of precipitation, as the latter process is much more difficult in a recrystallized matrix.

The decrease in the nose P_f temperature is more visible in the Watanabe et al. (43) data. This may be a consequence of Mo altering the solubility of Nb(CN), as does Mn. Note, however, that it does not seem to affect the diffusion rate of the Nb or, at least, it does so to a more limited extent (cf. Fig. 5.6(b)). Watanabe et al. argued that "since no significant amount of Mo appeared in the Nb(CN) phase, ... the precipitation kinetics must be influenced indirectly by Mo." They also suggest the possibility that Mo slows down the nucleation rate. The results of Kanazawa et al. (70,71) support the view that the effect of Mo is not through its precipitation in the austenite phase, as the evidence indicates that only a very limited quantity of Mo is found in the precipitates. The above authors (71) also found that Mo addition accelerates the dissolution of the Nb carbonitride in austenite, in agreement with the comments made above regarding Mn addition.

The present author considers that the retardation of Nb(CN) precipitation by Mo addition is due to the increased solubility of the carbonitride, and that this in turn is a consequence of the net effect that Mo has on the activity coefficients of Nb, C and N. The latter conclusion is consistent with the results of Wada et al. (72,73), and of Nishizawa (74), who showed that Mo lowers the activity coefficient of C, as well as with those of Nishizawa (74). To date, no data are available to indicate whether the effect of Mo on the activity of Nb parallels that of Mn.

5.1.3 Dynamic Precipitation of VN in Austenite

The PTT curve for the V steel is presented in Fig. 5.9, together with the curve of Fig. 5.3 for the Nb steel at the same level of Mn concentration. It can be seen that the nose of the curve is at a somewhat lower temperature (885 vs. 905) in keeping with the lower estimated solubility temperature of VN (985 vs. 996°C), which is discussed in greater detail below. Of greater importance are the time coordinates of the noses of the curves, situated at 16 and 26 s for the Nb and V steels, respectively. The present observations indicate that the rate of precipitation of VN during deformation is only slightly slower than the corresponding rate of precipitation of Nb(CN). It is, in fact, about equal to the precipitation rate of Nb(CN) in pre-strained austenite as determined, for example, by the method of Weiss and Jonas (21,29,30).

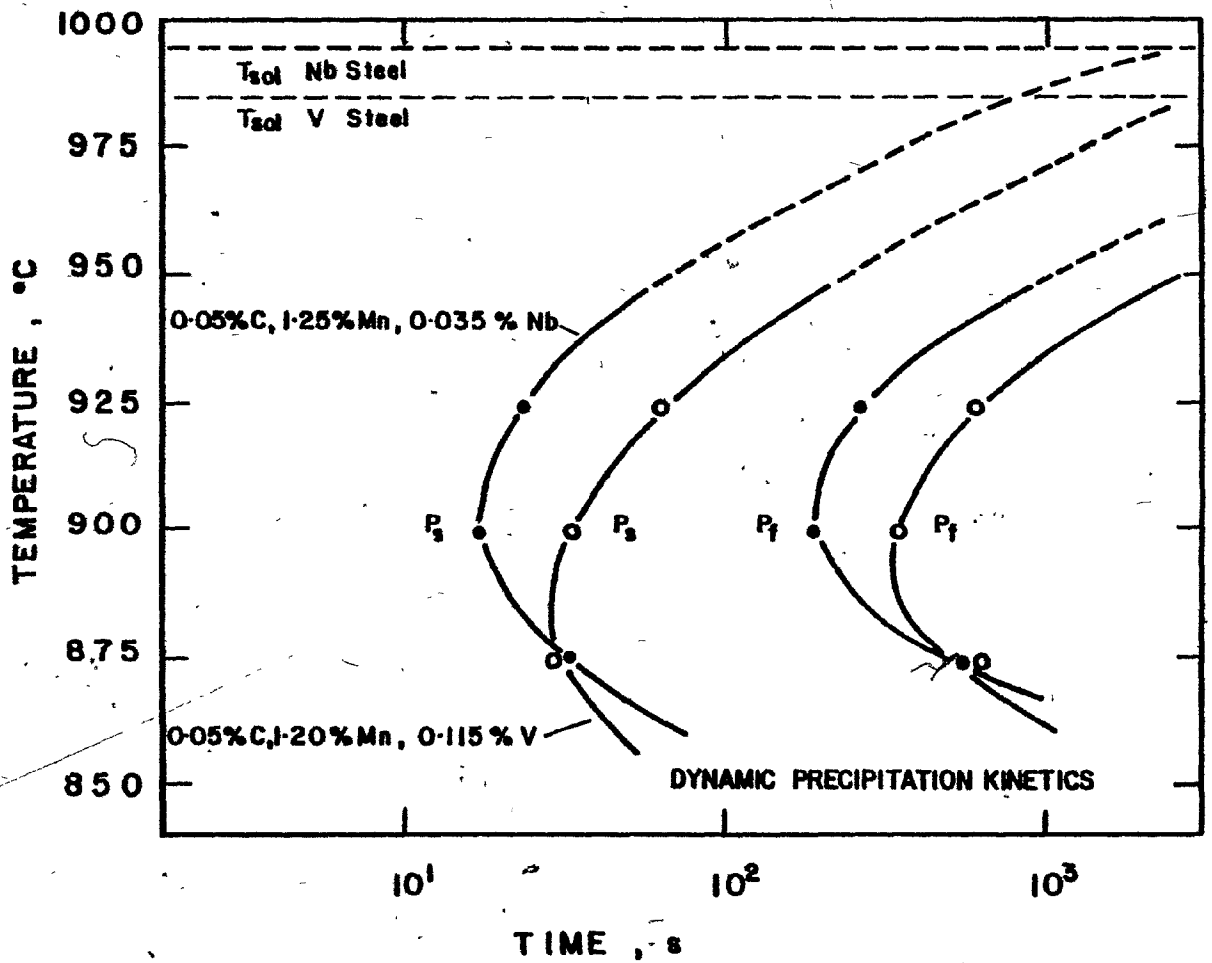

Figure 5.9 Comparison of the dynamic PTT curve for the precipitation of VN with that for Nb(CN) in austenites of similar Mn levels.

The work of Roberts (34), in which he compared the hot deformation behavior of a V and a Nb microalloyed steel, is also of interest in this respect. Roberts estimated the position of the PTT curve for 20% precipitation of V(NC) after 30% pre-strain at a strain rate of 1 s^{-1} (Fig. 5.10). He based this curve on the time to 50% recrystallization (after the above-mentioned pre-deformation) in the two steels, with a foreknowledge of the Nb(CN) precipitation kinetics. At 900°C, his estimated time for 20% precipitation is 60 seconds (Fig. 5.10) and can be expected to be somewhat less for (say) 5% precipitation. The Roberts P_s time for strain induced precipitation is thus longer than the dynamic P_s time for the present V steel. This is consistent with the higher Mn concentration of the Roberts material (compare Figs. 5.9 and 5.10).

The solubility temperature of VN (985°C) shown in Fig. 5.10 was calculated from the following expression (2):

$$\log(V)(N) = -\frac{7733}{T} + 2.99 \qquad (5.5)$$

The Mn levels of the steels on which this relation is based are not known, but are believed to be in the proximity of 1.2% as will become more evident from the relationships described below. Irvine et al. (16) reported the solubility equation for a 1.5% Mn steel as

$$\log(V)(N) = -\frac{8330}{T} + 3.46 \qquad (5.6)$$

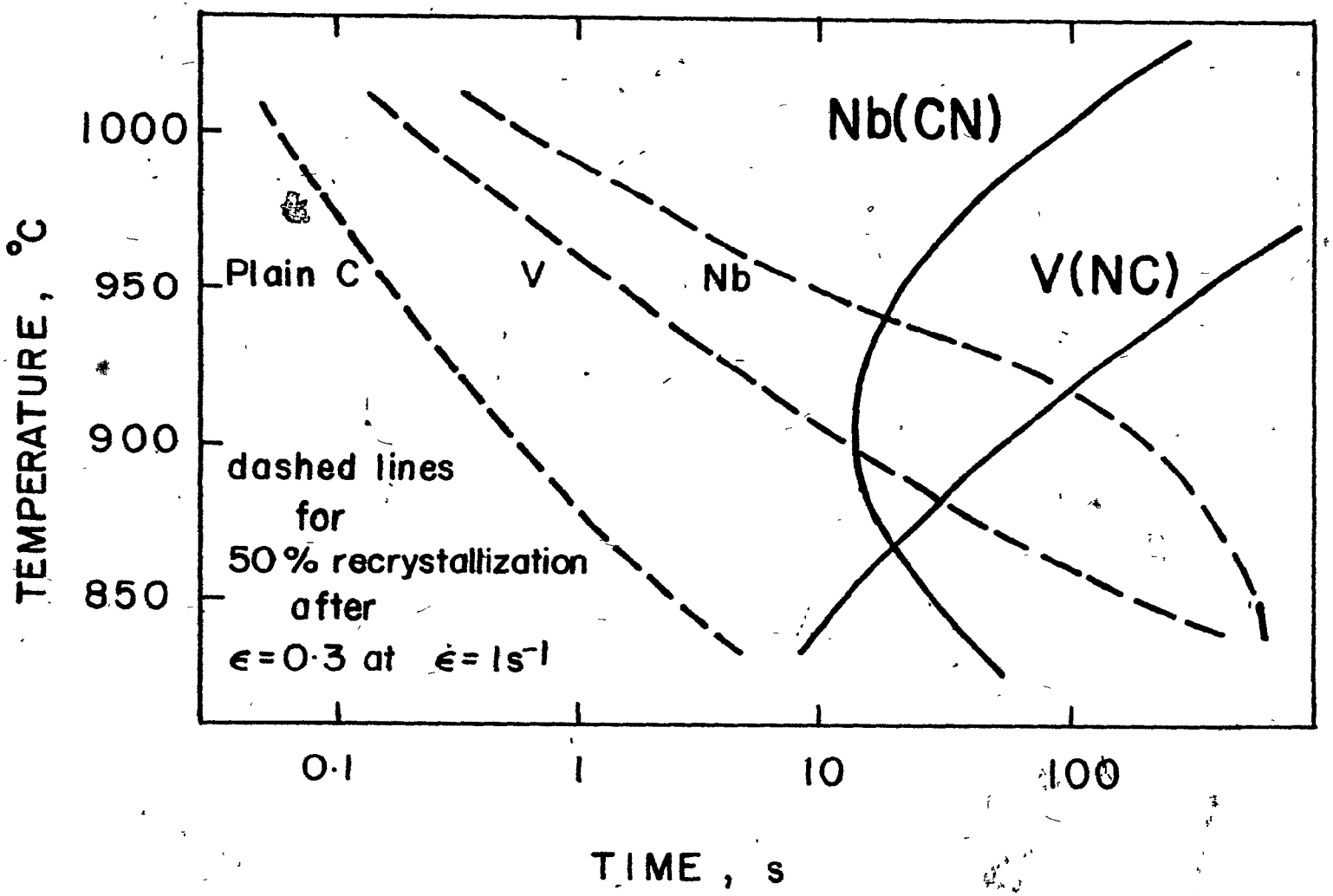

Figure 5.10 Schematic representation of the kinetics for (say) the 20% precipitation of V(NC) and Nb(CN) in austenite. The steel compositions are plain C steel: 0.12% C, 1.11% Mn, Nb steel: 0.18% C, 1.17% Mn, 0.025% Nb, and for the V-steel: 0.09% C, 1.35% Mn and 0.09% V (after Roberts (34)).

They found that the solubility of VN depended on the Mn concentration, and expressed this as:

$$\log(V)(N) = -\frac{8330}{T} + 3.40 + 0.12(\%\ Mn) \qquad (5.7)$$

They suggested that this effect is due to the decrease in the activity coefficient of N caused by Mn addition. (We have adopted here an anologous view regarding the effect of Mn addition on C activity.) The solubility temperature of VN in the present 1.2% Mn, 0.115% V and 0.006% N steel can be estimated as 985, 1025 or 970°C, depending on whether Eq. (5.5), (5.6) or (5.7) is employed, respectively. The solubility temperature of VN can also be estimated from the relationship determined by Frohberg and Graf (75):

$$\log(V)(N) = -\frac{7070}{T} + 2.29 \qquad (5.8)$$

This last equation is for a steel with no Mn; it can therefore be expected to lead to a high solubility temperature. For the present material, this is 1025°C, as is also obtained from Eq. (5.6). These relations (5.5 to 5.8), indicate that the dissolution of VN in the present austenite occurs in the 970-1025°C temperature range, with the lower temperature perhaps being the more likely one. These temperatures are close to the lower end of the Nb(CN) solubility temperature range in steels of similar Mn concentrations.

It should be added that the presence of vanadium carbide precipitates is not expected above 850°C (2) because of their solubility above this temperature, as calculated from (2)

$$\log(V)^{4/3}(C) = -\frac{10800}{T} + 7.06 \qquad (5.9)$$

5.1.4 Precipitation in the Nb-V Austenite

The experimentally determined dynamic precipitation kinetics in the Nb-V steel are compared in Fig. 5.11 with the dynamic PTT curves of Nb(CN) and VN in steels of similar C and Mn concentrations. There are several things worthy of note in this figure:

(i) The precipitation kinetics are slower in the Nb-V steel than in the Nb steel. (V addition retards the precipitation of Nb(CN).)

(ii) Above 900°C, precipitation starts earlier in the Nb-V steel than in the V steel. Below this temperature, the reverse is observed, though to a lesser degree. (This suggests Nb addition retards the precipitation of VN.)

(iii) Precipitation ends later in the Nb-V steel than in the Nb and V steels, the difference in time being smaller at the lower temperatures.

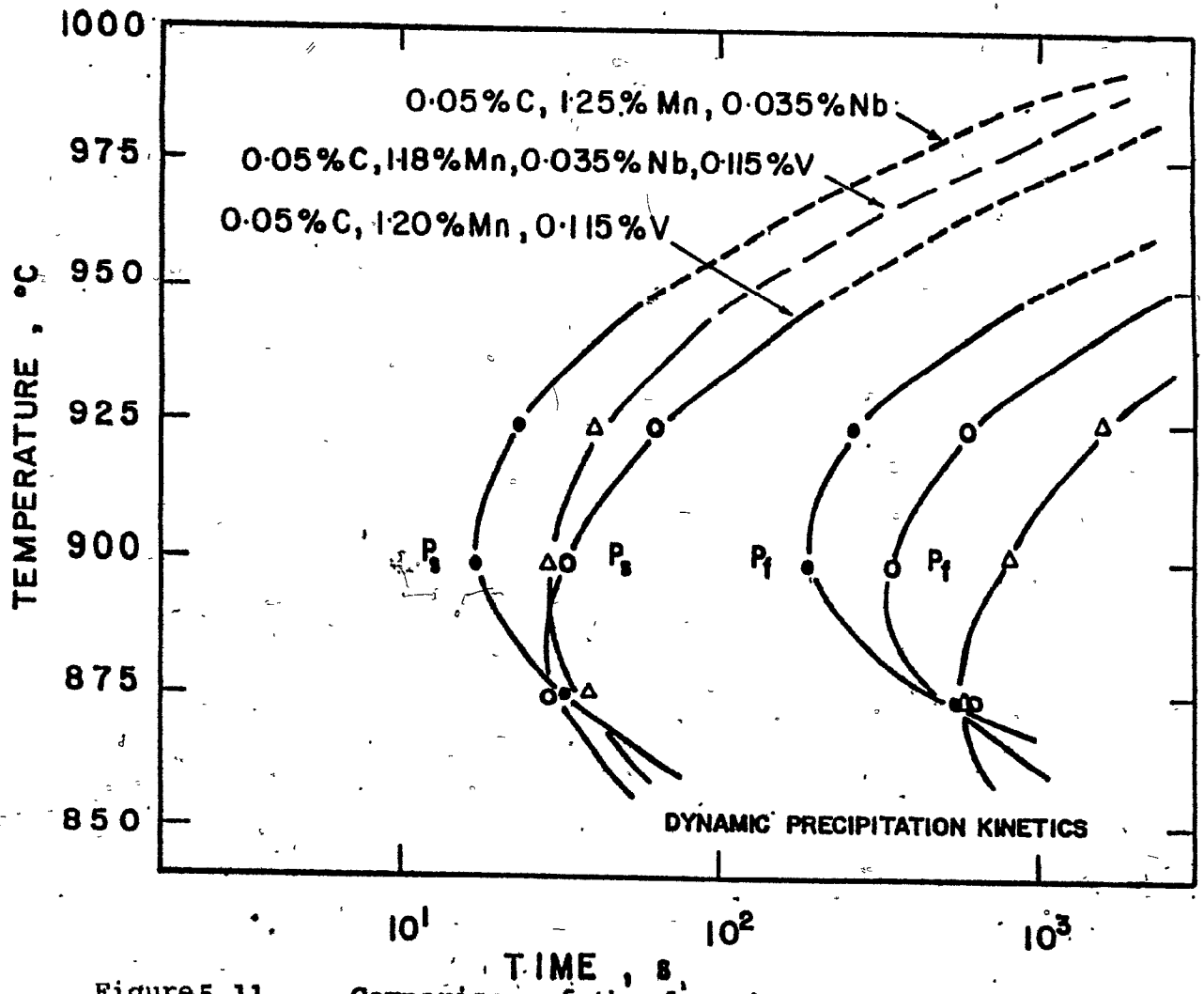

Figure 5.11 Comparison of the dynamic PTT curves for precipitation in three steels: a Nb-bearing steel, a V-bearing steel, and a Nb-V steel.

(iv) The nose of the Nb-V steel PTT curve drops to lower temperatures in going from P_s to P_f, in a manner similar to the drop caused by the addition of Mo to a Nb steel.

The explanation for the first item above lies largely in the expected increase in Nb(CN) solubility due to V addition; much like the effect of Mn and Mo, V addition decreases the activity coefficient of C (72) and also of N (75), as shown in Fig. 5.12. In a similar manner, the addition of Nb to a V steel can be considered to increase the solubility of VN and, therefore, to retard the rate of precipitation of VN in the Nb-V steel below 900°C. Although this approach is an over-simplification, it can account to some extent for conclusion (ii) above, as described in more detail in the next paragraph.

Above 900°C, the Nb-rich precipitates form earlier than the V-rich ones, largely due to the greater supersaturation of the former in this temperature range. At approximately 900°C, the nucleation and diffusion controlled branches of the Nb(CN) PTT curves intersect and are equally rate controlling; cf. Fig. 5.6(a). Below this temperature, the process becomes diffusion controlled for the Nb rich phase. For the V-rich phase, on the other hand (see Fig. 5.9), there is a heavy degree of supersaturation below 900°C, without the process being largely diffusion controlled. Hence, it can be anticipated that the V-rich phase precipitates sooner than the Nb one.

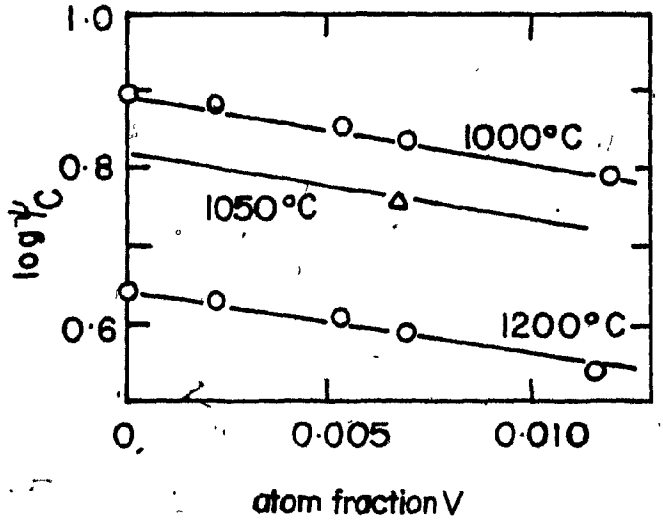

(a)

Figure.12 (a) Effect of V addition to austenite on the activity coefficient of C (after Wada et al. (72)).

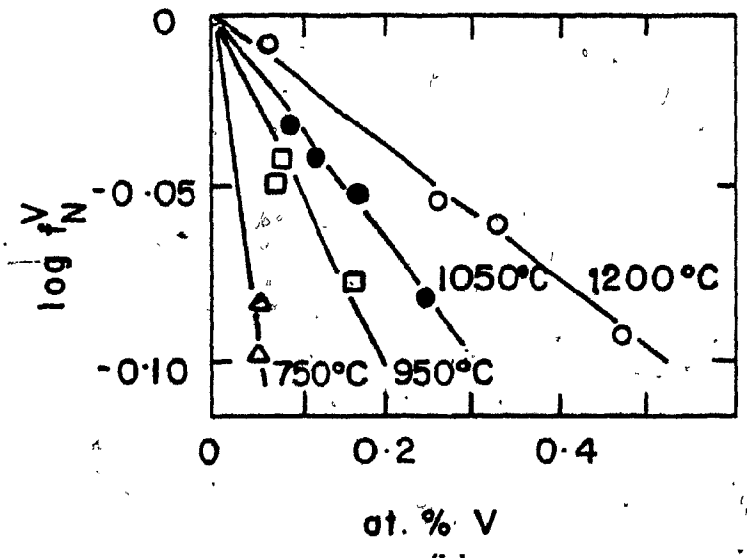

(b)

Figure 5.12 (b) Effect of V addition to austenite and ferrite on the activity coefficient of N (after Frohberg and Graf (75)).

We turn now to a consideration of items (iii) and (iv) above, which involves some knowledge of the composition of the precipitate in the Nb-V steel. The nature of this phase was not investigated, and was not within the scope of this study. It is, however, believed to be a complex (Nb,V)(CN), being very lean in V at the higher temperatures and at earlier times. Near the end of precipitation, due to the longer time and greater density of available nucleation sites, e.g. the existing Nb(CN) particles, a V-N rich phase is expected to precipitate. Behavior similar to this in nature has been observed in Ti-Nb steels where the Ti-rich phase precipitates almost instantly and the Nb-rich ones precipitate at lower temperatures and longer times onto the previously formed phase (76).

It was suggested above that, based on the shapes of the PTT curves in Fig. 5.3, it was possible that Mn addition decreased the diffusion rate of Nb in γ-Fe. It will now be hypothesized that both Mo and V addition decrease the rate of diffusion of Nb in γ-Fe. Furthermore, the possibility that Nb addition decreases the rate of diffusion of V in austenite will also be examined. These effects, if they occur, will modify the shapes of the PTT curves along the lines already discussed above for Mn addition. First of all, they will prevent the nose of the curve from dropping to the extent expected when the diffusion rate of the controlling species is not modified by an alloying addition. This has to do with the direct link between diffusion rate and the lower branch

of the PTT curve. However, it is possible that the decrease in diffusion rate also affects the upper branch of the curve, and in particular the finish time, rather than the start time (i.e. the growth rather than the nucleation process). Thus, the present results are consistent with the proposition that precipitation in the Nb-V steels takes longer than in either the base Nb or the base V steel because the addition of Nb to a V steel retards the rate of diffusion of V, and vice versa.

5.2 Dynamic Recrystallization-Time-Temperature (RTT) Curves

5.2.1 Recrystallization Start Time

The time to the onset of dynamic recrystallization R_s can be determined from:

$$R_s = \varepsilon_p / \dot{\varepsilon} \qquad (5.10)$$

in a manner analogous to the determination of the P_s and P_f times previously described. Here, ε_p is the peak strain at the associated strain rate $\dot{\varepsilon}$. The actual recrystallization start times are estimated to be approximately 5/6 of R_s, based on the work of Rossard et al. (77). For the strain rates used in this investigation, as will become evident below, this difference is of no practical significance.

To construct RTT curves for the current materials, compression tests were performed at a single strain rate of $3.7 \times 10^{-2} s^{-1}$. This strain rate was selected because it was the lowest that could be used under the condition that little or

no precipitation takes place prior to the attainment of the peak strain. (The latter was limited to 0.8 with the equipment available.) For all the six steels, this stipulation was likely to be respected, even at the lowest testing temperature (see Figs. 4.8 and 4.9). This is because, at the selected strain rate, the time of the test to a strain of 0.8 is 20 seconds, which is just long enough for some limited precipitation to start, if any at all.

The tests were conducted in the temperature range 875-1075°C. The flow curves are presented in Appendix B, and have all been reproduced in case they are of utility for the calculation of rolling loads. The R_s times were determined from the peak strains in these flow curves, and the RTT curves that resulted are presented in Fig. 5.13. The R_s times are shortest for the plain C steel, followed by the V steel, in good agreement with observations in the literature. The Nb bearing steels all have longer R_s times.* The delay produced by V addition (compare the curves for the plain C and the V steels) is approximately the same over the whole range of

---

*Note that the plain C and V steels for the 925 and 875°C tests were austenitized at 1075°C (the highest testing temperature) for 15 minutes rather than at 1030°C and at 1045°C respectively for the usual 30 minutes. These higher temperatures were used to compensate for the somewhat smaller grain sizes in these two steels in comparison to the Nb-bearing ones, which had been heat treated at 1100°C for half an hour.

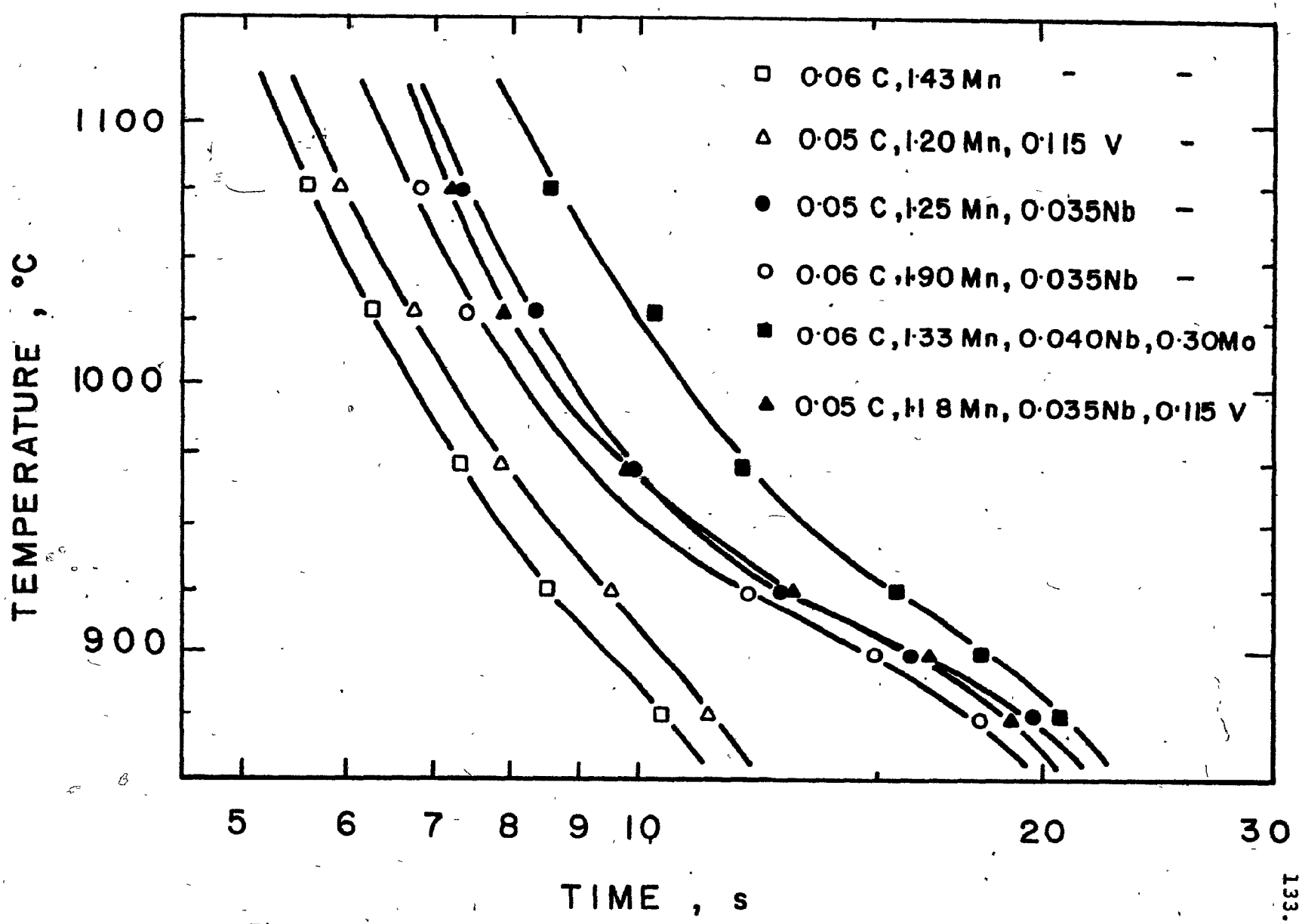

Figure 5.13 Experimentally determined recrystallization start times for the six steels investigated, deformed at a strain rate of $3.7 \times 10^{-2} s^{-1}$.

temperatures investigated and is due to the solute retardation effect of V on dynamic recrystallization. The addition of Nb at similar Mn levels (compare the curves for the plain C and the 1.25% Mn, 0.035% Nb steels), however, leads to greater delays in recrystallization below 925°C than at the higher temperatures. This can be attributed to the interaction between precipitation and recrystallization in the Nb steel, which is elaborated on in the next section. At 900°C, where the nose of the PTT curve for Nb(CN) precipitation is located, some precipitation starts just before the peak strain is reached (see Fig. 5.13). This probably causes the delay in the recrystallization start time beyond that due to the solute retarding effect of Nb.

It is clear from Fig. 5.13 that Nb alone has a greater solute retarding effect than V. Somewhat unexpectedly, the addition of V to the Nb steel does not lead to an increase in retardation. Instead, the R_s time follows the behaviour of the simple Nb steel and the R_s times for these two steels are almost indistinguishable. The RTT curve for the Mn-Nb steel is located at shorter times than the curve for the Nb steel. Although more complex explanations are possible, this lack of difference between the Nb-V and the Nb steels may be due to the somewhat smaller grain size in the former, as in the case of the Mn-Nb steel (see Table 3.1). As shown by Sah et al. (18), smaller grain sizes lead to smaller peak strains, and therefore to shorter R_s times. For the same grain size as the Nb steel, the R_s curve for the Mn-Nb steel

is expected to lie at about the same location, or possibly slightly to the right of the curve for the Nb steel.

When Mo is added to the Nb steel, the greatest postponement in recrystallization is produced among the five HSLA steels investigated. The probable reason why the RTT curve for this steel is not deflected rightward and upward below 925°C will be considered in more detail in the next section.

5.2.2 Recrystallization Finish Times

The R_s and R_f (recrystallization start and finish) times for the plain C, V and Nb steels are presented in Fig. 5.14. The R_f times were calculated from

$$R_f = \varepsilon_f / 3.7 \times 10^{-2}$$

Here ε_f is the strain at which the first cycle of recrystallization is terminated (78). The R_f times are incomplete at the lower temperatures in the Nb bearing steels. This is because the strain was limited to 0.8 in the test method adopted, so that the test could not be continued to the end of the first cycle of recrystallization. The R_f values were not included in Fig. 5.13 to make the figure clearer.

5.2.3 Solute and Precipitate Retardation of Recrystallization

Dynamic R_s times were also calculated (as described above) from the data of Weiss (79) at a strain rate of 3.7×10^{-2} s^{-1}. The results obtained for a plain C and a Nb steel are presented in Fig. 5.15 with the plain C and Nb steel data from

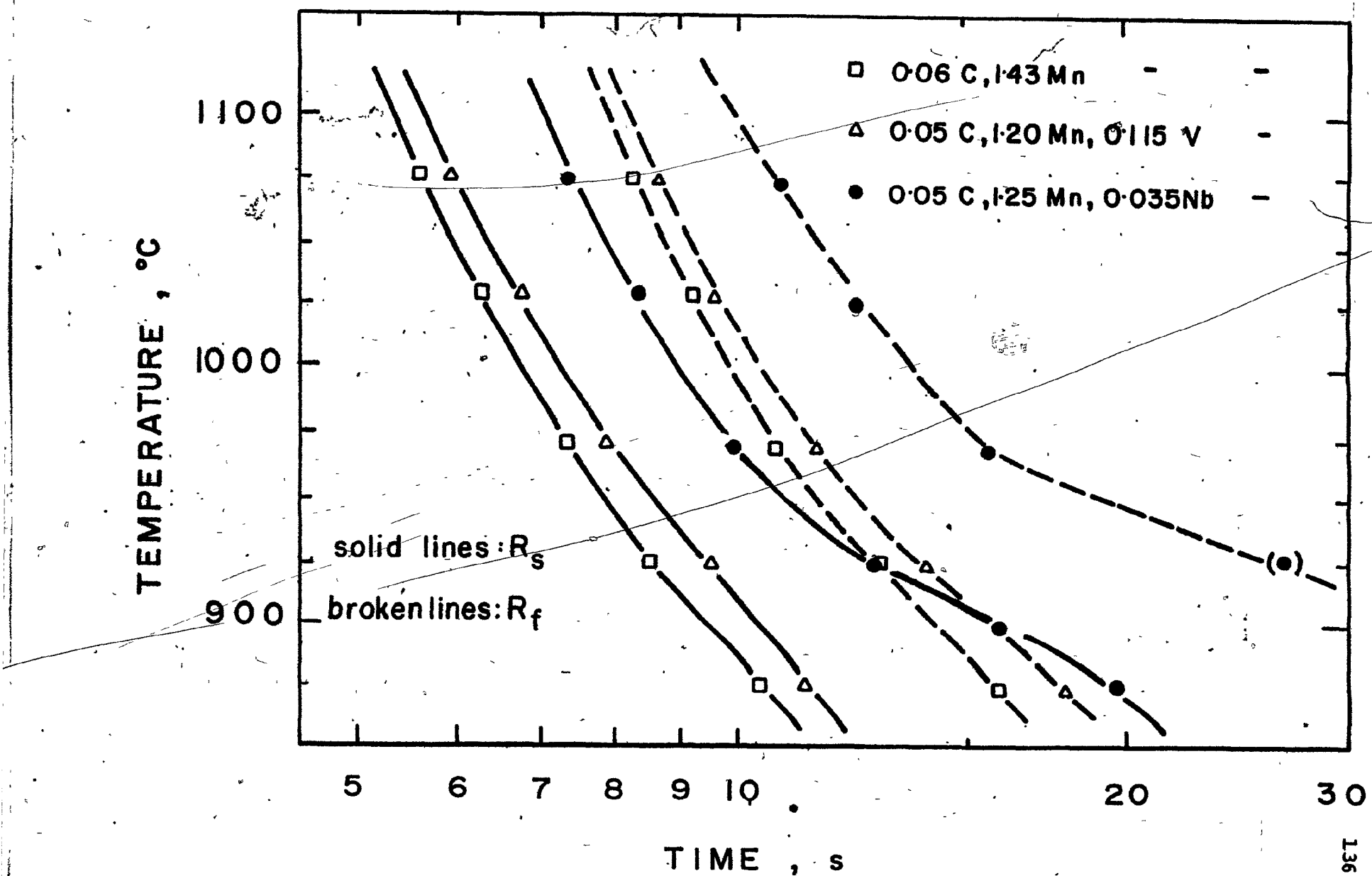

Figure5.14 Recrystallization start (R_s) and finish (R_f) times for the plain C, Nb and V steels, deformed at a strain rate of $3.7 \times 10^{-2} s^{-1}$.

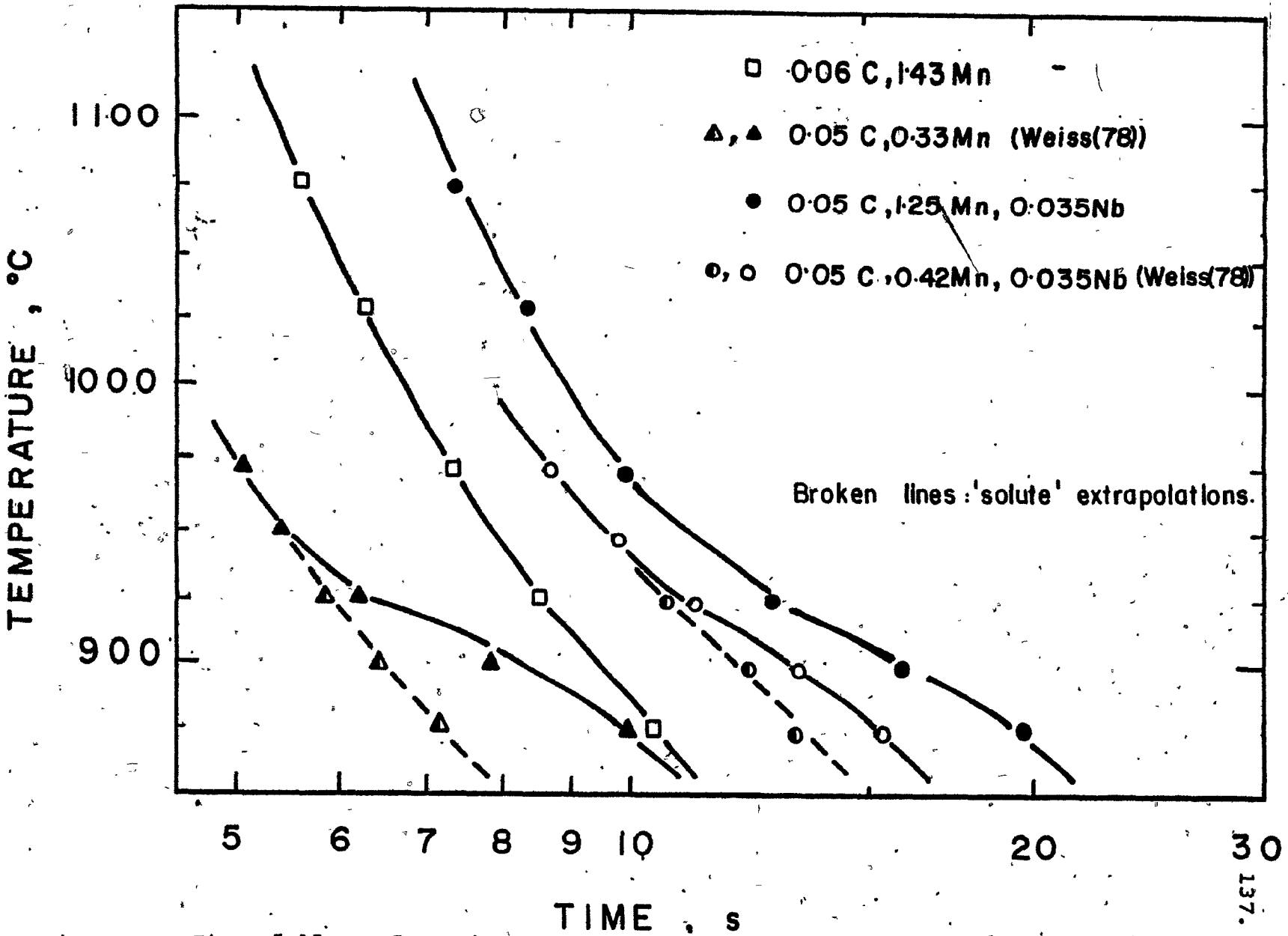

Figure 5.15 Comparison of R_s times in the present plain C and Nb steels with the data due to Weiss (79) for plain C and Nb steels of different base chemistries.

this investigation. The differences between the overall time coordinates for the two plain C steels are probably due to the considerably different chemistries of these steels. The steel studied by Weiss contained 0.007% Si, 0.33% Mn, 0.09% Al and 0.021% S and can be compared with the present composition of 0.24% Si, 1.43% Mn, 0.025% Al and 0.012% S. The greater concentration of Mn and Si in the current research accounts for the longer R_s times in the current steel. For example, at 975°C, R_s is around 5 s in the Weiss plain C steel compared with more than 7 s in the present one. The pronounced change in the slope of the curve for the Weiss plain C steel below 950°C is possibly due to AlN precipitation, which is expected to occur dynamically at these strain rates and temperatures, as shown by Michel and Jonas (32). In the absence of precipitation, this curve would be expected to be parallel to the other plain C steel curve, as indicated by the dashed line.

In a like fashion, the dashed line for the Weiss steel in Fig. 5.15 indicates the expected solute retardation due to Nb addition. These points were calculated from the hypothetical peak strains expected in the absence of precipitation; i.e. they correspond to the peak strains represented by the dashed line B in Fig. 5.1. The points on the solid line were calculated from the experimentally observed peak strains. The R_s times for solute and precipitate retardation shown in Fig. 5.15 were readily calculated for the Weiss Nb steel because the faster precipitation kinetics in this steel

(see Section 5.1.2 and Fig. 5.3) permitted the two effects to be more easily distinguished at this strain rate.

5.2.4 Comparison between Static and Dynamic Recrystallization Kinetics

Classical (static) and post dynamic recrystallization kinetics are considerably different, in terms of time, than the dynamic ones discussed above. For example, the static R_s times for the plain C grades are generally about an order of magnitude shorter than suggested by Fig. 5.13 to Fig. 5.15. Furthermore, the static times for the microalloyed grades can actually be longer than the dynamic times indicated in the above figures. Thus, the dynamic times for the full range of steels appear to be more 'compressed' than are the static times usually reported for the same steels. The data of Le Bon et al. (28) for a 0.17% C, 1.35% Mn and a 0.17% C, 1.35% Mn, 0.040% Nb steel indicate that above 950°C recrystallization starts in less than one second for both steels (Fig. 5.16). In fact, recrystallization starts in less than a second at temperatures as low as 800°C in the plain C steel. In the Nb steel, the process is delayed by more than an order of magnitude at 900°C and the R_s times are of the order of 10-50 seconds at 850°C. (The so-called "reverse-knee" at 900°C is due to the 'interaction' between recrystallization and precipitation, which will be considered in more detail below.) The static R_s times change in the Nb steel by more than two orders of magnitude in time over a 200°C temperature range. By contrast, in the

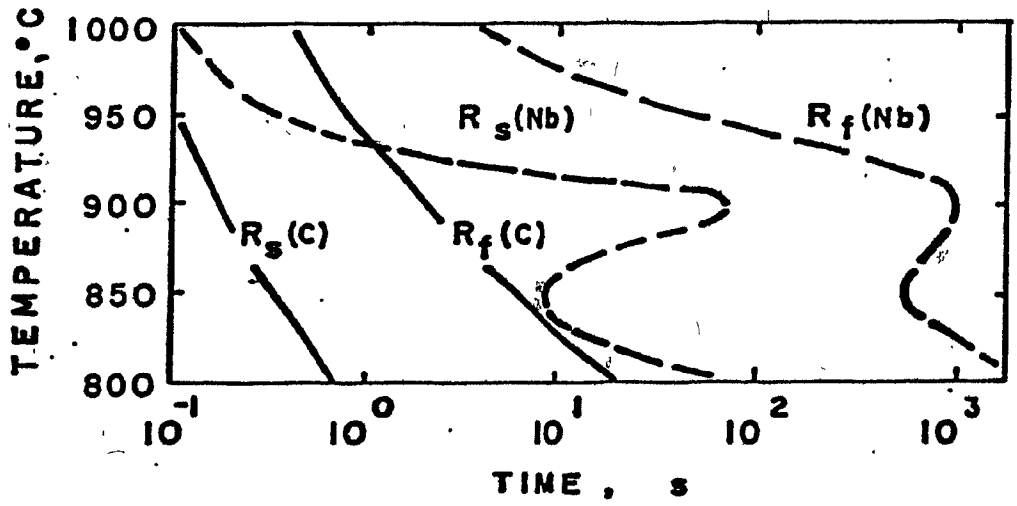

Figure 5.16 Comparison of the recrystallization kinetics of the plain C and Nb-modified steels, as reported by Le Bon et al. (28).

case of dynamic recrystallization over the same temperature range, the R_s times increase by only half an order of magnitude in time, or perhaps even less (see Fig. 5.13) for the strain rate selected here. (A different strain rate shifts the RTT curves along the log (time) axis.) It should be noted that the shape of the plain C curve of the present study does not change when shifting from the static to dynamic case. In the Nb or V steel, on the other hand, whether or not a shift occurs depends on the particular strain rate selected. At strain rates greater than $3.7 \times 10^{-2} s^{-1}$ (i.e. further to the right of the 'humps' in Figs. 4.8 and 4.9), the slight "reverse-knee" evident below 925°C in Fig. 5.13 will generally disappear almost completely, as the whole curve shifts to shorter times. At lower strain rates (i.e. within the 'hump'), the "reverse-knee" is expected to become more noticeable. Under these conditions, the curve moves to generally longer times.

It is apparent from the above discussion that the relation between the static and dynamic times is not a simple one. Nevertheless, many fewer tests are required to determine the dynamic than the static RTT curves. It is, therefore, of considerable interest to find a "calibration factor" relating the two types of recrystallization processes. (It is unfortunately, unlikely to be a constant.) The relationship could be determined by running both types of test on a given material, for example, on a non-precipitating, plain C steel, and for a selected Nb steel. If this were done, and if a "parallel" behavior were to be found for the materials of each type, then

it is possible that simple extrapolations could be performed to estimate the static RTT curves from the more easily established dynamic ones.

5.3 Interaction between Recrystallization and Precipitation

5.3.1 The Dynamic Case

In the preceding section, the RTT curves for the six steels investigated were discussed. The "reverse-knee" seen in the Nb steel curves was ascribed to the initiation of precipitation prior to recrystallization. This explanation will now be considered much more closely. For this purpose, the RTT curves for the Nb and the V steels are reproduced together with the Nb(CN) and the VN PTT curves in Fig. 5.17. It can be seen that the RTT curve of the Nb steel is intersected by the 5% Nb(CN) PTT curve in the vicinity of 900°C. The rightward deviation of the RTT curve can be explained on the following basis. First, an extrapolation is made of the 'no-precipitation' (solute modified, only) RTT curve for the Nb steel. (This is depicted as a broken line.) Then an estimate was made of the 0% Nb(CN) PTT curve as shown (broken line). It is the intersection of the 0% PTT line (P_s) with the solute modified RTT curve that leads to the deflection of the observed RTT curve. This argument has been advanced in more detail by Weiss and Jonas (21,29), Kreye and Hornbogen (80), Hansen et al. (13) and Akben et al. (63), amongst others.

Turning now to the case of the V steel, it is apparent that there is no hint of a "reverse-knee" in the V RTT data.

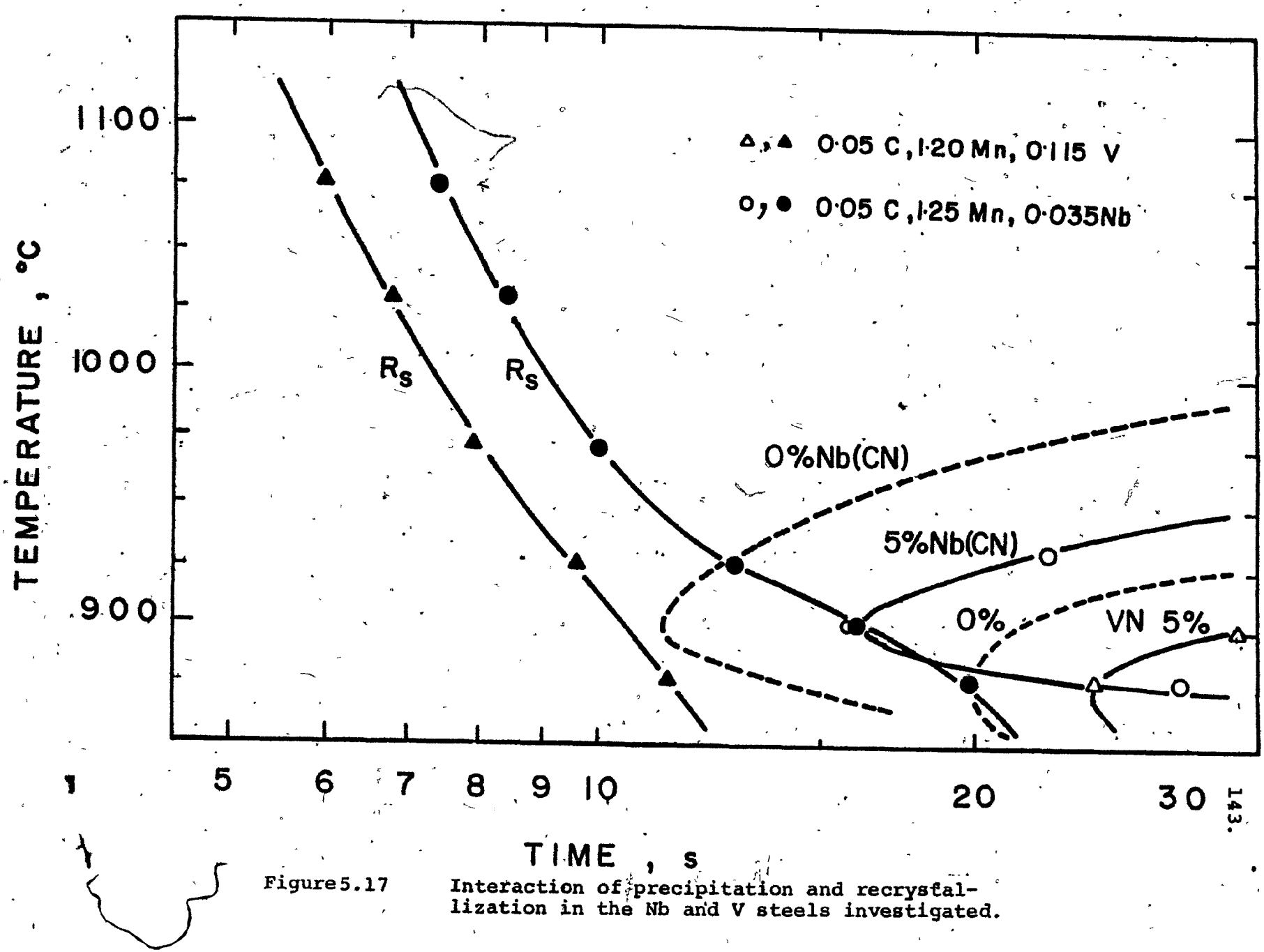

Figure 5.17 Interaction of precipitation and recrystallization in the Nb and V steels investigated.

In terms of the present model, this is because neither the 5% nor the estimated 0%, VN PTT curve intercepts the RTT curve. These two sets of curves are typical of the kinds of interactions between recrystallization and precipitation that are found in microalloyed steels. In this way, they lead to an insight into why a microalloying element such as Nb is particularly effective as a controlled rolling reagent, whereas others, such as V and Al, are less so.

5.3.2 The Strain Induced (Industrial) Condition

The above example is for the interaction between dynamic recrystallization and dynamic precipitation. In the controlled rolling process dynamic precipitation can occur during a particular rolling pass, but it is unlikely to be as important as static precipitation. This is because the elapsed time during rolling (i.e. during passage through the deformation zone) ranges from about 0.1 ms in the finishing stages of strip rolling to about 100 ms during the roughing stages of the ingot or slab breakdown, whereas the time between passes is much longer, falling in the range 100 ms for strip rolling to 10 s for ingot breakdown. That is, the time available for static precipitation is generally about two orders of magnitude greater than for dynamic precipitation.

A given rolling pass may, or may not, be followed by static recrystallization during the interpass time.*

---

*see following page

Generally speaking, the statically and dynamically formed precipitates (if they can nucleate on dislocations) prevent or delay both recovery and recrystallization after each pass. When this operation is carried out successfully, as was described in Chapter 2, the resulting austenite grain structure is pancaked. When these austenite grains transform, the ferrite grains are fine and uniform.

5.3.3 Solute and Precipitate Contributions

Two static cases analogous to the dynamic cases of Fig. 5.17 are illustrated in Figs. 5.18(a) and (b). In Fig. 5.18(a), the retarding effect of Nb in solution on recrystallization is indicated by the shift to the right of the RTT diagram with respect to the one for the plain C steel. By means of this shift, the solute-modified RTT diagram intersects the PTT diagram for the deformed material. When recrystallization precedes precipitation, e.g. at 1000°C, the prestrain dislocations are removed, and the onset of precipitation is delayed, as given by the static PTT curve (13,63,79), which is not shown on the diagram. Alternatively, when precipitation

---

*The possibility of metadynamic recrystallization is almost completely excluded because very large prestrains are required to initiate it at rolling mill strain rates and finishing temperatures (81). Even when recrystallization is absent and the strain is effectively 'accumulated' over a number of passes, the total strain is unlikely to reach the high levels required to provoke dynamic recrystallization, largely because the critical strain when the temperature is continuously decreasing is more than double that observed under isothermal conditions (81).

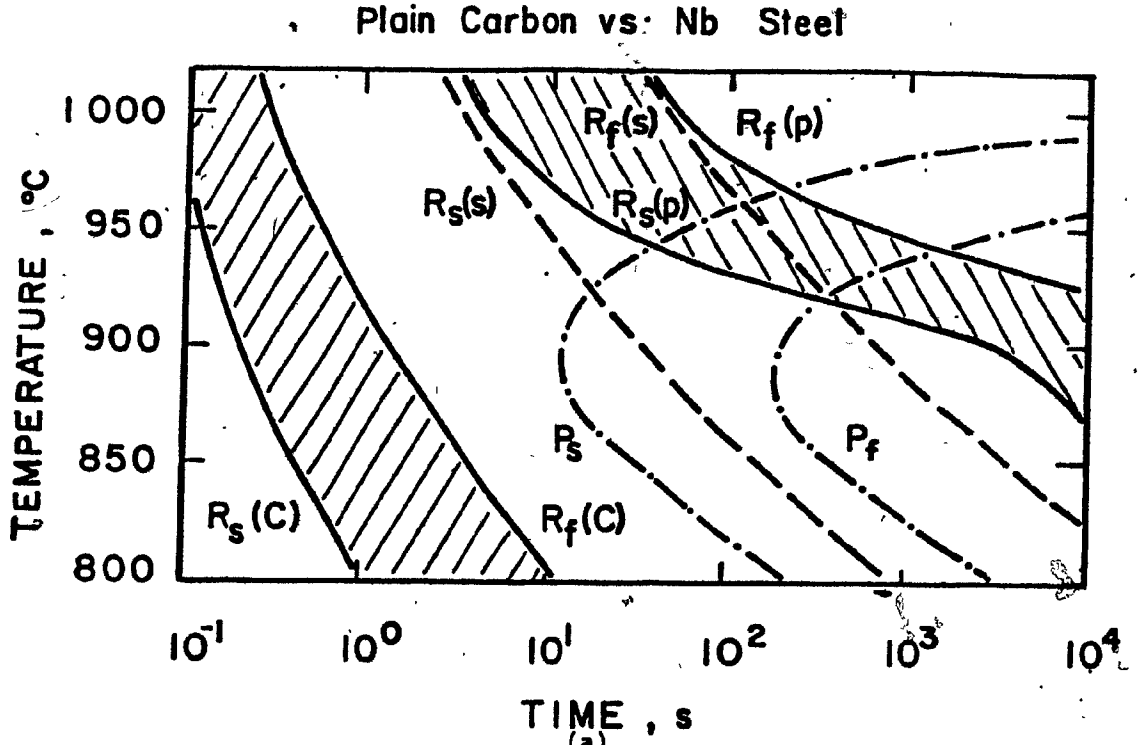

(a)

Figure 5.18 (a) Comparison of the RTT curves for a plain C and a Nb-bearing steel, illustrating the intersection of the RTT and PTT curves in the latter case.

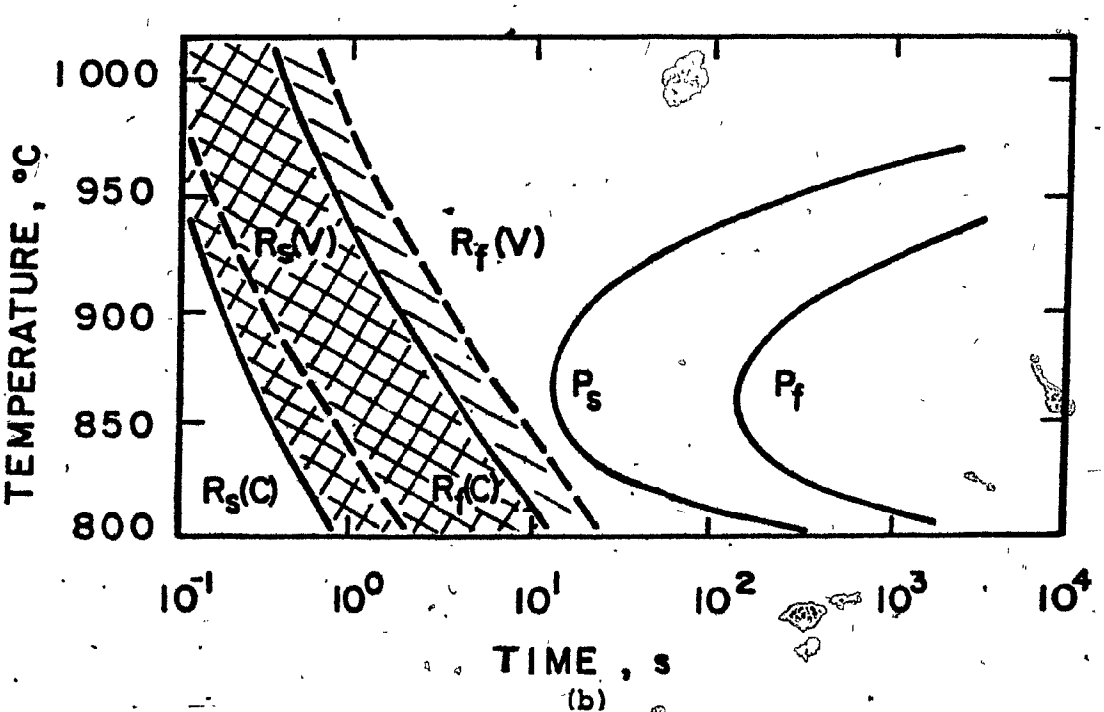

(b)

Figure 5.18 (b) Comparison of the RTT curves for a plain C and a V steel, and the PTT curve for VN in austenite.

begins earlier than the recrystallization start time indicated by the solute modified RTT curve, as it does at 900°C, the recrystallization is delayed significantly (21,29,30), and produces the desired pancaked grain structure during finish rolling.

In Fig. 5.18(b), the expected behaviour of a V steel containing no Nb is depicted. The solute-modified RTT curve is only slightly displaced to the right of the plain C curve. This small displacement is insufficient to cause this curve to intersect the PTT curve for VN. Once the steel starts recrystallizing and the dislocations are removed, it becomes increasingly difficult for strain-induced precipitation to occur. In this way VN precipitation is considerably delayed, and may not take place at all. Thus, the V concentration selected cannot prevent recrystallization, even at 900°C, not because the precipitation of VN is too slow (see Fig. 5.9), but because the solute retarding effect of V is too small. In fact, the solute retarding effect of V appears to be so low that, when used in combination with Nb, it cannot be distinguished from the effect of Nb alone (see Fig. 5.13).

The retarding effect of Mo in solution is much more noticeable, even in the presence of Nb. This is suggested by the dynamic RTT curves of Fig. 5.13, although it is the static curve which is of industrial interest. Even though the RTT curve for the Nb-Mo steel is shifted to longer times, in comparison with the Nb steel, due to the solute effect, the "reverse-knee" which could be expected to be more pronounced,

is barely detectable. This can be rationalized as follows: (a) the PTT curve is also shifted to longer times in this steel (Fig. 5.2) due to the effect of Mo addition on the C activity; (b) the nose temperature of this curve is decreased by the addition of Mo; and (c) as a result of (a), the PTT curve moves more than the RTT curve, so that they no longer intersect. This explanation could be checked out by conducting experiments at lower strain rates, and possibly at lower temperatures, under which conditions the knee would probably become more pronounced.

5.4 Rationalization of Relative Effects of Different Elements on High Temperature Flow Behaviour of Austenite

The roles of the microalloying elements in austenite are not well understood. This is partly because, at low concentrations (e.g. 0.02, 0.1 and 0.25 at.% of Nb, V and C respectively) detectable effects are not generally expected. However, there are reasons (both experimental and theoretical) for considering that the transition elements, and even some of the non-transition elements, can have important solute effects in the austenite range. As an example, Ouchi et al. (82) have recently shown that increasing the Mn concentration from 0.57% to 1.30% in a 0.12% C steel delays static recovery and recrystallization times by one half to one order of magnitude in time at 1000, 900 and 800°C. The experiments of Luton et al. (38) on decarburized and denitrided Nb steel have also shown that Nb in solution retards both static recovery and static recrystallization by about one order of magnitude in

time compared to an equivalent plain C steel. Similarly, the work of White and Owen (41) on a V steel conducted above the solubility temperatures of VN and VC has demonstrated that V in solution retards the dynamic recrystallization of austenite with respect to a reference plain C steel. With regard to the retardation of dynamic recrystallization, in addition to the references already mentioned, the torsion data of Fig. 4.9(a) and (c) determined at 3 s^{-1} indicate that the peak strains for V and Nb bearing steels are higher than for C steels, even when there is no time for precipitation to take place. The results of cam plastometer tests carried out at 55 s^{-1} (and therefore in about 20 ms) lead to a similar conclusion (83). Torsion testing on a series of Al-N steels by Michel and Jonas (32), e.g. at 0.6 s^{-1} also resulted in larger peak strains in a 0.08% C, 0.084% Al steel than in an Al-free steel, even when the precipitation of AlN was not taking place.

A number of possibilities exists as to why these elements can have significant solute retardation effects on recovery and recrystallization. The various possibilities will now be considered in turn and are evaluated below.

5.4.1 Atomic Size Differences in γ-Fe Solutions

The diameter difference between gamma iron and a given solute atom can be an important factor with regards to segregation to both dislocations and grain boundaries. The

ranking order for these size differences is presented in Table 5.2. The atomic sizes are taken from the reference by Pearson (84), and are for a coordination number of 12 and for metallic bonding. It is apparent from this table that, at equal atom fractions in solution in γ-Fe, Nb and Al at size differences of 15% and 12%, respectively, are expected to have stronger effects than, say V at 6%. In a similar way Mo, with a size difference of 10%, is expected to have an effect intermediate between Nb and V, whereas Mn, at 2%, is likely to have only a small effect. On this basis, Cr and Ni, which have approximately the same atomic diameter as iron, should have a negligible effect.

Although there is reasonable qualitative agreement between the atomic size differences and the observed "solute effects" there are important exceptions. For example, with almost equal atomic diameters, Al and Nb should have similar effects. As illustrated schematically in Fig. 5.19, the increase in the peak strain produced by Nb addition is considerably larger (by a factor of more than three) than that due to Al addition. A possible reason for this inconsistency, which may involve differences in the electronic structure of iron and of each element (32,63), will be considered in Section 5.4.3 below, in detail.

5.4.2 Modulus Differences

The changes in the modulus of γ-Fe as a result of different solute additions are hard to compare with each other

TABLE 5.2

Elements in Decreasing Order of Atomic Size Difference with Iron*

$r_x > r_{Fe}$			$r_x < r_{Fe}$		
Symbol	r_x (Å)	$(r_x - r_{Fe})/r_{Fe}$	Symbol	r_x (Å)	$-(r_x - r_{Fe})/r_{Fe}$
Y	1.801	0.41	C	0.916	0.28
Zr	1.602	0.26	B	0.98	0.23
Hf	1.578	0.24	Be	1.128	0.11
Hg	1.573	0.23	Ni	1.246	0.02
U	1.56	0.22	Co	1.252	0.02
Nb	1.468	0.15	S	1.27	0.003
Ta	1.467	0.15			
Ag	1.445	0.13			
Al	1.432	0.12			
W	1.402	0.10			
Mo	1.400	0.10			
Se	1.400	0.10			
Zn	1.394	0.09			
Pt	1.387	0.09			
Pd	1.376	0.08			
Tc	1.360	0.07			
Ir	1.357	0.07			
V	1.346	0.06			
Rh	1.345	0.06			
Si	1.312	0.03			
Mn	1.304	0.02			
Cr	1.282	0.01			
P	1.28	0.005			

$r_{Fe} = 1.274$ Å

*Based on a CN of 12 and metallic bonding (84).

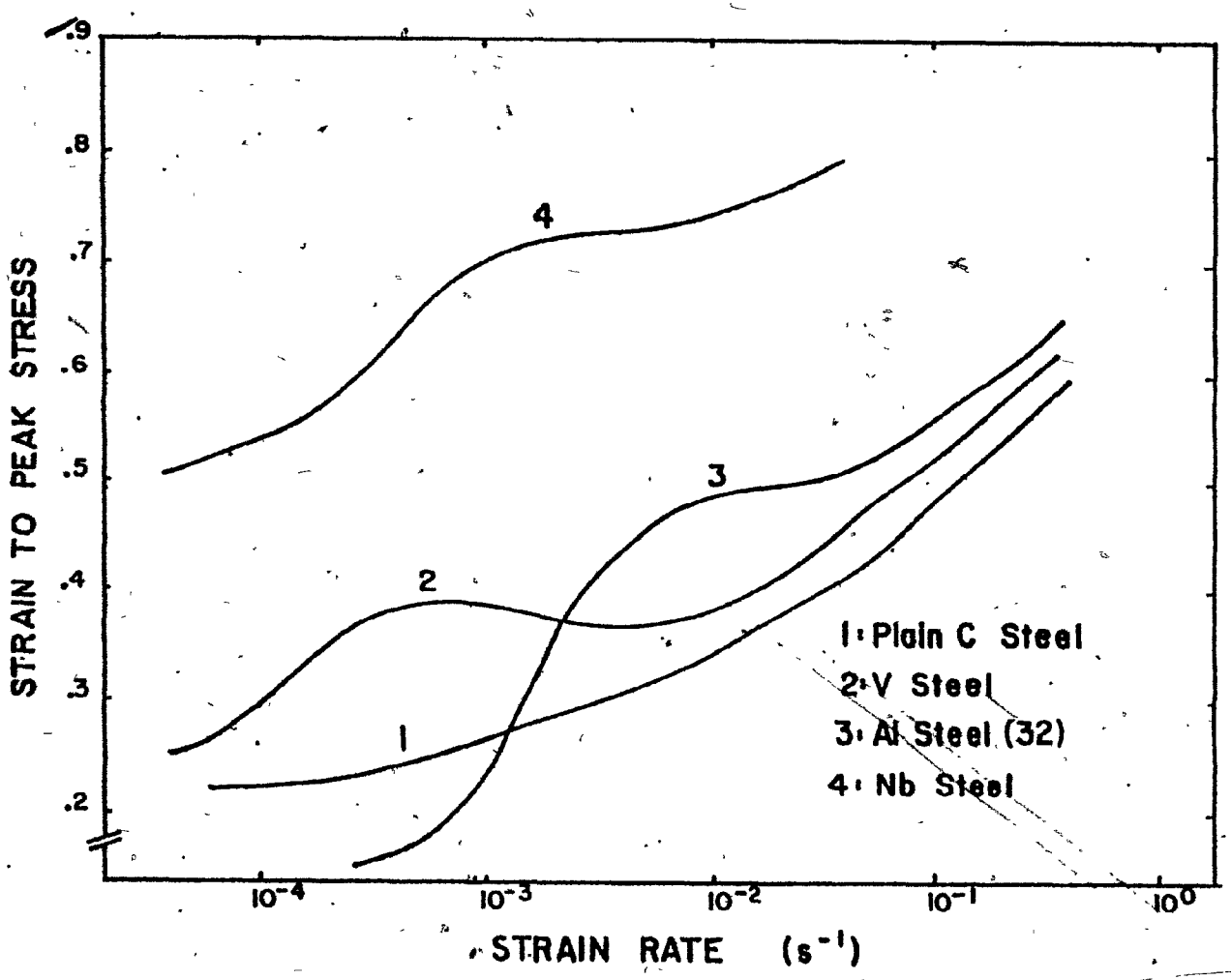

Figure 5.19 Comparison of the peak strain vs. strain rate relationship expected for steels in which Nb(CN), VN or AlN is precipitating during testing.

for a number of reasons. One is that such data are scarce. Another reason is that the extrapolation of room temperature data (for α-iron) to the high temperatures of concern here may be inaccurate due to the change in lattice structure. A recent survey of the literature relating to modulus effects published by Michel and Jonas (32) is reproduced in part in Table 5.3 for Al, C, Mn, N, Nb and V. The data are presented as normalized differences and as the modulus mismatch parameters $(1/E)(dE/dc) \cdot 100$ and $(1/\mu)(d\mu/dc) \cdot 100$, where c is the atomic concentration.

According to this table, each of the above elements produces a decrease in the Youngs modulus of Fe with increasing concentration, and all but one also lower the shear modulus (the exception in the second case is V, which is expected to lead to a slight increase). Data for Nb are lacking. The softening due to C and N is anticipated, as these interstitial elements strongly dilate the lattice. However, a clear drop in the modulus of γ-Fe is also produced when Al is added. The retardation of recovery and recrystallization described above, and the strengthening effects described below, therefore, cannot be attributed to the decrease in modulus (as long as these trends are also followed in γ-Fe). They would require an increase in modulus on the addition of solute. It therefore seems apparent that the observed differences in the rates of recovery and recrystallization are probably due to the electronic effects, which are described immediately below.

TABLE 5.3

Influence of Al, C, Mn, N, Nb, Si and V Addition on the Elastic Modulus of Iron*

Element	Relative Difference in Young's Modulus $\frac{E_x - E_{Fe}}{E_{Fe}} \times 100$	Relative Increase in Young's Modulus with Concentration $\frac{1}{E} \cdot \frac{dE}{dc} \times 100$	Relative Increase in Shear Modulus with Concentration $\frac{1}{\mu} \cdot \frac{d\mu}{dc} \times 100$
C	-	- 63 at 1000°C -102 at 1050°C	-
N	-	< 0 and similar to C	-
Al	-65	-125	-132
Si	-	-130	-139 to -200
V	-33	~0	+12
Mn	-19	-42	-29
Nb	-47	-	-

*From Michel and Jonas (32).

5.4.3 Electronic Differences between Solute and Solvent

For the present purposes, the relevant electronic difference is defined as the difference in the number of electrons contained in the outermost shell or shells. For example, iron has 2 s, 6 p and 6 d shell electrons in the outermost layer. In what follows, the basic approach of Abrahamson and co-workers (85-88) has been adopted. Accordingly, the expected effect of solute addition on the recrystallization behavior of Fe depends primarily on the number of s, p and d electrons in the outer shell of the particular elements in their ground state. Abrahamson's original plot is reproduced here as Fig. 5.20, with the addition of several elements, identified by crosses, which were not included in his investigation of 1960. The rank order of these elements is listed in Table 5.4.

According to Abrahamson, even when elements have the same number of s, p and d shell electrons, their relative effects can still be distinguished. With regard to their influence on the recrystallization temperature of α-Fe, as shown in Fig. 5.20, at a given number of s and d electrons, the rank order will be based on the atomic size order given in Table 5.2. It is evident from Fig. 5.20 that the number of free electrons has a significantly stronger influence on recrystallization behavior than the number of filled electron shells. (It is the latter which is closely associated with the atomic size of each element.*)

---

*see page 158.

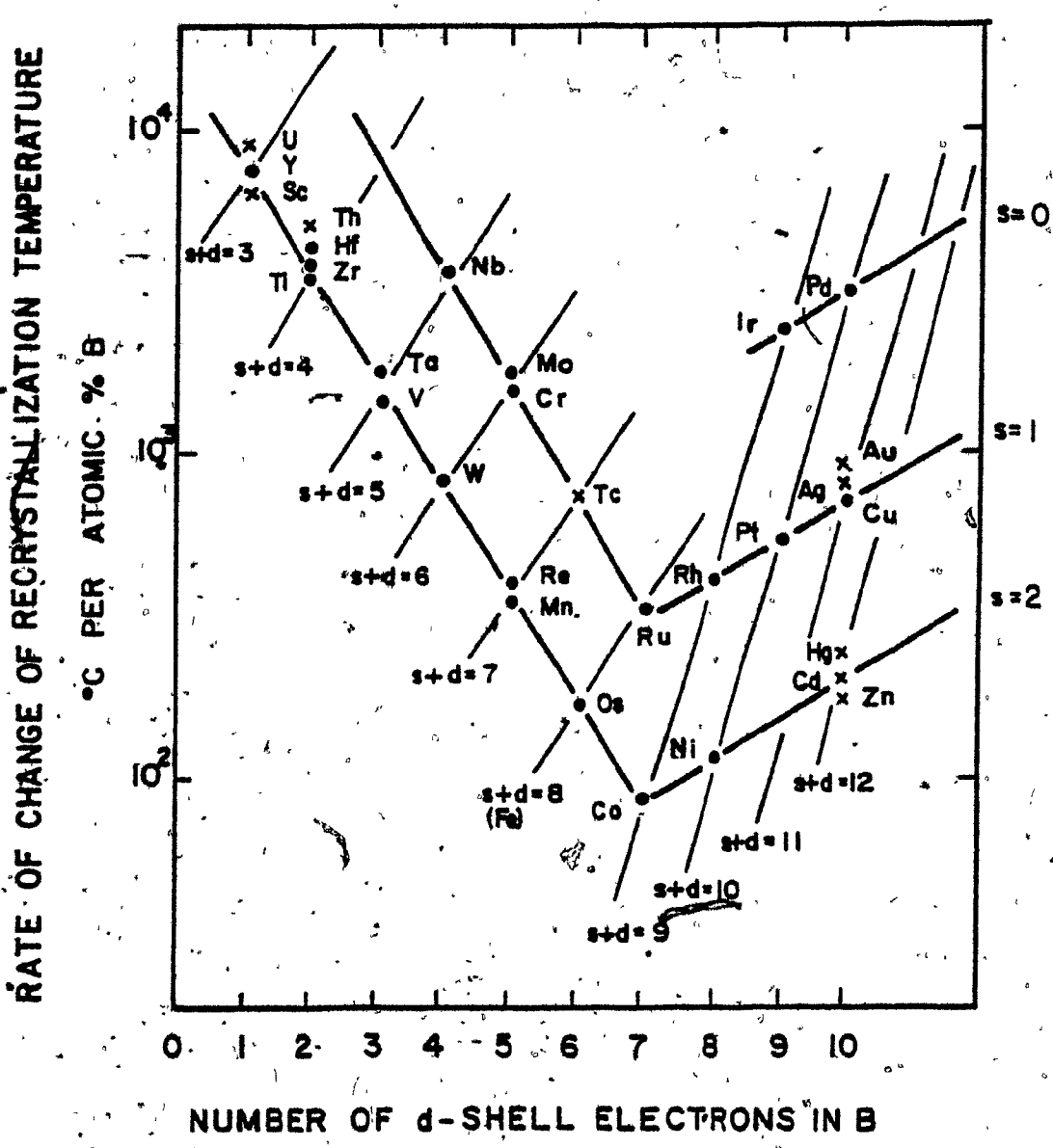

Figure 5.20 Effect of the addition of transition elements on the recrystallization temperature of deformed α-iron (after Abrahamson (87)).

TABLE 5.4

Transition Elements in Decreasing Order of Rate of Change of Recrystallization Temperature

U, Y, Sc

Th, Hf, Zr, Ti, Nb

Ir, Pd

Ta, Mo, V, Cr

W, Tc

Au, Ag, Cu, Pt

Re, Mn, Rh, Ru

Os, Hg, Cd, Zn

Ni, Co

It is apparent from Fig. 5.20 that Nb has a much more powerful effect on the recrystallization kinetics of α-Fe than V, and also that V and Mo have similar effects, with Mo having a somewhat larger one. The addition of Mn on the other hand, only leads to a small change. The elements Al, B, C, N and Si, amongst others, are not represented in this figure because they have no d shell electrons. It is, however, possible to rank these elements according to the number of p shell electrons, and this has been done by Michel and Jonas (32), following a pattern originally proposed by Abrahamson and Grant (88).

5.4.4 The Role of 'Associated Solutes'

Abrahamson's model, useful as it is for predictive and correlative purposes, has one serious flaw: it gives no indication WHY the various solutes line themselves up as shown in Fig. 5.20. Why, for example, does Nb in solution have an

*Before comparing Abrahamson's model to the present situation, however, two assumptions must be made. The first is that the ranking of Table 5.4 determined experimentally for alpha iron applies to gamma iron. This has not been demonstrated, but is reasonable in that (a) the phase transformation does not affect the electronic structure; and (b) the Abrahamson correlation has been demonstrated to be valid for fcc (85) and hcp (86), as well as bcc (87) structures. The change in coordination number, on the other hand, implies that the slope in Fig. 5.20 does not apply to gamma iron, which will have a different proportionality factor. The second assumption concerns the conversion from isochronal to isothermal conditions, and stipulates that the rate of recrystallization at a fixed temperature follows the ranking given in Table 5.4 for the temperature of recrystallization at a fixed time, inasmuch as these are kinetically equivalent.

order of magnitude more influence than V, and two orders of magnitude more than Mn? Some light is thrown on this matter by the concepts introduced by W.C. Leslie (89,90), which will now be described briefly. According to Leslie, a type of clustering can occur which effectively inhibits the recrystallization of worked ferrite. The clustering involves two or more solutes, which display a strong attraction for each other, so that they are associated in solution. The relevant solutes may be any combination of interstitial or substitutional elements. The results are most pronounced when the solutes are present in very low concentrations. An example he cites is in a ferrite containing less than 0.1% Mn and 0.02% S, where recrystallization becomes very sluggish compared to a higher Mn steel of the same low C level. The effect is said to be due, neither to MnS nor to Mn or S singly in solution, but rather to their association in solution. For this reason, Leslie has used the expression "associated solutes" for this phenomenon.

The idea that clusters of elements, e.g. Nb, C and N, can form without necessarily creating a compound or precipitate is a rather welcome one. It helps to bridge the gap between the 'precipitate' and 'solute' retardation theories of recrystallization discussed earlier in this section. The idea that Mo or V or Mn might form with C and N some sort of ordered region or cluster, and that this formation is not a distinct precipitate, might also help us to understand the physical processes by means of which the activity coefficient

of the latter two elements (C and N) are reduced.

Observations of this type have already been reported (90) for the case of Ti, C and N. Given the commercial importance of steel processing, it will clearly be of importance to determine the extent of this phenomenon in high temperature austenite, and to subject Leslie's idea of 'associated solutes' to further investigation.

5.5 High Temperature Flow Stresses

The solution strengthening produced by single or multiple addition of Mn, Mo, Nb and V, and listed in Table 4.2 (b) is reproduced below as Table 5.5 for convenience. The magnitude of strengthening produced by single additions of these elements follows that expected from the Abrahamson plot of Fig. 5.20 for recrystallization. In this table, Nb has almost 10 times the strengthening effect of V and about 50 times that of Mn (i.e. 70 vs. 7 vs. 1,3%, respectively). A possible explanation for the correlation between strengthening and recrystallization effects is the following. First of all, recrystallization is generally preceded by static recovery, a process which is required for nucleus formation. The yield, or flow stresses, on the other hand, are controlled (at high temperatures) by dynamic recovery (24,31). It is even considered by some (31) that the high temperature 'yield' strength is the stress level at which appreciable dynamic recovery is initiated, so that the flow corresponds roughly to the stage III deformation

TABLE 5.5

Strengthening Due to Microalloy Additions at a Strain Rate of $3.2/3.7 \times 10^{-2} s^{-1}$ in the 875-1075°C Temperature Range

Solute Element (s)	Comparison Base	$\Delta\sigma y/\sigma y$ (base) % Per 0.1 at.% Solute (s)	$\Delta\sigma y/\sigma y$ (base) % Per 0.1 wt.% Solute (s)	Overall Average* Per 0.1 at.% Solute (s)	Overall Average* Per 0.1 wt.% Solute (s)
V	Plain C	3.3	3.3	7	6
Nb	Plain C	78	55	70	50
Mn + Nb (in Mn-Nb steel)	Plain C	5	5	5	5
Mn (in Mn-Nb steel)	Nb Steel	0.6	0.6	1.3	1.3
Nb + V (in Nb-V steel)	Plain C	18	18	19	19
V (in Nb-V steel)	Nb Steel	5	6	8	8
Nb (in Nb-V steel)	V Steel	80	56	80	56
Mo (in Mo-Nb steel)	Nb Steel	8	4	9	5
Mo + Nb (in Mo-Nb steel)	Plain C	17	10	18	10

*Includes data from Table 4.2 (a).

of single crystals. Thus, on the assumption that static and dynamic recovery are affected in a similar manner when solute additions are made, it does not seem unreasonable that both yield strengths and static recovery rates should follow the Abrahamson pattern.

We turn now to a related question, and that is the effect produced by the combined addition of Nb and V, and to a lesser degree, to that of Mn and Nb. As mentioned above, the simple addition of 0.1 at % Nb leads to a 70% increase in strength. However, in the presence of V, this amount increases to 80%. The greater effectiveness of Nb in the company of V may be related to a change in the activity coefficient of Nb due to V addition. The effect of adding V to a Nb steel retards the precipitation of Nb(CN), as discussed in Section 5.13. This was attributed to the decrease in the activity coefficients of C (72) and N (75), which leads in turn to an increase in the solubility of the carbonitride. The effect was considered to be parallel to that of Mn. Mn addition has been shown to increase the activity coefficient of Nb in steel (66). This can, in physical terms, be interpreted as signifying that, when Mn is added, the steel behaves as though there were more Nb present. This type of phenomenon is often termed a 'synergistic' effect, implying that the two elements 'work' together.

It is usual to discuss the activities of elements in solution with respect to the formation of precipitates and

solubilities, as was done above. However, when it comes to solute strengthening effects, the term 'activity' is not conventionally employed to evaluate or describe the synergistic effects. With respect to the Nb-V system, the present author is not aware of any evidence that V raises the activity coefficient of Nb, as does Mn. However, it can be anticipated that it does so qualitatively, but perhaps to a different degree. Similar results have been reported in the literature for the Nb-Mo pair (70,71). Because a reference Mo steel was not used in this investigation, the extent of synergism in the latter case could not be determined. Returning to the Nb-V system, it seems possible that if V addition increases the activity coefficient of Nb with respect to carbonitride formation, it may also increase the activity coefficient of Nb with respect to solute strengthening.

The strengthening resulting from the addition of solutes reported in the literature is summarized in Table 5.6. Table 5.6(a) shows the strengthening produced by 0.1 wt% of alloy addition and Table 5.6(b) that for an atom fraction of 0.001. Those due to Tegart and Gittins (35) are for solute strengthening as such, as are those reported by Michel and Jonas (32), and the ones produced in the present investigation. Only part of the results of Everett et al. (91), on the other hand, are for solute strengthening alone. These are marked by an asterisk. The other values from this source are for the combination of work hardening (retardation of recrystallization), and precipitate and solute strengthening, because they correspond to 2nd, 3rd or 4th mill pass simulations.

TABLE 5.6 (a)

Comparison of the Solute Strengthening Produced by Alloy Additions, per Atom Fraction of 0.001

Element: Nb	Mn	V	Mo	Si	Al	C	T°C	Reference
–	0.52	–	2.2	0.4	0.8	–	1000	Tegart & Gittins (35)
31	–	7	–	1.2	4.2	1.4	1000	Everett et al. (92)
183	–	10.4	–	1.6	–	–	925	ibid.
–	1.6	–	–	0.7	6.8	0.3	875	Everett et al. (91)
44.4	–	–	–	1.6	21.8	–	975	ibid.
110	2.4	–	–	–	–	0.3	875 (a)	ibid.
–	–	–	–	2.1	15	–	975 (b)	ibid.
–	–	–	–	–	12 (a)	–	875-925	Michel and Jonas (32)
29.5	1.3	8	2.9	–	–	–	875-925	present study

TABLE 5.6 (b)

Comparison of the Solute Strengthening Produced by Alloy Additions, per 0.1 wt.%

–	5.3	–	1.3	0.8	1.6	–	1000	Tegart & Gittins (35)
18.5	–	7.5	–	2.5	8.8	6.5	1000	Everett et al. (92)
110	–	11.4	–	3.1	–	–	925	ibid.
–	1.6	–	–	1.4	14.1	1.2	875	Everett et al. (91)
26.7	–	–	–	3.2	45.2	–	975	ibid.
66	2.4	–	–	–	–	1.2	875 (a)	ibid.
–	–	–	–	4.1	31	–	975 (b)	ibid.

(a) and (b) also include precipitation strengthening.

That Nb causes the greatest solution strengthening in steel is once again evident from this table, as has already been pointed out above. The magnitude of the effect is slightly smaller in these published results than has been reported here, but this may be due to the different methods used. The agreement is better for the cases of V and Mn. The reason for the large discrepancy between the two Mo results in this table is not known. The data for Si and Al are included because they are common and important elements in steel.

CHAPTER 6

CONCLUSIONS

In the present investigation, two mechanical testing methods were employed to distinguish the effects of Mn, Mo, Nb and V addition on the high temperature flow and recrystallization behavior of six microalloyed steels. The method of I. Weiss (1977) based on the strain rate dependence of the peak strain was utilized to determine the dynamic precipitation kinetics of the microalloy carbonitrides in the 875-925°C temperature range. The dynamic RTT curves for these steels were established by testing at a strain rate of $3.7 \times 10^{-2} s^{-1}$ in the temperature range 875-1075°C. As a result of this study, the following conclusions were drawn:

Precipitation Kinetics

1. Increasing the Mn concentration in a 0.05/06% C, 0.035% Nb steel from 0.42% to 1.90% leads to a delay in the dynamic precipitation kinetics of Nb(CN) by more than an order of magnitude in time. This effect is attributed to the greater solubility of Nb(CN) that results from the sharp decrease in the activity coefficient of C caused by the addition of Mn. (The accompanying increase in the activity coefficient of Nb is insufficient to compensate for the decrease in the C activity.)

2. The temperature at the nose of the dynamic PTT curve for Nb(CN) is not appreciably changed by the addition of Mn. This suggests that Mn also decreases the diffusivity of Nb in austenite.
3. The addition of Mo to a 0.035% Nb steel leads to a decrease in the rate of dynamic precipitation of Nb(CN) in austenite, the amount diminishing near 875°C. The effect is attributed (by analogy to the case of Mn addition), to the probable increase in the solubility of the carbonitride that accompanies Mo addition through the decrease in the activity coefficient of C.
4. The nose of the dynamic PTT curve for Nb(CN) precipitation is moved to lower temperatures, indicating that the effect of Mo on the diffusivity of Nb is probably small.
5. The dynamic precipitation kinetics in the present Nb-V steel are slower than in the Nb steel and faster than in the V steel each having a similar base composition. The retardation in comparison with the Nb steel is taken to be a result of the increased solubility of the carbonitride attributable to the presence of V, which like Mn and Mo lowers the activity coefficients of C and N.
6. The lower nose temperature in the Nb-V steel, in comparison with the Nb steel, is due to the

greater supersaturation of VN than of Nb(CN) at the lower temperatures, leading to the earlier precipitation of the former particle.

Recrystallization Kinetics

1. Among the microalloying elements investigated, the solute retarding effect of Nb by far was the strongest. The more marked effectiveness of Nb than of V or Mo is primarily due to the greater electronic difference between Fe and Nb than between Fe and V or Fe and Mo. It is also related to the larger difference in atomic size between Nb and Fe than between either V or Mo and Fe.
2. The magnitude of the retarding effect of the dual microalloy additions on the dynamic recrystallization rate is, in decreasing order: 0.3% Mo-0.035% Nb, 1.90% Mn-0.035% Nb, and 0.115% V-0.035% Nb. The retardation of recrystallization of a plain C steel by the dual addition of 0.3% Mo and 0.035% Nb is approximately twice that due to the single addition of 0.035% Nb and is possibly greater than expected from the simple addition of the effect of each element when added alone. This synergism may be related to the increase in activity coefficients of Nb and Mo that occurs when these elements are added

jointly.

3. The Nb-V pair behaves much like Nb alone in terms of retarding dynamic recrystallization.
4. The limiting factor that affects the retardation of austenite recrystallization in HSLA steels is not the rate of precipitation of the microalloy carbonitrides, but rather the minimum amount of solute retardation that is required. Unless the solute effect is strong enough to delay recrystallization until the onset of static precipitation, the latter process cannot prevent recrystallization.

Solute Strengthening

1. Single additions of Nb and V produce yield strength increases of 70% and 7% respectively per 0.1% at.% addition. The strengthening due to Nb and V in the present 0.115% V-0.035% Nb steel are 80% and 8% respectively per 0.1 at.% addition. This greater effect in comparison with the single addition of each element is attributed to a synergism in their strengthening effects.
2. The addition of Mo or of Mn increased the yield strength of a 0.035% Nb steel by 9 and 1.3% per 0.1 at.% addition.

3. The rank order of strengthening produced by the alloy additions (per at.%) is primarily associated with the electronic difference between each element and iron and secondarily with the atomic size factor. The extent of synergism produced by dual additions is probably related to the effect of each element on the activity coefficient of the other element.
4. Over the range of temperatures and strain rates investigated, the addition of Mn, Mo or V to a 0.05% C, 1.25% Mn and 0.035% Nb steel does not change the peak stress in a systematic manner.

STATEMENT OF ORIGINALITY AND CONTRIBUTION TO KNOWLEDGE

The results of the present study have led to the following original contributions:

1. The investigation showed that an increase in the Mn level of a Nb steel delays the dynamic precipitation of Nb(CN) in austenite. In the temperature range where the precipitation is nucleation controlled, the delay is due to the increased solubility of Nb(CN). This effect is considered to be associated with the decrease in the activity coefficient of C, and possibly also of N, in the presence of increased Mn concentrations. At lower temperatures, where the precipitation is diffusion (and growth) controlled, the delay is linked to a possible decrease in the diffusivity of Nb associated with the increased Mn level. This interpretation is relevant to industrial rolling practices in that a decrease in the solubility temperature means that lower soaking and roughing temperatures can be used, which can lead in turn to energy savings.
2. It has been shown that the addition of Mo or V delays Nb(CN) precipitation in austenite in a manner similar to Mn, but to a greater extent

per atomic percent of addition. These delays are also linked to the increased solubility of the carbonitride, which probably results from the way in which these two elements reduce the activity coefficients of C and N.

3. The dynamic precipitation kinetics of VN in austenite were determined and demonstrated to be slightly slower than those of Nb(CN) in a steel of the same Mn concentration containing 0.035% Nb. On this basis it has been suggested that the markedly lower pancaking efficiencies observed in controlled rolling practice in V steels as compared to equivalent Nb steels is not due to the sluggishness of VN precipitation, but rather to the distinctly reduced solute retardation produced by V addition. To the present author's knowledge, the dynamic precipitation kinetics of VN in austenite have not been previously determined. Neither has the relative inefficiency of V addition for preventing austenite recrystallization during control rolling been attributed to its rather limited effect in solution in γ-Fe.

4. Dynamic Recrystallization-Time-Temperature (RTT) curves have been constructed for the first time from mechanical test data, rather than by the usual metallographic methods. The relative

retardation of dynamic recrystallization produced by single or multiple additions of Mn, Mo, Nb and V has thus been determined over a wide temperature range (875-1075°C) for a preselected deformation rate. It is suggested that this technique is capable of predicting the relative retardations under industrial conditions of static recrystallization.

5. The present research contributes to an understanding of control rolling by highlighting the probable importance of the electronic difference between the microalloying element and γ-Fe. These differences are likely to play a primary role in determining the relative effectiveness of individual alloy additions with respect to the retardation of austenite recrystallization. The importance of solute effects was underlined in the present work by the contrast between (a) the early recrystallization in the V steel (compared to the Nb steel), and (b) the late recrystallization in the Nb-Mo steel (compared to the Nb steel) where dynamic recrystallization is retarded by the addition of Mo as solute.
6. A systematic study of the single and combined strengthening effects of Mn, Mo, Nb and V was made on a series of steels of similar base compositions. The normalized strengthening produced (on an atomic percent basis) was

demonstrated to be related to the electronic differences between each element and iron. The synergistic effects observed, for example: Nb alone vs. Nb with V, have been associated with possible changes in the activity coefficients of these elements due to their combined presence.

REFERENCES

1. J.P. Orton: "Microalloying 75", Union Carbide Corporation, New York, NY (1977), 334.

2. J.N. Cordea: Symposium on Low Alloy High Strength Steels, Nurnberg, BRD, May (1970), Metallurg Companies.

3. F.B. Pickering: "Microalloying 75", Union Carbide Corporation, New York, NY (1977), 32.

4. H.W. Paxton: Met. Trans., 10A (1980), 1.

5. E.O. Hall: Proc. Phys. Soc., Series B, 64 (1951), 747.

6. N.J. Petch: J. Iron and Steel Inst., 174 (1953), 25.

7. F.B. Pickering and T. Gladman: "Metallurgical Developments in C Steels", Iron and Steel Inst. (1963), 10.

8. H.J. Wiester and H. Ulmer: Stahl und Eisen, 79 (1959), 1120.

9. W.C. Leslie: "The Relationship between Structure and Mechanical Properties of Metals", NPL Conference Proceedings, Her Majesty's Stationery Office (1963), 334.

10. W.B. Morrison and J.H. Woodhead: J. Iron and Steel Inst., 201 (1963), 43.

11. W.B. Morrison: ibid., 201 (1963), 317.

12. W.B. Morrison and J.A. Chapman: Phil. Trans. Roy. Soc., Series A, 282 (1975), 289.

13. S.S. Hansen, J.B. Van der Sande and M. Cohen: Met. Trans., 11A (1980), 387.

14. M. Cohen and S.S. Hansen: "MiCon 80: Optimization of Processing, Properties and Service Performance Through Microstructural Control", ASTM STP 672 (1979), 34.

15. L. Meyer and H. de Boer: J. Met., 29, No. 1 (1977), 17.

16. K.J. Irvine, F.B. Pickering and T. Gladman: J. Iron and Steel Inst., 205, part 2 (1967), 161.

17. J.M. Gray: Presented at Instituto Latin Americano del Fierro el Acero, Buenos Aires, Argentina, May 9-13 (1976).

18. J.P. Sah, G.J. Richardson and C.M. Sellars: Met. Sci., 8 (1974), 325.

19. T. Gladman and D. Dulieu: Met. Sci., 18 (1974), 167.

20. R.A. Petkovic, M.J. Luton and J.J. Jonas: Can. Met. Quart., 14 (1975), 137.

21. I. Weiss and J.J. Jonas: Met. Trans., 10A (1979), 831.

22. "Microalloying 75", Union Carbide Corporation, New York, NY (1977).

23. "Hot Deformation of Austenite", J.B. Ballance, ed., AIME, NY (1977).

24. J.J. Jonas and H.J. McQueen: "Mise en forme des métaux et alliages", B. Baudelet, ed., Centre National de la Recherche Scientifique, Sept. (1975).

25. J.D. Jones and A.B. Rothwell: "Deformation Under Hot Working Conditions", Iron and Steel Inst. Pub. 108 (1968), 78.

26. D. McCutcheon and R.M. Jamieson: Can. Met. Quart., 12 (1973), 105.

27. R.A.P. Djaic and J.J. Jonas: Met. Trans., 4 (1973), 621.

28. A. LeBon, J. Rofes-Vernis and C. Rossard: Met. Sci., 9 (1975), 36.

29. I. Weiss and J.J. Jonas: Met. Trans., 11A (1980), 403.

30. J.J. Jonas and I. Weiss: Met. Sci., 13 (1979), 238.

31. "Recrystallization of Metallic Materials", F. Haessner, ed., Dr. Rieder-Verlag GMBH, Stuttgart (1978).

32. J.P. Michel and J.J. Jonas: Acta Met., in press.

33. R.W.K. Honeycombe and K. Pethen: J. of the Less Common Metals, 28 (1972), 201.

34. W. Roberts: Swedish Institute for Metals, Research Report No. IM-1333, Nov. (1978).

35. W.J. McG. Tegart and A. Gittins: "Hot Deformation of Austenite", J.B. Ballance, ed., AIME, NY (1977), 1.

36. P.J. Wray: ibid., 86.

37. R. Coladas, J. Masoumave and J.P. Bailon: ibid., 341.

38. M.J. Luton, R. Dorvel and R.A.P. Petkovic: Met. Trans., 11A (1980), 411.

39. M. Lamberigts and T. Greday: "Hot Deformation of Austenite", J.B. Ballance, ed. AIME, NY (1977), 286.

40. W. Roberts: Swedish Institute for Metals Research, Report No. IM-1211 (1977).

41. M.J. White and W.S. Owen: Met. Trans., 11A (1980), 597.

42. R. Simoneau, G. Begin and A.H. Marquis: Met. Sci., 12 (1978), 381.

43. H. Watanabe, Y.E. Smith and R.D. Pehlke: "The Hot Deformation of Austenite", J.B. Ballance, ed., NY (1977), 140.

44. A.T. Davenport, R.E. Miner and R.A. Kot: ibid., 186.

45. Y. Mishima, R.H. Horn, V.F. Zackay and E.R. Parker: Met. Trans., 11A (1980), 431.

46. R.K. Amin and F.B. Pickering: Preprint from "Sheffield International Conference on Hot Working and Deformation Processing", Sheffield, England (1979).

47. J. Jizaimaru, H. Kobayashi and T. Kosaka: Tetsu-to-Hagane, 60, No. 4 (1974), 177.

48. C. Ouchi, T. Sanpei, T. Okita and I. Kozasu: "Hot Deformation of Austenite", J.B. Ballance, ed., NY (1977), 316.

49. M.F. Ashby and R. Ebeling: Trans. AIME, 236 (1966), 1396.

50. V.M. Farber, O.M. Mikhailova, V.N. Davydov and N.N. Chesnokova, Steel in the USSR, Aug. (1977), 667.

51. R. Phillippo and F.A.A. Crane: J. Iron and Steel Inst., 211 (1973), 653.

52. T. Chandra, I. Weiss and J.J. Jonas: submitted to Metal Science.

53. J.W. Cahn and J. Nutting: Trans. AIME, 215 (1959), 526.

54. J.E. Hilliard: Trans. AIME, 224 (1962), 906.

55. C.M. Sellars and A.F. Smith: J. of Mater. Sci., 2 (1967), 521.

56. A.T. Davenport, L.C. Brossard and R.E. Miner: Republic Steel Project #12, 051, April (1977).

57. T.M. Hoogendorn and M.J. Spanraft: "Microalloying 75", Union Carbide Corporation, New York, NY (1977), 75.

58. M.J. Luton: Ph.D. Thesis, McGill University, Montreal (1971).

59. S. Fulop, K.C. Cadien, M.J. Luton and H.J. McQueen: J. Testing and Evaluation, 5 (1977), 419.

60. D.S. Fields, Jr. and W.A. Backofen, Proc. Am. Soc. Test. Mater., 57 (1957), 1259.

61. G.R. Canova, private communication.

62. G.R. Canova, S. Shrivastava, J.J. Jonas and C. G'Sell: J. of the Mechs. and Phys. of Solids, in press.

63. M.G. Akben, I. Weiss and J.J. Jonas: Acta Met., in press.

64. V.R. Golik, V.A. Dubrov, N.I. Sandler and V.M. Yunash: Fiz. Metal. Metalloved., 14, No. 4 (1962), 555.

65. J.H. Woodhead: "Vanadium '79", Vanadium Int. Tech. Committee (1980), 3.

66. Shinji Koyama, Turuo Ishii and Kiichi Narita: Journal of the Japan Institute of Metals, 35 (1971), 1089.

67. T. Wada, H. Wada, J.F. Elliot and J. Chipman: Met. Trans., 3 (1972), 1657.

68. K.J. Irvine, F.B. Pickering and T. Gladman: J. Iron and Steel Inst., 205 (1967), 161.

69. H. Nordberg and B. Aronsson: J. Iron and Steel Inst., 206 (1968), 1263.

70. S. Kanazawa, A. Nakashima, K. Okamoto and T. Suzuki: Trans. I.S.I.J., 11, #3 (1971), 184.

71. S. Kanazawa, A. Nakashima, K. Okamoto, K. Tanabe and S. Nakazawa: J. of the Japan Institute of Metals, 31 (1962), 171.

72. T. Wada, H. Wada, J.F. Elliot and J. Chipman: Met. Trans., 3 (1972), 2865.

73. T. Wada, Y.E. Smith and W.E. Lauprecht: "Vanadium 79", Vanadium Int. Tech. Committee (1980), 61.

74. T. Nishizawa: Scand. J. Metallurgy, 1 (1972), 41.

75. M.G. Frohberg and H. Graf: Stahl u. Eisen, 80 (1960), 539.

76. D. Houghton, private communication.

77. C. Rossard: Proc. Int. Conf. Strength Metals and Alloys, 3rd, Vol. II (1973), 175.

78. G. Glover and C.M. Sellars: Met. Trans., 4 (1973), 765.

79. I. Weiss: Ph.D. Thesis, McGill University, Montreal (1977).

80. H. Kreye and E. Hornbogen: J. Mat. Sci., 5 (1970), 89.

81. A.H. Ucisik, I.Weiss, H.J. McQueen and J.J. Jonas : Can. Met. Quart., in press.

82. C. Ouchi, T. Okita, M. Okado and Y. Noma: "International Conference on Steel Rolling", Iron and Steel Inst. of Japan (1980), 1272.

83. M.J. Stewart: "Hot Deformation of Austenite", J.B. Ballance, ed., AIME, NY (1977), 47 and 233.

84. W.B. Pearson: "The Crystal Chemistry and Physics of Metals and Alloys", Wiley-Interscience, New York, NY (1972), 151.

85. E.P. Abrahamson, II: Trans. AIME, 224 (1962), 727.

86. E.P. Abrahamson, II and J.A. Alexander: Trans. ASM, 56 (1963), 377.

87. E.P. Abrahamson, II and B.S. Blakeney, Jr.: Trans. AIME, 218 (1960), 1101.

88. E.P. Abrahamson II and N.J. Grant: Trans. ASM, 50 (1958), 705.

89. W.C. Leslie, private communication.

90. W.C. Leslie: "Physical Metallurgy of Steels", McGraw Hill, to be published in 1981.

91. J. Everett, A. Gittins, G. Glover and M. Toyama: pre-print from "International Conf. on Manf. Eng.", Melbourne, 25-27 Aug. (1980).

92. J. Everett, A. Gittins, G. Glover and M. Toyama: pre-print from Sheffield Int. Conf. on Hot Working and Forging Processes, Sheffield, England (1979).

APPENDIX A

REAL TIME PROGRAM USED FOR TORSION TESTING

```
BKBEN  16-DEC-80  MTS BASIC V01B-02D

100 REM"*****************************************************"
101 REM"  TORSION TESTING PGM USED"
102 REM"  ADOPTED FROM THE TORTEST PGM WRITTEN BY G.R.CANOVA"
103 REM"*****************************************************"
104 REM"  DETERMINATION OF THE TEST CONDITIONS"
105 EDMP
106 PRINT "DO YOU WANT TO RUN A TEST?"\INPUT Y1$
107 IF Y1$="YES " THEN 108\GO TO 308
108 PRINT "SAMPL #?"\INPUT N$
109 PRINT "STRAIN-RATE?"\INPUT D
110 R=3.175
111 L=25.4
112 DIM X(201),A(110,20),B(110,20),A1(110)
113 DIM B1(110),E(10),T(10)
114 DIM C1(20),D1(20)
115 REM"*****************************************"
116 REM"  THE NEXT 5 LINES ARE FOR INTERRUPTED TESTS ONLY"
117 REM"*****************************************"
118 PRINT "HOW MANY INTERRUPTIONS?"\INPUT N
119 FOR I=1 TO N
120 PRINT "INTR STRAIN"\INPUT E(I)
121 PRINT "INTR TIM?"\INPUT T(I)
122 NEXT I
123 REM"*********************************"
124 REM"  SETS UP SYSTEM FOR TESTING"
125 REM"*********************************"
126 QUIT
127 MSW1(2)
128 DACQ(0,K9,2,0)
129 FOR I=K9 TO 0 STEP -1
130 FG1(I)
```

```
131 NEXT I
132 PRINT "IS TST READY?"\INPUT A$
133 IF A$<>"YES" THEN 132
134 REM"*****************************************"
135 REM"  RUNS TEST AND CARRIES OUT DATA ACQUISITION"
136 REM"*****************************************"
137 G9=0
138 FOR J=1 TO N
139 MSW1(2)
140 P=E(J)*L/2/PI/R*SQR(3)
141 PRINT "# OF TURNS",P
142 IF J>1 THEN 149
143 X(1)=4095/2*D/E(J)
144 IF J>1 THEN 149
145 Y1=P*162
146 X(2)=Y1
147 G9=Y1
148 GO TO 153
149 P2=E(J-1)*L/2/PI/R*1\X(1)=4095/2*D/(E(J)-E(J-1))/100
150 H9=(P-P2)*162
151 X(2)=H9+G9
152 G9=X(2)
153 X=2
154 IF J<>1 THEN 156
155 V=10*E(J)/D\GO TO 157
156 V=10*(E(J)-E(J-1))/D
157 FG1(X,1,7,7)
158 DACQ(3,A1,0,V)\DACQ(3,B1,2,V)
159 PRINT "GO"
160 STAR
161 BUF1(2)
162 IF Z>-1 THEN 161
163 QUIT
164 PRINT "STOP"
165 IF Y1$="YES" THEN 183
```

```
166 FOR I=1 TO 500
167 O=0
168 NEXT I
169 U=G9-10
170 FG1(U)
171 MSW1(0)\FG1(0)
172 PRINT "FINISH"
173 X(1)=4095/T(J)
174 FOR I=2 TO 201\X(I)=0\NEXT I
175 X=201
176 V1=100*T(J)
177 DACQ(3,C1,0,V1)\DACQ(3,D1,2,V1)
178 FG1(X,1,7,0)
179 STAR
180 BUF1(Z)
181 IF Z>-1 THEN 180
182 QUIT
183 IF Y1$="YES" THEN 185
184 M1=110\GO TO 186
185 M1=100
186 FOR I=1 TO M1
187 A(I,J)=A1(I)-9
188 B(I,J)=B1(I)
189 IF I<101 THEN 193
190 IF Y1$="YES" THEN 193
191 I1=I-100
192 A(I,J)=C1(I1)-9\B(I,J)=D1(I1)
193 NEXT I
194 MSW1(2)
195 NEXT J
196 REM"**********************"
197 REM"  LISTING OF DATA"
198 REM"**********************"
199 CNTR(3)
200 PRINT "TORQUE","EQU STR","TIME"
```

```
201 A8=0
202 FOR J=1 TO N
203 U=10*(E(J)-E(J-1))/D
204 FOR I=1 TO 100
205 A8=A8+U/1000
206 PRINT A(I,J)/10.2,(B(I,J)-B(1,1))/162*2*PI*R/L/SQR(3),A8,I
207 NEXT I
208 IF Y1$="YES" THEN 214
209 FOR I=101 TO 110
210 U1=100*T(J)
211 A8=A8+U1/1000
212 PRINT A(I,J)/10.2,(B(I,J)-B(1,1))/162*2*PI*R/L/SQR(3),A8,I
213 NEXT I
214 NEXT J
215 INPUT Y6$
216 CNTR(3)
217 REM"*************************"
218 REM"  PLOTS TORQUE VS. TIME"
219 REM"*************************"
220 T9=A8
221 CNTR(3)\CNTR(0)\PHYL(100,900,80,700)
222 SCAL(0,0,T9,-10,75)\AXES(0,0)
223 CNTR(2)\PLOT(0,0)
224 LABL("TIME","TORQUE",T9/5.5,1)\X=0\FOR J=1 TO N
225 IF J<>1 THEN 226\U=10*E(J)/D\GO TO 227
226 U=10*(E(J)-E(J-1))/D
227 FOR I=1 TO 100
228 X=X+U/1000\Y=A(I,J)/10.2\MARK(".",X,Y)\NEXT I
229 IF Y1$="YES" THEN 232
230 FOR I=101 TO 110\X=X+100*T(J)/1000
231 Y=A(I,J)/10.2\MARK(".",X,Y)\NEXT I
232 NEXT J
233 INPUT G7$
234 REM
235 REM
```

```
236 REM"*****************************"
237 REM"  PLOTS TORQUE VS. STRAIN"
238 REM"*****************************"
239 REM
240 CNTR(3)\CNTR(0)
241 PHYL(100,900,80,700)
242 SCAL(0,0,E(J),0,75)
243 AXES(0,0)
244 CNTR(2)\PLOT(0,0)
245 B9=INT(E(J)+.1)
246 LABL("STRAIN","TORQUE",B9/10,10,0)
247 LABL(".",".",B9/20,10,2)
248 CNTR(2)\PLOT(0,0)\CNTR(0)
249 FOR J=1 TO N
250 FOR I=1 TO 100
251 X=A(I,J)/10.2
252 Y=(B(I,J)-B(1,1))/162*2*PI*R/L/SQR(3)
253 MARK(".",Y,X)
254 NEXT I
255 IF Y1$="YES" THEN 261
256 FOR I=101 TO 110
257 X=A(I,J)/10.2
258 Y=(B(I,J)-B(1,1))/162*2*PI*R/L/SQR(3)
259 MARK(".",Y,X)
260 NEXT I
261 NEXT J
262 CNTR(2)\INPUT G9$
263 REM"*************************************"
264 REM"  PLOTS TORQUE VS. LOG(STRAIN)"
265 REM"*************************************"
266 CNTR(3)\CNTR(0)\PHYL(100,900,80,700)
267 SCAL(3,.01,E(J),10,75)\AXES(.01,10)\CNTR(2)\PLOT(.01,10)
268 LABL("STRAIN","TORQUE",1,1,1)
269 FOR J=1 TO N\FOR I=1 TO 100
270 X=A(I,J)/10.2
```

```
271 Y=(B(I,J)-B(1,1))/162*2*PI*R/L/SQR(3)
272 IF X<=0 THEN 274\IF Y<=0 THEN 274
273 MARK(":",Y,X)
274 NEXT I
275 NEXT J
276 CNTR(2)\INPUT G9$\CNTR(3)
277 PRINT "DO YOU WANT TO KEEP THIS EXP.?"\INPUT C$
278 IF C$="YES" THEN 283
279 GO TO 300
280 REM"*****************************************"
281 REM"  STORES THE DATA ON THE FLOPPY DISC"
282 REM"*****************************************"
283 OPEN "DX1:TOR"&N$ FOR OUTPUT AS FILE #1
284 FOR J=1 TO N
285 Q=(J-1)*4\R=Q+1
286 Q1=R+1\R1=Q1+1
287 FOR I=1 TO 110
288 A1(I)=A(I,J)\B1(I)=B(I,J)
289 NEXT I
290 FOR I=1 TO 100
291 AOUT(A1,1,Q,E1)
292 AOUT(B1,1,R,E2)
293 NEXT I
294 NEXT J
295 CLOSE #1
296 CNTR(3)
297 REM"********************"
298 REM"  END OF THE TEST"
299 REM"********************"
300 PRINT "DO YOU WANT TO RUN ANOTHER/"\INPUT C$
301 IF C$<>"YES" THEN 309
302 PRINT "DO YOU WANT THE SAME TEST CONDITIONS?"\INPUT C$
303 IF C$="YES" THEN 126
304 GO TO 106
305 REM
```

```
306 REM"*************************************************************"
307 REM"  THIS PART IS TO RECALL DATA FROM THE FLOPPY DISC"
308 REM"*************************************************************"
309 PRINT "DO YOU WANT TO RECALL DATA?"\INPUT Y6$
310 IF Y6$<>"YES" THEN 332
311 PRINT "ENTER SAMPLE#, RADIUS,LENGTH,EXP.TIME"
312 INPUT N$\INPUT R\INPUT L\INPUT T9
313 PRINT "ENTER N,M1"\INPUT N\INPUT M1
314 FOR J=1 TO N
315 PRINT "ENTER INTER. TIME&STRAIN"\INPUT T(J)\INPUT E(J)
316 PRINT "STRAIN-RATE"\INPUT D
317 NEXT J
318 OPEN "DX1:TOR"&N$ FOR INPUT AS FILE #1
319 FOR J=1 TO N
320 Q=(J-1)*2\R1=Q+1
321 FOR I=1 TO 100
322 AINP(A1,1,Q,E1)\AINP(B1,1,R1,E2)
323 NEXT I
324 FOR I=1 TO 100
325 A(I,J)=A1(I)\B(I,J)=B1(I)
326 NEXT I
327 NEXT J
328 CLOSE #1
329 GO TO 216
330 REM"MAKES ABSURD REMARK TO THOSE WHO REALLY HAVE NOTHING TO DO WITH"
331 REM"THIS PGM"
332 PRINT "TOURIST!"\STOP

READY
```

APPENDIX B

FLOW CURVES OF THE STEELS TESTED AT A STRAIN RATE OF $3.7 \times 10^{-2} s^{-1}$ AT 975, 1025 AND 1075°C

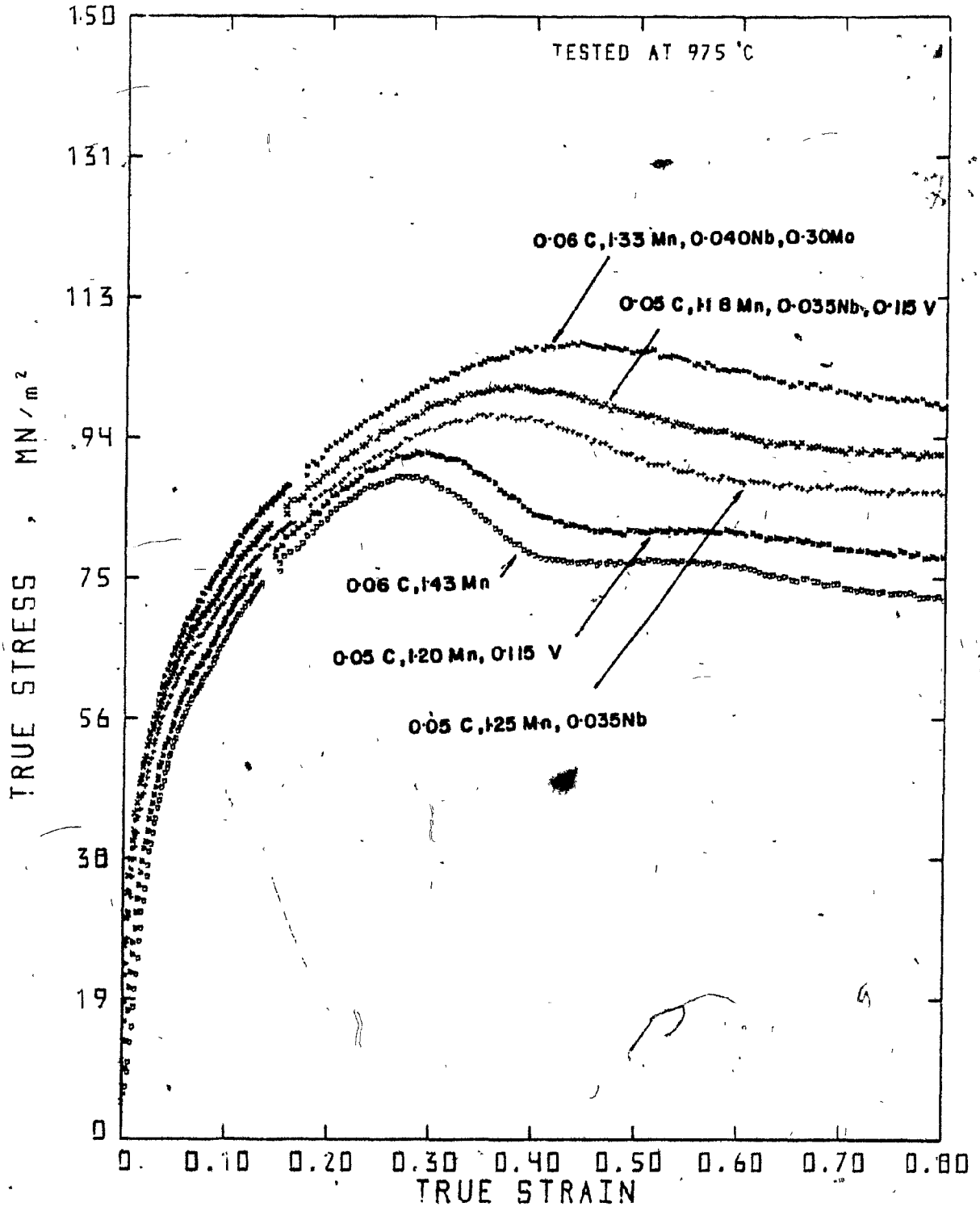
TESTED AT 975 °C
0·06 C, 1·33 Mn, 0·040Nb, 0·30Mo
0·05 C, 1·18 Mn, 0·035Nb, 0·115 V
0·06 C, 1·43 Mn
0·05 C, 1·20 Mn, 0·115 V
0·05 C, 1·25 Mn, 0·035Nb
TRUE STRESS , MN/m²
150
131
113
94
75
56
38
19
0
0.
0.10
0.20
0.30
0.40
0.50
0.60
0.70
0.80
TRUE STRAIN

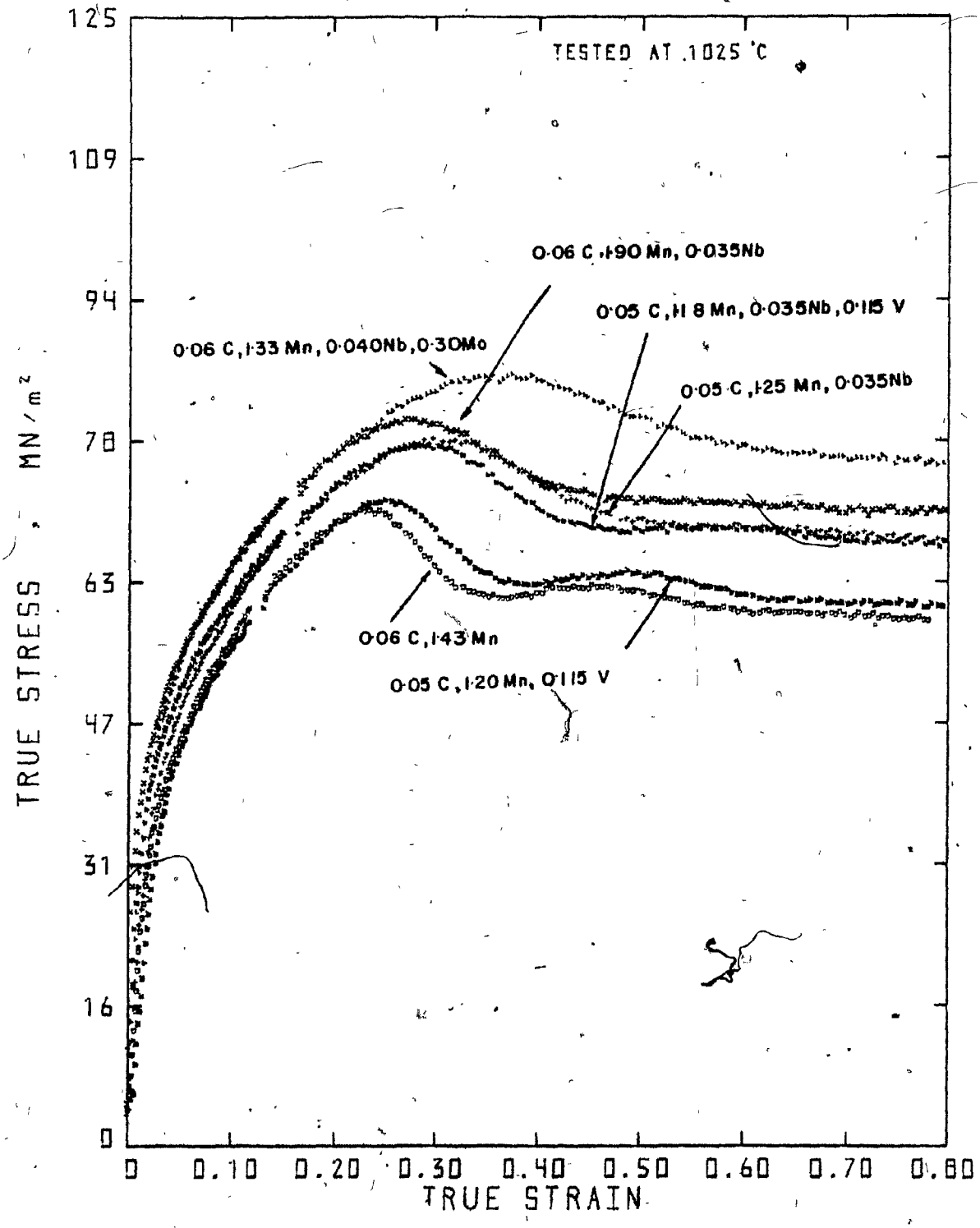
TESTED AT 1025 °C
0·06 C, 1·90 Mn, 0·035Nb
0·05 C, 1·18 Mn, 0·035Nb, 0·115 V
0·06 C, 1·33 Mn, 0·040Nb, 0·30Mo
0·05 C, 1·25 Mn, 0·035Nb
0·06 C, 1·43 Mn
0·05 C, 1·20 Mn, 0·115 V
TRUE STRESS , MN/m²
125
109
94
78
63
47
31
16
0
0
0.10
0.20
0.30
0.40
0.50
0.60
0.70
0.80
TRUE STRAIN

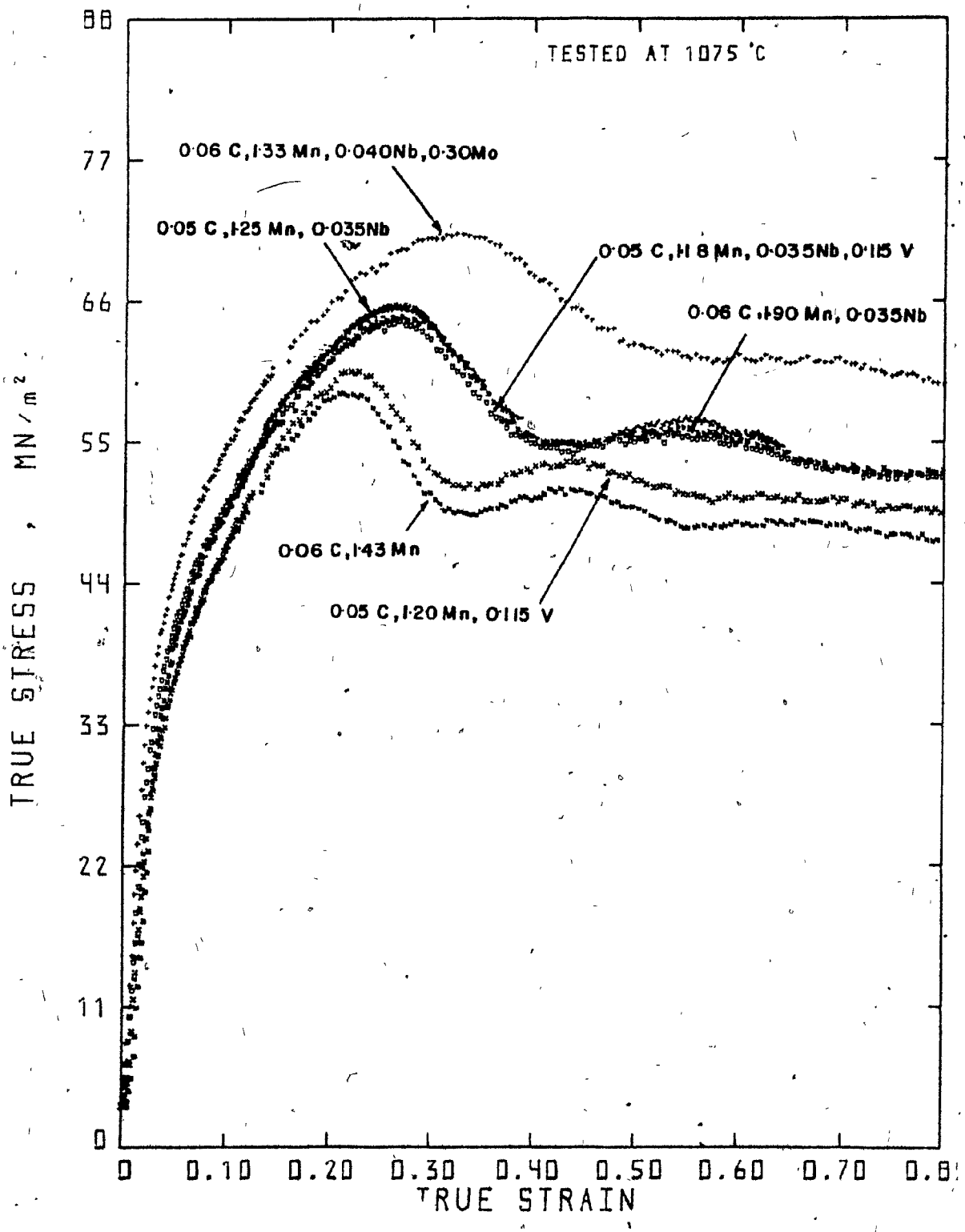
TESTED AT 1075 °C
0·06 C, 1·33 Mn, 0·040Nb, 0·30Mo
0·05 C, 1·25 Mn, 0·035Nb
0·05 C, 1·18 Mn, 0·035Nb, 0·115 V
0·06 C, 1·90 Mn, 0·035Nb
0·06 C, 1·43 Mn
0·05 C, 1·20 Mn, 0·115 V
TRUE STRESS , MN/m²
88
77
66
55
44
33
22
11
0
0
0.10
0.20
0.30
0.40
0.50
0.60
0.70
TRUE STRAIN